



HAL
open science

Etudes théoriques de dérivés (HqX) de la 8-hydroxyquinoléine : complexes $\text{Al}(\text{qX})_3$ et monocouches sur $\text{Al}(111)$

Yann Bulteau

► **To cite this version:**

Yann Bulteau. Etudes théoriques de dérivés (HqX) de la 8-hydroxyquinoléine : complexes $\text{Al}(\text{qX})_3$ et monocouches sur $\text{Al}(111)$. Matériaux. Institut National Polytechnique de Toulouse - INPT, 2020. Français. NNT : 2020INPT0142 . tel-04172899

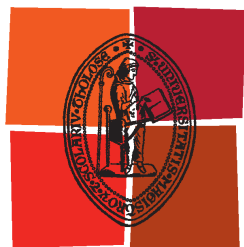
HAL Id: tel-04172899

<https://theses.hal.science/tel-04172899>

Submitted on 28 Jul 2023

HAL is a multi-disciplinary open access archive for the deposit and dissemination of scientific research documents, whether they are published or not. The documents may come from teaching and research institutions in France or abroad, or from public or private research centers.

L'archive ouverte pluridisciplinaire **HAL**, est destinée au dépôt et à la diffusion de documents scientifiques de niveau recherche, publiés ou non, émanant des établissements d'enseignement et de recherche français ou étrangers, des laboratoires publics ou privés.



Université
de Toulouse

THÈSE

En vue de l'obtention du

DOCTORAT DE L'UNIVERSITÉ DE TOULOUSE

Délivré par :

Institut National Polytechnique de Toulouse (Toulouse INP)

Discipline ou spécialité :

Science et Génie des Matériaux

Présentée et soutenue par :

M. YANN BULTEAU

le vendredi 18 décembre 2020

Titre :

Etudes théoriques de dérivés (HqX) de la 8-hydroxyquinoléine: complexes Al(qX)₃ et monocouches sur Al(111)

Ecole doctorale :

Sciences de la Matière (SDM)

Unité de recherche :

Centre Interuniversitaire de Recherche et d'Ingénierie des Matériaux (CIRIMAT)

Directeur(s) de Thèse :

MME CORINNE DUFAURE

Rapporteurs :

MME DOMINIQUE COSTA, CHIMIE PARISTECH

MME TZONKA MINEVA, ECOLE NLE SUP DE CHIMIE DE MONTPELLIER

Membre(s) du jury :

MME NADINE PEBERE, CNRS TOULOUSE, Président

M. ESMAIL ALIKHANI, UNIVERSITE SORBONNE, Membre

M. HERVE BULOUP, UNIVERSITE DE STRASBOURG, Membre

MME ANNE HEMERYCK, LAAS TOULOUSE, Membre

MME CHRISTINE LEPETIT, LABORATOIRE DE CHIMIE DE COORDINATION, Invité(e)

MME CORINNE DUFAURE, TOULOUSE INP, Membre

MME NATHALIE TARRAT, CEMES TOULOUSE, Invité(e)

Contents

Remerciements	vii
Résumé en Français	1
0.1 Introduction et Etat de l'Art	1
0.1.1 Présentation de la molécule Hq et de ses dérivés	1
0.1.2 Applications de la molécule Hq et de ses dérivés	3
0.2 Étude des molécules et des complexes isolés	4
0.2.1 Analyse ELF des molécules qX^{n-} ($n = 1$ ou 2)	4
0.2.2 Analyses ELF et QTAIM des complexes $Al(qX)_3^{n-}$ ($n = 0$ ou 3)	6
0.3 Étude de l'adsorption de molécules sur une surface Al(111)	8
0.3.1 Adsorption des molécules qX sur une surface Al(111) dans le vide	9
0.3.2 Adsorption des molécules qX sur une surface Al(111) dans l'eau	13
0.3.3 Adsorption des anions qX^{n-} ($n = 1$ ou 2) sur une surface Al(111) dans l'eau	13
0.4 Étude de la formation d'un complexe sur une surface Al(111)	14
0.4.1 Complexes Alq_3 adsorbés sur une surface Al(111)	14
0.4.2 Adsorption de trois molécules q sur une surface d'Al-Al(111)	17
0.5 Conclusions et Perspectives	21
General Introduction	25
1 State of the art	29
1.1 The Hq molecule and its derivatives	29
1.2 Complexes formed between Hq and its derivatives and metallic ions	31
1.3 The Hq molecule and its derivatives as chelating compounds	32
1.4 The Hq molecule and its derivatives as aluminum corrosion inhibitors	33
1.4.1 Corrosion of aluminum	33
1.4.2 Aluminum corrosion inhibition by chromates	34
1.4.3 Aluminum corrosion inhibition by organic molecules	35

1.4.4	Aluminum corrosion inhibition by Hq and its derivatives	36
1.5	Conclusion	37
2	Theoretical Methods & Calculation Parameters	39
2.1	Theoretical Background	39
2.1.1	Ab-initio calculations	39
2.1.2	Van der Waals interactions	45
2.1.3	Molecular dynamics	46
2.1.4	Solvent model	47
2.1.5	Topological analysis	48
2.2	Computational details	52
2.2.1	GAUSSIAN09 calculation parameters	52
2.2.2	VASP calculation parameters	52
2.2.3	Topological analysis	54
2.3	Conclusion	55
3	Study of the chelation of an aluminum cation by Hq derivatives	57
3.1	Computational Details	57
3.1.1	Presentation of the molecules	57
3.1.2	DFT calculations	58
3.2	Free molecules and anions	59
3.2.1	Geometries of the molecules	59
3.2.2	Topological analyses of qX^{n-} ($n = 1$ or 2) anions	62
3.3	$Al(qX)_3^{n-}$ ($n = 0$ or 3) complexes	64
3.3.1	Formation energies of $Al(qX)_3^{n-}$ ($n = 0$ or 3) in vacuum and in water	65
3.3.2	Geometries of the $Al(qX)_3^{n-}$ ($n = 0$ or 3) complexes	66
3.3.3	Topological analysis of $Al(qX)_3^{n-}$ ($n = 0$ or 3) complexes	66
3.4	Conclusion	69
4	Periodic calculations: Free molecules and complexes, bare surfaces	71
4.1	Free molecules and complexes	71
4.1.1	Computational details	71
4.1.2	Free Hq molecules, dehydrogenated and deprotonated species	75
4.1.3	Free Alq_n ($n = 1, 2$ or 3) complexes	76
4.2	Bare aluminum surface	78

4.2.1	Bulk aluminum	79
4.2.2	Aluminum surface model	80
4.2.3	Flat Al(111) surface	82
4.2.4	Defective Al(111) surface: Al-Al(111)	84
4.3	Conclusion	85
5	Adsorption of Hq derivatives on an Al(111) surface	87
5.1	Computational Details	88
5.1.1	Calculation parameters for qX species on Al(111) in vacuum	88
5.1.2	Calculation parameters for qX species on Al(111) in water	89
5.1.3	Calculation parameters for qX ⁿ⁻ (n = 1 or 2) species on Al(111) in water	89
5.1.4	Adsorption, interaction, and deformation energies	90
5.2	qX molecules adsorbed on Al(111) in vacuum	91
5.2.1	qX molecules adsorbed on Al(111) at θ_1 coverage in vacuum	92
5.2.2	qX molecules adsorbed on Al(111) at θ_2 coverage in vacuum	98
5.2.3	qX molecules adsorbed on Al(111) at θ_3 coverage in vacuum	100
5.2.4	QTAIM analysis of the bonding of qX molecules on Al(111) in vacuum	102
5.3	qX and qX ⁿ⁻ (n = 1 or 2) species adsorbed on Al(111) in water	105
5.3.1	qX molecules adsorbed on Al(111) at θ_1 and θ_3 coverage in water	106
5.3.2	qX ⁿ⁻ (n = 1 or 2) species adsorbed on Al(111) at θ_1 coverage in water	107
5.3.3	qX ⁿ⁻ (n = 1 or 2) species adsorbed on Al(111) at θ_3 coverage in water	111
5.3.4	Conclusion	112
6	Alq₃ complexes on an aluminum surface	115
6.1	Computational details	116
6.1.1	Adsorption of an Alq ₃ complex on an Al(111) surface.	116
6.1.2	Adsorption of n q molecules (n = 1 or 3) on an Al-Al(111) surface	117
6.1.3	Geometry exploration by <i>ab initio</i> molecular dynamics	118
6.2	Alq ₃ complexes adsorbed on an Al(111) surface.	118
6.3	Formation of Alq ₃ complexes on an Al-Al(111) surface	122
6.3.1	One q molecule adsorbed on an Al-Al(111) surface.	122
6.3.2	Three q molecules adsorbed on an Al-Al(111) surface.	124
6.3.3	Overall Discussion	132
6.4	Conclusion	132

General conclusion	135
A	139
A.1 Free molecules and complexes	139
B	141
B.1 Molecule adsorbed on an Al(111) surface	141
C	145
C.1 Complex adsorbed on an Al(111) surface	145
Bibliography	147

Remerciements

Je remercie tout d'abord ma directrice de thèse Corinne Dufaure pour son aide pendant ces 3 années de thèse. J'ai apprécié sa grande disponibilité, sa patience et ses qualités tant humaines que scientifiques qui m'ont permis de mener à bien ma thèse dans un contexte idéal. Je remercie Dominique Costa et Tzonka Mineva pour avoir bien voulu rapporter ma thèse, et Nadine Pébère, Hervé Bulou, Esmail Alikhani, Anne Hemeryck et Corinne Dufaure pour avoir accepté de former mon jury de thèse. Je remercie toutes les personnes avec qui j'ai travaillé sur des publications en commun ou qui m'ont donné des conseils pour mon travail de thèse : Nathalie Tarrat, Christine Lepetit, Nadine Pébère, Dominique Costa et Fatah Chiter.

En parallèle de ma thèse, l'expérience d'enseigner à l'ENSIACET a été très enrichissante. Je remercie pour cela Pascal Floquet qui m'a conseillé et supervisé, et aussi mes collègues de TD Moukrane Dehmas, Benoit Malard et Aurélie Vande Put.

Pendant mes 3 années de thèse, j'ai rencontré et sympathisé avec un grand nombre de personnes qui ont contribué à faire de ce temps passé au CIRIMAT une excellente expérience. Je remercie tous ceux que j'ai la chance d'avoir eu comme collègues de bureau : Yoann Gazal qui m'a accueilli à mon arrivée au CIRIMAT. Adeline Miquelot, Simon Ponton et Samuel Leleu, du bureau des doctorants SURF, avec qui j'ai partagé cafés et mots croisés, et Laura Villareal qui parlait beaucoup mais savait quand même quand s'arrêter ! Je remercie aussi d'autres collègues du CIRIMAT et des laboratoires de l'ENSIACET avec qui j'ai passé de très bons moments : Giorgos Gakis et notre escapade à Madrid, Ionela Illescu avec qui c'était toujours un plaisir de discuter, Tom Sanviemvongsak qui m'a aidé à mettre en place la journée sportive du CIRIMAT et enfin, mes amis Pedro Navarrete, Alejandro Monton, Manuel Flores et Camila Rivera avec lesquels j'ai passé de très bonnes soirées...

Je remercie enfin mes parents pour m'avoir soutenu tout au long de cette thèse.

Résumé en Français

0.1 Introduction et Etat de l'Art

0.1.1 Présentation de la molécule Hq et de ses dérivés

Au cours de cette thèse, nous avons étudié trois molécules : la 8-hydroxyquinoléine (appelée Hq ici), et deux de ses dérivés, la 5,7-dibromo-8-hydroxyquinoléine (appelée HqBr ici) et l'acide 8-hydroxyquinoléine-5-sulfonique (appelée HqSH ici). L'ensemble des trois molécules est noté HqX. Les structures de ces molécules sont indiquées dans la Figure 1, et les groupements X1 et X2 correspondants sont donnés dans le Tableau 1. Dans les molécules HqBr et HqSH, les atomes H aux positions ortho et para du cycle phénol (X2 et X1) sont remplacés par des atomes Br dans le cas de la HqBr et par un groupement SO_3H en X1 pour la HqSH. En solution, les formes sous lesquelles ces molécules sont présentes dépendent des pKa associés aux différents groupements de ces molécules. Pour la Hq, les pKa des groupements OH/O^- et NH^+/N sont respectivement de 9.89 et 5.13 [1, 2]. Dans la molécule HqSH, le pKa associé au groupement $\text{SO}_3\text{H}/\text{SO}_3^-$ est très faible, ce qui indique que la forme SO_3H est prédominante seulement dans un environnement extrêmement acide.

Ces molécules ont des propriétés dites chélatantes, ce qui signifie qu'elles peuvent former des complexes avec des cations métalliques tels que Cu^{2+} , Zn^{2+} , Co^{3+} et Al^{3+} [3, 4]. Dans le cas de complexes formés entre des molécules HqX et un cation Al^{3+} , deux isomères peuvent exister. Ces isomères sont appelés méridional (*mer*) et facial (*fac*) [5], et sont présentés dans la Figure 2. Les groupements X1 et X2 correspondants sont donnés dans le Tableau 2. Les molécules sont déprotonées, c'est à dire avec le groupement hydroxyle OH/O^- sous forme O^- . Dans l'isomère *mer*, les trois atomes O forment un plan perpendiculaire au plan formé par les trois atomes N. Dans l'isomère *fac*, ces mêmes plans sont presque parallèles, et les atomes O forment une face tandis que les atomes N en forment une autre, orientée dans le sens opposé.

FIGURE 1: Molécules de HqX. X1 and X2 correspondent aux groupes présentés dans le Tableau 1.

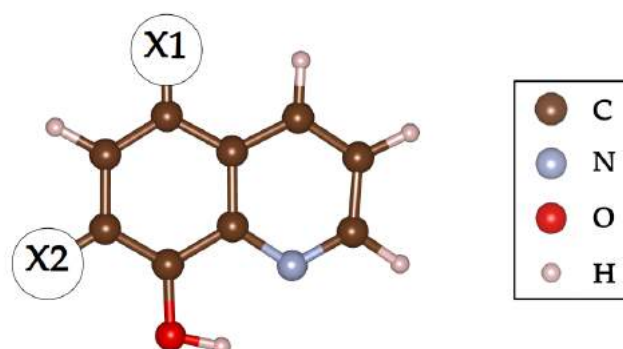


TABLE 1: Molécules de HqX : Notations.

Molécules	Hq	HqBr	HqSH
X1	H	Br	SO ₃ H
X2	H	Br	H

FIGURE 2: Complexes Al(qX)₃. X1 and X2 correspondent aux groupes présentés dans le Tableau 2. À gauche : l'isomère *mer*. À droite : l'isomère *fac*.

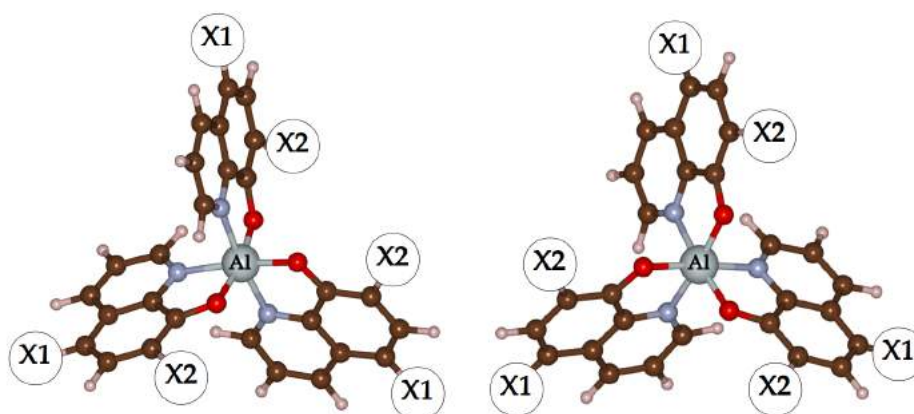


TABLE 2: Complexes Al(qX)₃ : Notations.

Complexes	Alq ₃	Al(qBr) ₃	Al(qSH) ₃
X1	H	Br	SO ₃ H
X2	H	Br	H

0.1.2 Applications de la molécule Hq et de ses dérivés

Les propriétés chélatantes de ces molécules sont utilisées pour diverses applications. Premièrement, la capture de cations métalliques par ces molécules est utilisée pour dépolluer des solutions contaminées [6, 7]. Les propriétés électroluminescentes des molécules HqX et de leurs complexes sont utilisées pour la détection d'ions métalliques en solution [8]. En effet, l'intensité et la longueur d'onde d'émission changent avec la complexation de la molécule [8]. Ces propriétés électroluminescentes sont aussi utilisées dans les diodes électroluminescentes organiques (OLED) [9, 10]. Elles peuvent être composées de complexes de HqX présents sous forme de films, dont la longueur d'onde d'émission peut être ajustée par l'utilisation de différentes molécules et différents cations [11].

L'application sur laquelle porte ce travail de thèse est l'inhibition de la corrosion de l'aluminium. Les alliages d'aluminium sont largement utilisés dans l'industrie, notamment aéronautique, en raison de leur bonne résistance naturelle à la corrosion, grâce à la formation d'une couche passive d'oxyde. Cependant, des processus de corrosion localisée, appelés corrosion par piqûre, peuvent causer d'importants dommages, ce qui rend nécessaire le traitement de l'aluminium contre la corrosion. Les traitements à base de chrome hexavalent $\text{Cr}_2\text{O}_7^{2-}$ sont appliqués pour l'utilisation industriel d'alliages d'aluminium. Cependant, les réglementations REACH imposent aujourd'hui leur remplacement par des alternatives moins toxiques [12]. Pour cela, une des pistes étudiées est l'utilisation de molécules organiques, qui s'adsorbent à la surface de l'aluminium pour modifier sa réactivité et stopper la corrosion. Dans cette optique, la molécule Hq a été étudiée expérimentalement, et montre de bonnes propriétés inhibitrices [13]. Les molécules de HqBr et HqSH ont été étudiées expérimentalement et ne montrent quand à elles pas d'efficacité en tant qu'inhibiteurs de corrosion [14, 15].

Pour mieux comprendre les mécanismes responsables de l'inhibition de la corrosion de l'aluminium par la Hq, une étude théorique par DFT a été menée par Fatah Citer [16]. Il a montré que la Hq, sous forme déshydrogénée, peut se chimisorber sur une surface Al(111) et former des couches compactes et stables, bloquant la réaction de réduction de l' O_2 , qui est une des réactions de la corrosion [17, 18].

Dans notre travail, nous étudions les molécules de Hq, HqBr et HqSH à l'aide de la Théorie de la Fonctionnelle de la Densité comprenant les forces de dispersion (DFT-D) [19,

20], avec comme objectif de mieux comprendre pourquoi, bien que proches de la Hq dans leurs structures, les molécules HqBr et HqSH ne sont pas de bons inhibiteurs de corrosion.

Dans ce résumé, nous présentons notre travail en trois parties. Tout d'abord, le travail effectué sur les molécules de HqX et les complexes formés avec un cation d'aluminium, sous formes isolées. Ensuite, la modélisation de l'adsorption des molécules de HqX sur une surface d'aluminium. Enfin, les géométries d'adsorption de complexes de Hq sur une surface d'aluminium.

0.2 Étude des molécules et des complexes isolés

Dans cette section, nous nous intéressons aux systèmes finis que sont les molécules isolées, et les complexes isolés formés à partir de trois molécules et d'un ion aluminium. Parmi les différentes formes des dérivés HqX présents dans l'eau, la forme déprotonée est celle pouvant se lier le plus fortement à un ion ou à une surface, comme montré par Chiter *et. al.* dans sa thèse [16] dans le cas d'une surface Al(111). C'est donc cette forme que nous avons étudiée pour toutes les HqX. La forme déprotonée se distingue de la forme native par la forme O⁻ du groupe hydroxyle au lieu de la forme OH. C'est donc une forme électronique chargée, notée qXⁿ⁻ (n = 1 ou 2). Dans le cas de la molécule HqSH, deux formes sont étudiées, l'une avec le groupe sulfo dans sa forme SO₃⁻, notée qS²⁻, et l'autre dans sa forme SO₃H, notée qSH⁻. Bien qu'en conditions expérimentales, la forme qS²⁻ soit la plus probable, la présence d'un H sur le groupe sulfo permet de modéliser l'influence d'un contre-ion sur le groupement.

0.2.1 Analyse ELF des molécules qXⁿ⁻ (n = 1 ou 2)

L'analyse ELF (Electron Localization Function) [21, 22], menée à bien avec l'aide de Christine Lepetit du LCC à Toulouse, utilise la probabilité de paire, i.e. la probabilité de trouver deux électrons de même spin dans une même zone, pour cartographier la molécule et répartir la population électronique en bassins pouvant être assimilés à des doublets de la théorie de Lewis. Dans le cas de la molécule q⁻, les populations des bassins sont indiquées en rouge dans la Figure 4(b). Les populations des bassins associés aux doublets non liants de O1,

$V(O1)_a$ et $V(O1)_b$, sont respectivement de $2.88 e^-$ et $2.76 e^-$, pour un total de presque $6 e^-$, ce qui correspond au mésomère présenté Figure 4(c).

FIGURE 3: Molécules déprotonées qX^{n-} ($n = 1$ or 2) optimisées dans le vide.

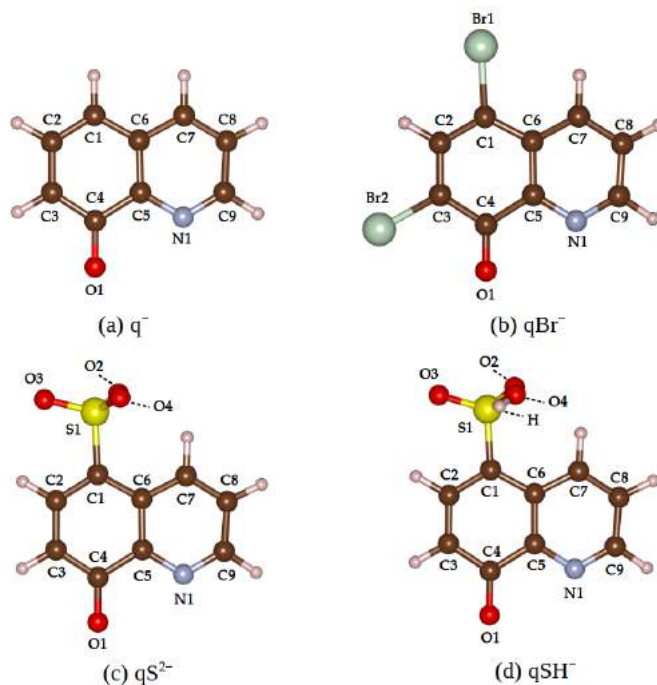
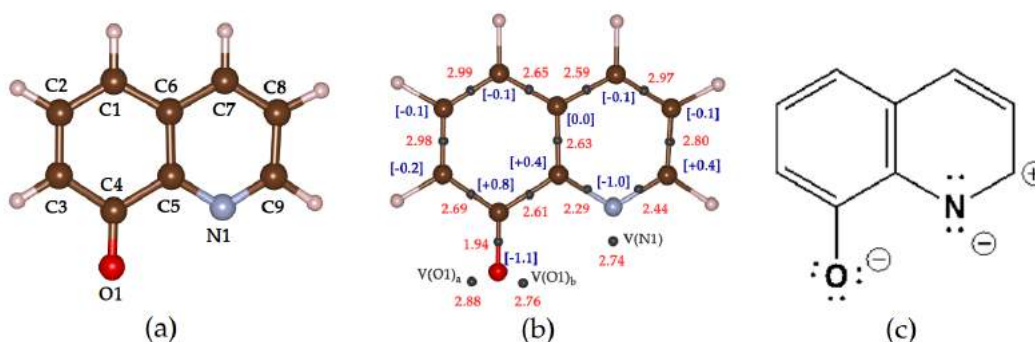


FIGURE 4: Molécule déprotonée q^- . (a) Indices des atomes. (b) Carte des attracteurs ELF et de leurs populations électroniques (en e^-) en rouge; Charges atomiques QTAIM (en e) en bleu. (c) Formes mésomères phénolate et pyridine.



Dans ce travail, nous nous intéressons aux populations proches des atomes mis en jeu dans la formation de liaisons avec l'aluminium, c'est à dire les atomes O1, N1, et C7 [16]. Afin de déterminer d'éventuelles variations de réactivité entre les dérivés, les populations de ces bassins ont été calculées pour chacun des quatre dérivés et sont présentées dans le Tableau 3. Les différences observées entre les espèces ne sont pas suffisantes pour indiquer une modification de réactivité sur les atomes O1, N1 et C7 suite à la substitution des atomes H des positions ortho et para du cycle phénol par les groupes Br, SO_3^- ou SO_3H .

TABLE 3: Comparaison des populations (en e^-) de certains bassins ELF des anions q^- , qBr^- , qS^{2-} et qSH^- .

Molécules	q^-	qBr^-	qS^{2-}	qSH^-
V(C4,O1)	1.94	2.00	1.88	2.02
V(O1) _a	2.88	2.83	2.92	2.82
V(O1) _b	2.76	2.76	2.79	2.79
V(N1)	2.74	2.72	2.76	2.73
V(C5,N1)	2.29	2.30	2.31	2.27
V(C9,N1)	2.44	2.44	2.43	2.45
V(C7,C6)	2.59	2.60	2.57	2.63
V(C7,C8)	2.97	2.94	2.96	2.91

0.2.2 Analyses ELF et QTAIM des complexes $Al(qX)_3^{n-}$ ($n = 0$ ou 3)

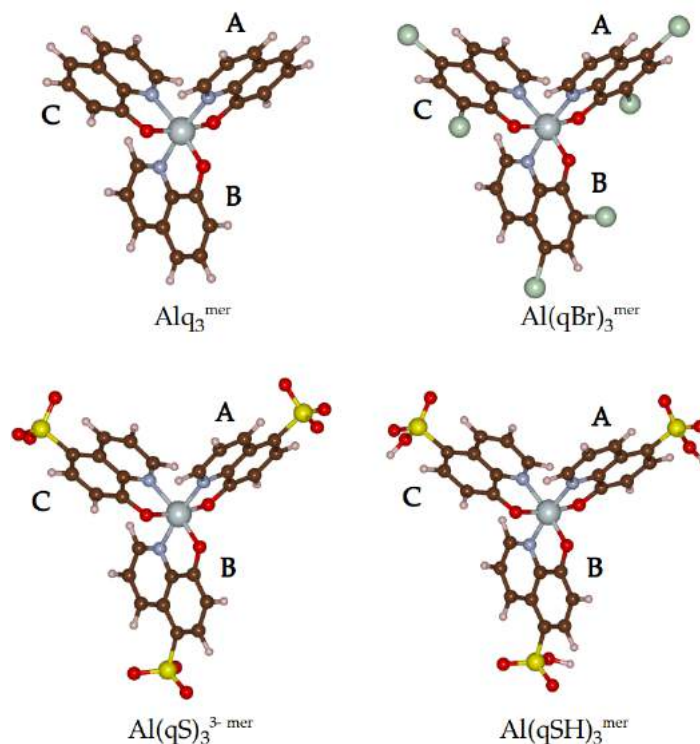
Les complexes $Al(qX)_3^n$ ($n = 0$ ou 3) existent sous deux formes isomères. La première, appelée meridional et notée *mer*, est caractérisée par une première face comprenant deux atomes O et un atome N. Dans l'isomère facial, noté *fac*, une des faces comprend trois atomes O, et l'autre trois atomes N. L'isomère *mer* étant celui observé expérimentalement en solution [23–26], ainsi que le plus stable dans le vide selon des calculs DFT [25], il est le seul à être étudié dans cette section. Les géométries des complexes $Al(qX)_3^{mer}$ sont présentées dans la Figure 5. Pour étudier les propriétés de chélation des différents dérivés, nous analysons la structure électronique des liaisons formées dans les complexes entre l'ion aluminium et les molécules. L'analyse ELF, présentée précédemment, montre toujours la présence de deux bassins $V(O1)_a$ et $V(O1)_b$. Par rapport à la molécule seule, le bassin $V(O1)_a$ perd des électrons, tandis que $V(O1)_b$ en gagne. La comparaison des différents complexes ne montre pas de différence significative dans les populations des bassins proches des atomes O1 et N1 (Tableau 4), ce qui indique que les quatre dérivés interagissent de manière similaire avec l'ion aluminium.

TABLE 4: Populations ELF (en e^-) autour de l'ion Al^{3+} dans les complexes Alq_3^{mer} , $Al(qBr)_3^{mer}$, $Al(qS)_3^{3-mer}$ et $Al(qSH)_3^{mer}$. Les populations sont moyennées sur les molécules **A**, **B** et **C** des complexes.

Complexe	Alq_3^{mer}	$Al(qBr)_3^{mer}$	$Al(qS)_3^{3-mer}$	$Al(qSH)_3^{mer}$
V(O1) _a	2.31	2.30	2.29	2.34
V(O1) _b	3.70	3.69	3.75	3.62
V(N1)	2.78	2.80	2.80	2.80

L'analyse QTAIM (Quantum Theory of Atoms in Molecule) [27, 28], utilise la densité de charge ρ pour i) calculer des charges atomiques ii) caractériser les liaisons à partir de valeurs de la densité de charge au niveau des BCP (Bond Critical Points), qui sont les points selle

FIGURE 5: Géométries des complexes $\text{Alq}_3^{\text{mer}}$, $\text{Al}(\text{qBr})_3^{\text{mer}}$, $\text{Al}(\text{qS})_3^{3-\text{mer}}$ et $\text{Al}(\text{qSH})_3^{\text{mer}}$ optimisées dans le vide. Les trois molécules composant un complexe sont notées A, B et C.



de ρ entre les atomes du système. La charge atomique sur Al est de $+2.49 \pm 0.01$ e pour l'ensemble des complexes, ce qui indique un état d'oxydation Al^{III} dans tous les cas. Dans le Tableau 5, les indicateurs $\frac{|V_{\text{bcp}}|}{G_{\text{bcp}}}$ et $\frac{H_{\text{bcp}}}{\rho_{\text{bcp}}}$, construits à partir des densités d'énergie potentielle V_{bcp} et cinétique G_{bcp} aux BCPs permettent une analyse plus fine de la nature des liaisons [29]. Dans tous les cas présentés, la faible valeur de ρ et le signe positif de $\Delta\rho_{\text{bcp}}$ montrent que la densité de charge est répartie de part et d'autre du BCP, pouvant indiquer plusieurs types de liaisons (ionique, dative, van der Waals...). Les charges sur Al et sur les atomes O et N (-1.2 ± 0.1 e) vont dans le sens de liaisons ioniques. Les indicateurs $\frac{|V_{\text{bcp}}|}{G_{\text{bcp}}}$ et $\frac{H_{\text{bcp}}}{\rho_{\text{bcp}}}$ montrent quant à eux un faible caractère covalent, ce qui nous permet de conclure que les liaisons O-Al et N-Al sont dans tous les cas ioniques et à faible caractère covalent, ce qui correspond à ce qui est indiqué dans la bibliographie pour des complexes formés entre la molécule q et des ions Co, Fe, et Mn [30]. Les valeurs des descripteurs ρ , $\Delta\rho_{\text{bcp}}$, $\frac{|V_{\text{bcp}}|}{G_{\text{bcp}}}$ et $\frac{H_{\text{bcp}}}{\rho_{\text{bcp}}}$ varient peu entre les complexes, ce qui confirme que les molécules qX^{n-} ($n = 1$ ou 2) étudiées dans ce travail interagissent de la même manière avec l'ion Al^{3+} .

TABLE 5: Descripteurs QTAIM (en u.a.) associés aux liaisons O1-Al et N1-Al dans les complexes $\text{Alq}_3^{\text{mer}}$. Les descripteurs sont moyennés sur les trois liaisons O1-Al and N1-Al.

Complexes	$\text{Alq}_3^{\text{mer}}$	$\text{Al}(\text{qBr})_3^{\text{mer}}$	$\text{Al}(\text{qS})_3^{3-\text{mer}}$	$\text{Al}(\text{qSH})_3^{\text{mer}}$
BCP O1-Al				
ρ_{bcp}	0.071	0.072	0.070	0.071
$\Delta\rho_{\text{bcp}}$	0.397	0.403	0.388	0.397
$\frac{ V_{\text{bcp}} }{G_{\text{bcp}}}$	1.06	1.06	1.06	1.06
$\frac{H_{\text{bcp}}}{\rho_{\text{bcp}}}$	-0.09	-0.08	-0.09	-0.08
BCP N1-Al				
ρ_{bcp}	0.053	0.053	0.053	0.054
$\Delta\rho_{\text{bcp}}$	0.223	0.223	0.219	0.227
$\frac{ V_{\text{bcp}} }{G_{\text{bcp}}}$	1.09	1.09	1.09	1.09
$\frac{H_{\text{bcp}}}{\rho_{\text{bcp}}}$	-0.10	-0.11	-0.11	-0.11

0.3 Étude de l'adsorption de molécules sur une surface Al(111)

Des travaux théoriques ont montré que pour trouver des corrélations entre des valeurs calculées par DFT et des données expérimentales d'efficacité de l'inhibition de la corrosion par des molécules, il est nécessaire d'utiliser un modèle de surface sur lequel sont adsorbées les molécules étudiées. Pour que les molécules soient susceptibles d'être de bons inhibiteurs de corrosion, un prérequis est qu'elles s'adsorbent fortement et puissent former une couche organique compacte [17, 18, 31–39]. Dans cette section, nous adsorbons les dérivés HqX sur une surface Al(111) afin de déterminer les éventuelles différences dans l'adsorption de ces molécules pouvant être reliées à leur efficacité comme inhibiteurs de corrosion. La forme déprotonée de la molécule a été dans un premier temps modélisée par une forme dite déshydrogénée. Cette forme correspond à la forme native à laquelle est retiré un atome H du groupe hydroxyle. La notation qX désigne les formes déshydrogénées de l'ensemble des dérivées de Hq . Cette forme déshydrogénée est utilisée car les formes chargées sont difficiles à étudier par des codes de calcul de systèmes périodiques. Cette approximation est largement utilisée dans ce type d'étude, et nous avons vérifié sa viabilité dans la section 0.3.3. Après la présentation des calculs réalisés dans le vide, nous utilisons un modèle de solvant afin de nous rapprocher des conditions expérimentales.

0.3.1 Adsorption des molécules qX sur une surface Al(111) dans le vide

La surface d'aluminium a été modélisée par un empilement de couches atomiques d'Al aussi appelé un slab. La périodicité du système permet d'obtenir une surface infinie dans les directions x et y, tandis que les images du slab dans la direction z sont isolées par suffisamment de vide pour que les interactions soient négligeables. L'adsorption des molécules est faite à trois taux de recouvrement, notés θ_1 ($4.72 \cdot 10^{-3}$ molécule $\cdot \text{Å}^{-2}$), θ_2 ($1.57 \cdot 10^{-2}$ molécule $\cdot \text{Å}^{-2}$) et θ_3 ($2.36 \cdot 10^{-2}$ molécule $\cdot \text{Å}^{-2}$), qui sont associés à des cellules élémentaires de tailles différentes, et donc à des périodicités du système différents. Le taux de recouvrement θ_1 correspond à l'adsorption de molécules isolées les unes des autres, θ_2 à l'adsorption de molécules en interaction les unes avec les autres, et θ_3 l'adsorption de molécules formant une couche de densité maximale. Le slab Al(111) est composé de 4 couches atomiques, dont deux sont libres de se relaxer avec l'optimisation géométrique du système, et est séparé d'environ 22.5 Å de son image périodique dans la direction z. Une correction dipolaire [40, 41] corrige l'interaction dipôle-dipôle entre les slabs images dans la direction de z.

L'adsorption des molécules peut s'effectuer selon plusieurs modes, appelés *tilt_{bridge}*, *tilt_{top}* et *para*. Les géométries correspondantes à ces modes sont présentées Figure 6 pour θ_1 et Figure 7 pour θ_3 . Pour les modes *tilt_{bridge}* et *tilt_{top}*, la molécule est orientée de manière oblique par rapport à la surface, avec l'atome O1 adsorbé respectivement sur un site bridge ou top de la surface Al(111), et l'atome N1 adsorbé sur un site top de la surface Al(111). Pour les modes *para*, la molécule est orientée de manière parallèle à la surface, avec les atomes O1, N1 et C7 adsorbés sur des sites top de la surface. La molécule qSH forme aussi une liaison par un atome O du groupe SO₃H avec Al(111). Dans le cas de θ_3 , la périodicité du système ne permet pas le mode d'adsorption *para*. Les valeurs énergétiques calculées sont l'énergie d'adsorption $E_{ads}^{mol/Al(111)}$, qui correspond à la variation d'énergie globale du système associée à l'adsorption de la molécule, l'énergie d'interaction entre la molécule et la surface $E_{int}^{mol/Al(111)}$, l'énergie d'interaction entre les molécules de la couche organique $E_{int}^{inter-mol}$, et l'énergie de déformation du système $E_{def}^{mol/Al(111)}$ associée aux déformations de la molécule et du slab induites par l'adsorption. Ces énergies sont données dans la Figure 7. Seulement le plus stable des modes *tilt_{bridge}* et *tilt_{top}* est indiqué. Les énergies d'adsorption montrent une forte adsorption dans tous les cas (au moins -3.48 eV), et le mode *para* est le plus stable pour toutes les molécules à θ_1 et θ_2 à l'exception du cas de la molécule q à θ_1 où le mode *tilt* est le plus stable. Les modes *para* ont une énergie de déformation nettement plus haute que les modes *tilt*, ce qui s'explique par la déformation du cycle pyridine induite par

la liaison de l'atome C7 avec la surface. Cette liaison, ainsi que l'interaction van der Waals entre la molécule et la surface, qui est plus forte lorsque la molécule est plus proche de la surface, donne une énergie d'interaction entre la molécule et la surface plus forte en valeur absolue pour les modes *paral* que pour les modes *tilt*. Enfin, sans surprise, l'interaction entre les molécules au sein d'une couche augmente avec le taux de recouvrement, à l'exception de la molécule qBr à θ_3 , pour des raisons expliquées dans le manuscrit. La molécule qS a aussi été étudiée et montre la même tendance que la molécule qSH. Ces résultats montrent que tous les dérivés étudiés peuvent former des couches compactes et fortement adsorbées. La différence notable entre les différents dérivés est le mode d'adsorption le plus stable à θ_1 , qui pourrait influencer le processus de formation de la couche.

FIGURE 6: Molécules qX adsorbées sur une surface Al(111) dans le vide au taux de recouvrement $\theta_1 = 4.72 \cdot 10^{-3}$ molécule $\cdot \text{Å}^{-2}$. En bleu : les atomes Al de la couche supérieure. En gris : les atomes Al des couches inférieures.

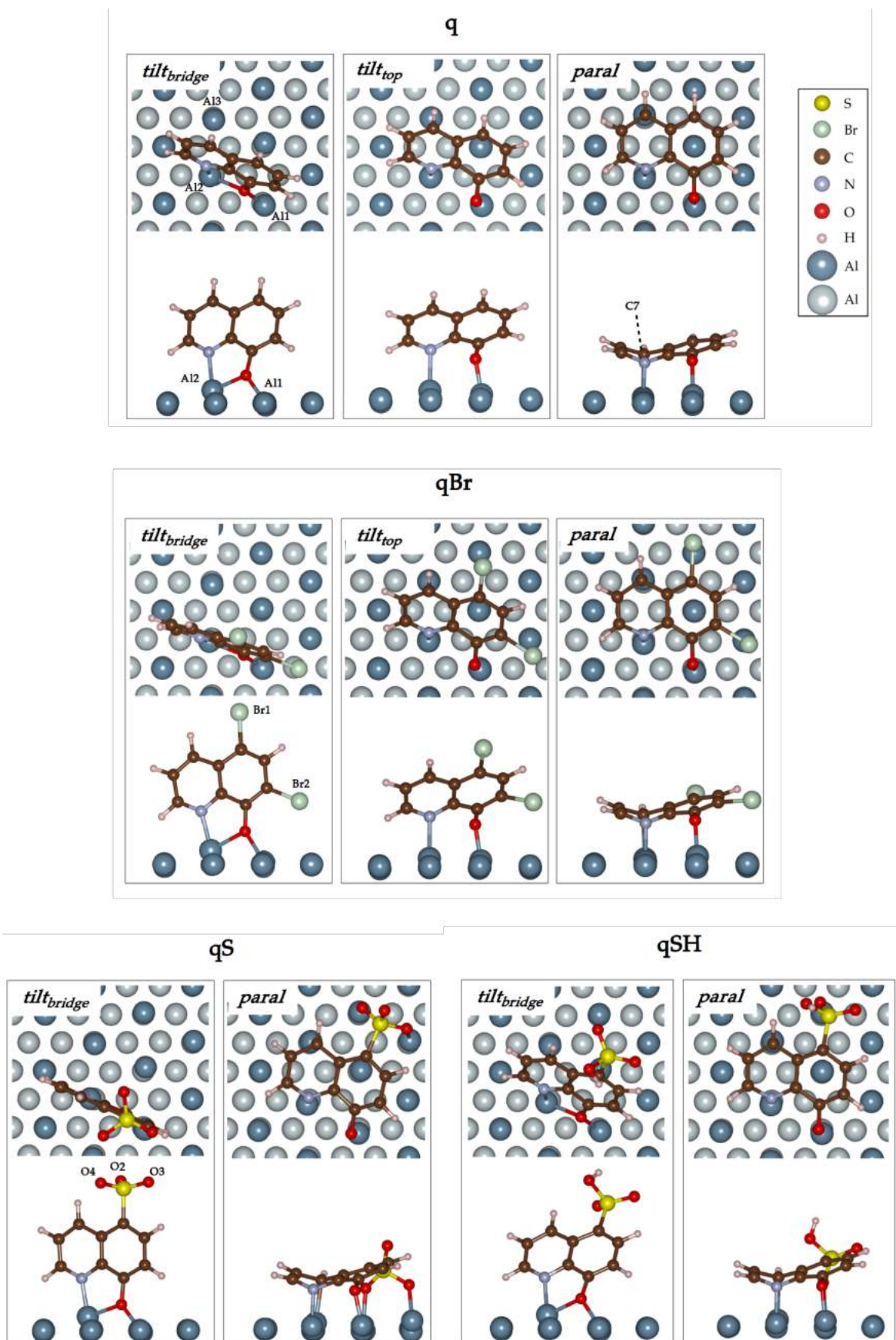


FIGURE 7: Molécules qX adsorbées sur une surface Al(111) dans le vide au taux de recouvrement $\theta_3 = 2.36 \cdot 10^{-2}$ molécule $\cdot \text{\AA}^{-2}$. En bleu : les atomes Al de la couche supérieure. En gris : les atomes Al des couches inférieures.

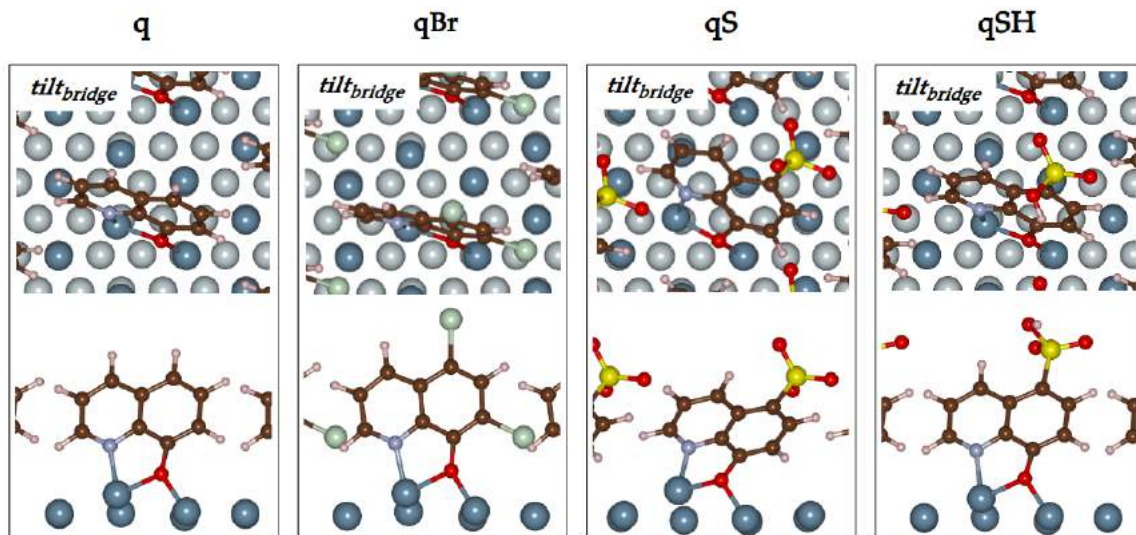
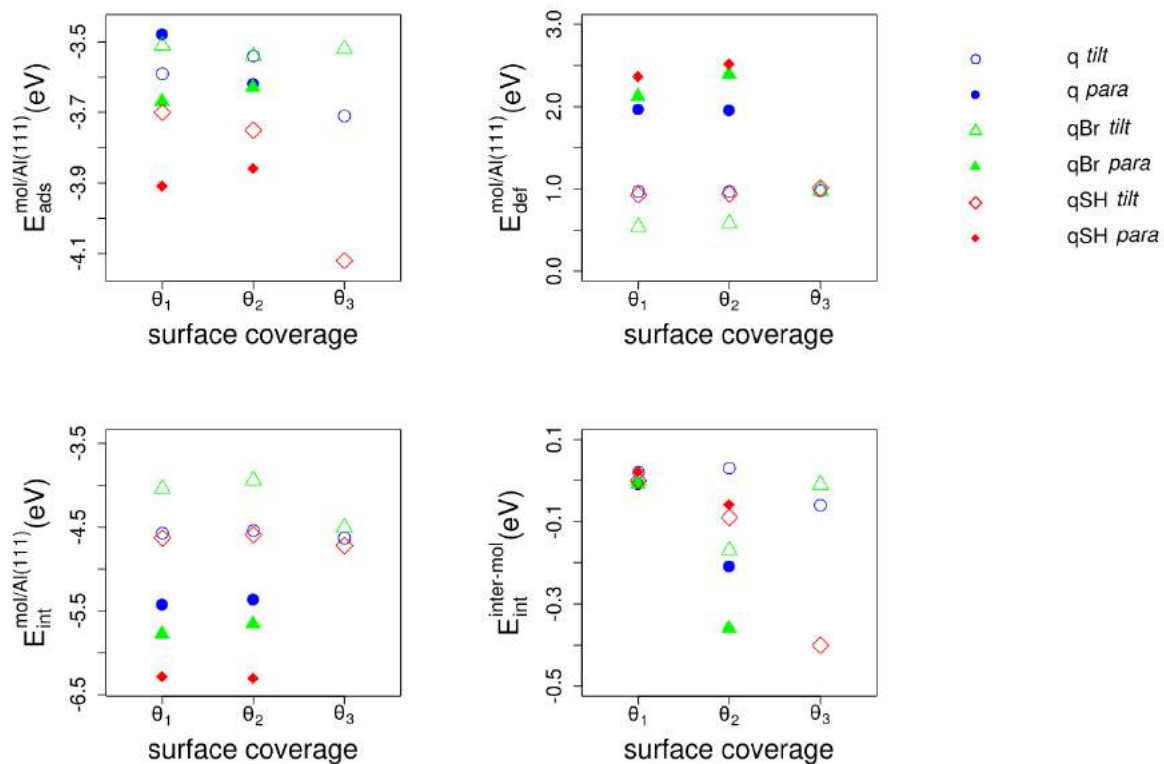


FIGURE 8: Molécules qX adsorbées sur une surface Al(111) dans le vide. Energie d'adsorption, énergie de déformation de la molécule et de la surface, énergie d'interaction entre la couche de molécules et la surface, énergie d'interaction entre les molécules de la couche.



0.3.2 Adsorption des molécules qX sur une surface Al(111) dans l'eau

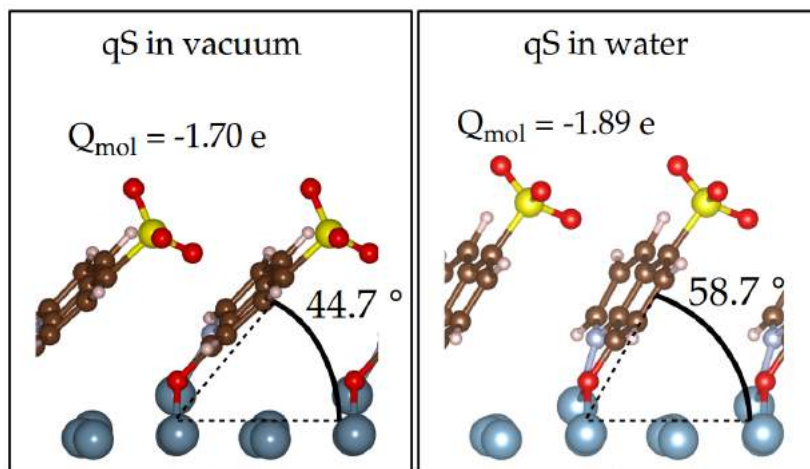
Afin de nous rapprocher des conditions expérimentales, nous avons utilisé un modèle de solvant implicite simulant l'effet de l'eau sur le système [42–44]. Les mêmes tendances que celles exposées précédemment sont constatées, avec globalement une adsorption diminuée mais toujours forte. Les plus grandes différences sont observées pour la molécule qS, qui comprend un groupe très hydrophile (SO_3). Le mode d'adsorption $\text{tilt}_{\text{bridge}}$ à θ_3 dans le vide et dans l'eau sont comparées Figure 9. L'angle décrivant l'orientation de la molécule par rapport à la surface est plus grand en présence de solvant que dans le vide. Cela peut s'expliquer par la stabilisation du groupe SO_3 dans l'eau par rapport à dans le vide. La charge sur la molécule est aussi environ 0.2 e plus forte en présence de solvant. Ce résultat montre qu'il est utile de prendre en compte le solvant dans les cas où la molécule étudiée contient un groupe chimique fortement hydrophile ou hydrophobe.

0.3.3 Adsorption des anions qX^{n-} ($n = 1$ ou 2) sur une surface Al(111) dans l'eau

Dans ce genre d'étude, où on simule l'adsorption d'une molécule déprotonée sur une surface, la molécule est généralement modélisée par la forme déshydrogénée, qui est électriquement neutre. On suppose alors que le modèle de surface joue le rôle de réservoir d'électrons et que l'état final du système est identique au cas de l'adsorption d'une molécule déprotonée. Pour vérifier cette hypothèse, nous avons modélisé l'adsorption d'une forme déprotonée grâce à l'ajout d'un contre-ion permettant de donner à la molécule la charge voulue tout en gardant la cellule neutre, ce qui est nécessaire dans VASP. Cela permet aussi d'évaluer la valeur de l'énergie d'adsorption d'une molécule déprotonée, qui est nécessairement différente de l'énergie d'adsorption d'une molécule déshydrogénée.

À bas taux de recouvrement θ_1 , on obtient des géométries et des charges similaires entre le cas des molécules q^- et qS^{2-} (déprotonées) et celui des molécules déshydrogénées q et qS, ce qui valide l'approximation présentée précédemment en ce qui concerne l'état final du système. L'énergie d'adsorption d'une forme déprotonée est plus faible en valeur absolue que celle d'une forme déprotonée, d'une différence d'environ 1 eV. Au taux de recouvrement θ_3 , des problèmes d'interaction entre le système slab + molécule et le contre-ion ou entre les images périodiques nous empêchent de conclure pour le moment.

FIGURE 9: Molécule qS adsorbée sur une surface Al(111), dans le vide et dans l'eau. Charge sur la molécule Q_{mol} et angle d'inclinaison de la molécule.



0.4 Étude de la formation d'un complexe sur une surface Al(111)

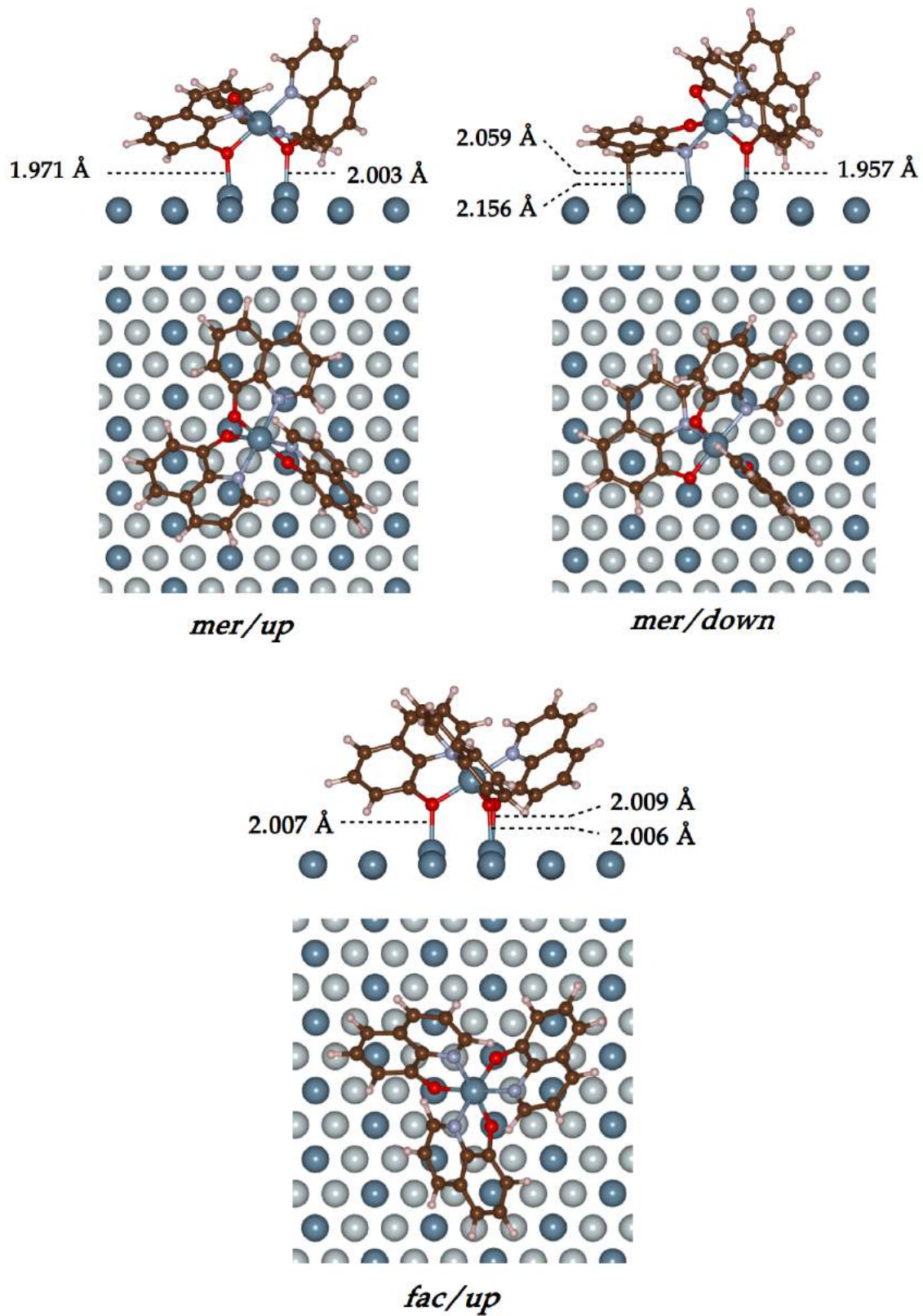
Dans de nombreux travaux expérimentaux, le mécanisme de l'inhibition de la corrosion proposé met en jeu des complexes insolubles formés à partir de Hq et d'ions d'Al, de Cu ou de Mg, présents sur la surface d'aluminium et empêchant le passage d'espèces agressives. Dans cette section, nous modélisons la formation de complexes sur une surface Al(111), à partir de deux processus de formation. Dans le premier, le complexe est préformé dans le vide puis adsorbé sur la surface. Dans le deuxième processus, trois molécules q sont adsorbées sur un adatome de la surface Al(111). Cette surface est notée Al-Al(111). La modèle de surface utilisé contient trois couches atomiques, et la périodicité du système correspond à un taux de recouvrement de $\theta = 6.64 \cdot 10^{-3} \text{ molecule} \cdot \text{\AA}^{-2}$.

0.4.1 Complexes Alq_3 adsorbés sur une surface Al(111)

Afin de trouver la géométrie d'adsorption la plus stable d'un complexe Alq_3 , les deux isomères Alq_3^{mer} et Alq_3^{fac} sont adsorbés sur la surface Al(111). Les géométries des modes de chimisorption sont présentées Figure 10. Les modes sont dénommés *up* et *down* selon l'orientation des moments dipolaires des complexes. Dans le mode *mer/up*, la face comprenant deux atomes O et un atome N est orientée vers la surface, avec la formation de deux liaisons O-Al. Dans le mode *mer/down*, la face comprenant un atome O et deux atomes N est orientée vers la surface, et un atome O et un atome N sont liés à la surface. Enfin, dans le mode *fac/up*, la face comprenant trois atomes O est orientée vers la surface, et les trois

O forment des liaisons avec la surface. Les énergies totales relatives de ces géométries, les charges sur l'atome Al du complexe et sur les molécules du complexes, ainsi que la position de l'atome Al par rapport à la surface, sont indiquées dans le Tableau 6. La géométrie *fac/up* est la plus stable. Dans les trois cas, la charge sur l'adatome reste proche de celle du complexe libre.

FIGURE 10: Isomères *mer* and *fac* du complexe Alq_3 adsorbés sur une surface $\text{Al}(111)$. En bleu : l'atome Al du complexes et les atomes Al de la couche supérieure. En gris : les atomes Al des couches inférieures.



0.4.2 Adsorption de trois molécules q sur une surface d'Al-Al(111)

L'adsorption de trois molécules q sur un adatome d'une surface Al-Al(111) mène à un système contenant un grand nombre de degrés de liberté. Pour pouvoir déterminer les géométries les plus stables, il est nécessaire d'utiliser une méthode permettant d'explorer l'espace des conformations du système. Pour cela nous avons utilisé la dynamique moléculaire *ab initio*, avec l'aide de Natalie Tarrat du CEMES à Toulouse. Cette méthode utilise la DFT, mais plutôt que de rechercher une géométrie correspondant à un minimum d'énergie, les atomes du système se déplacent en suivant une équation newtonienne, et simulent une température donnée en entrée par l'utilisateur. En partant de deux géométries initiales différentes, deux simulations de l'agitation thermique correspondant à 500 K sont réalisées, modélisant 10 ps chacune. Durant ces simulations, seules les molécules sont libres tandis que les atomes d'Al sont fixés. Dans la première simulation, appelée DM1, les molécules sont placées de sorte à être liées par O1 à l'adatome, en interagissant avec la surface Al(111). Dans la deuxième simulation, appelée DM2, les molécules sont placées de sorte à maximiser les interactions des molécules avec l'adatome. Une fois ces simulations réalisées, 20 géométries sont extraites à intervalle régulier le long de la simulation, ceci pour DM1 et DM2. L'énergie totale relative (la plus basse est la référence) et les liaisons existantes entre les molécules et la surface Al-Al(111) sont indiquées pour toutes ces géométries dans les Figures 11 (DM1) et 12 (DM2). Dans la simulation DM1, une grande diversité de géométries sont explorées, avec une variation du nombre de liaisons tout au long de la simulation. Les géométries les plus stables (1, 2, 9, 10, 11, 12, 13, 15 et 17) coïncident globalement avec des géométries où un grand nombre de liaisons entre les molécules et la surface Al-Al(111) existent. Dans la simulation DM2, la géométrie varie très peu au cours de la simulation. Dans tous les cas, deux O sont liés à la surface, deux N sont liés à l'adatome et un N est lié à la surface. Les seules géométries se démarquant des autres sont la géométrie 2, où un atome C9 est lié à la surface Al(111), ce qui correspond à un système moins stable, et les géométries 17 et 18, où un atome C7 est lié à la surface, ce qui correspond à un système plus stable. Les géométries les plus stables issues des deux simulations sont présentées dans la Figure 13. Les énergies totales de ces deux géométries, comparées à celles obtenues par adsorption d'un complexe préformé dans le vide, sont présentées dans le Tableau 6, avec la charge sur l'adatome et sur les molécules q, ainsi que la position de l'adatome par rapport à la surface Al(111).

Ces résultats suggèrent qu'un grand nombre de géométries peuvent exister pour ce système. Dans tous les cas, un pseudo-complexe est formé, avec l'atome Al du complexe (ou l'adatom Al) en état d'oxidation Al^{III}

TABLE 6: Propriétés des géométries 10 et 17 issues de l'exploration géométrique par DM, et des géométries issues de l'adsorption des complexes formés dans le vide. Énergies totales relatives (en eV, avec pour référence l'énergie totale de la géométrie 17), charge sur l'atome Al du complexe, charge sur l'adatom Al, charge sur les molécules **A**, **B** et **C** (en e); distance entre l'atome Al du complexe et la surface Al(111) et distance entre l'adatom Al et la surface Al(111) (en Å).

Géométrie	Géométrie 17	Géométrie 10	<i>fac/up</i>	<i>mer/up</i>	<i>mer/down</i>
ΔE	0	+0.38	+0.25	+0.79	+0.94
$q_{Al\ adatom}$	+2.48	+2.56			
q_{Al}^{cx}			+2.45	+2.44	+2.36
Q_{molA}	-0.97	-0.85	-1.08	-0.94	-1.26
Q_{molB}	-2.18	-1.25	-1.19	-1.26	-1.49
Q_{molC}	-1.25	-2.18	-1.14	-0.98	-1.25
$z_{Al\ adatom}$	2.738	3.206			
z_{Al}^{cx}			3.509	3.862	3.897

FIGURE 11: Trois molécules q adsorbées sur une surface Al-Al(111). 20 géométries issues de la trajectoire DM1; en noir : énergies totales relatives ΔE (en eV, avec comme référence l'énergie de la géométrie 10); en orange : nombre de liaisons entre les atomes O et la surface Al(111); en bleu foncé : nombre de liaisons entre les atomes N et l'adatom Al; en bleu clair : nombre de liaisons entre les atomes N et la surface Al(111); en marron : nombre de liaisons entre les atomes C7 et la surface Al(111). Deux atomes a et b sont considérés comme liés si $d_{a-b} < 2.3 \text{ \AA}$.

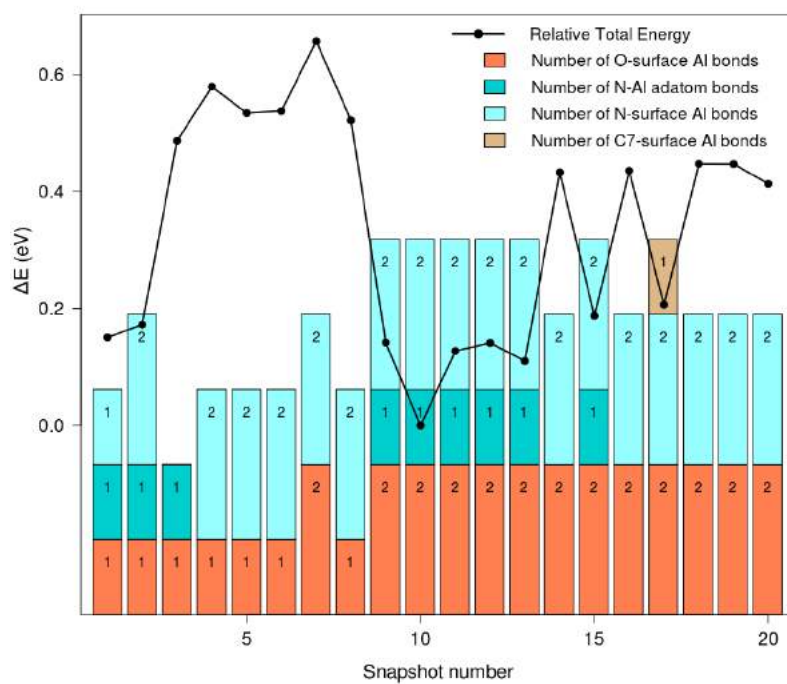


FIGURE 12: Trois molécules q adsorbées sur une surface Al-Al(111). 20 géométries issues de la trajectoire DM2; en noir : énergies totales relatives ΔE (en eV, avec comme référence l'énergie de la géométrie 17); en orange : nombre de liaisons entre les atomes O et la surface Al(111); en bleu foncé : nombre de liaisons entre les atomes N et l'adatom Al; en bleu clair : nombre de liaisons entre les atomes N et la surface Al(111); en marron : nombre de liaisons entre les atomes C7 et la surface Al(111); en beige : nombre de liaisons entre les atomes C9 et la surface Al(111). Deux atomes a et b sont considérés comme liés si $d_{a-b} < 2.3 \text{ \AA}$.

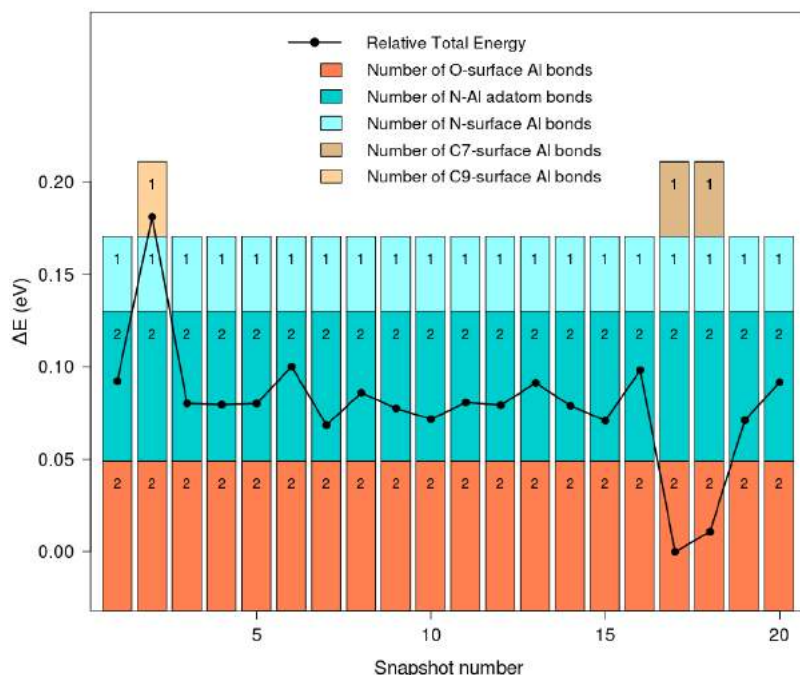
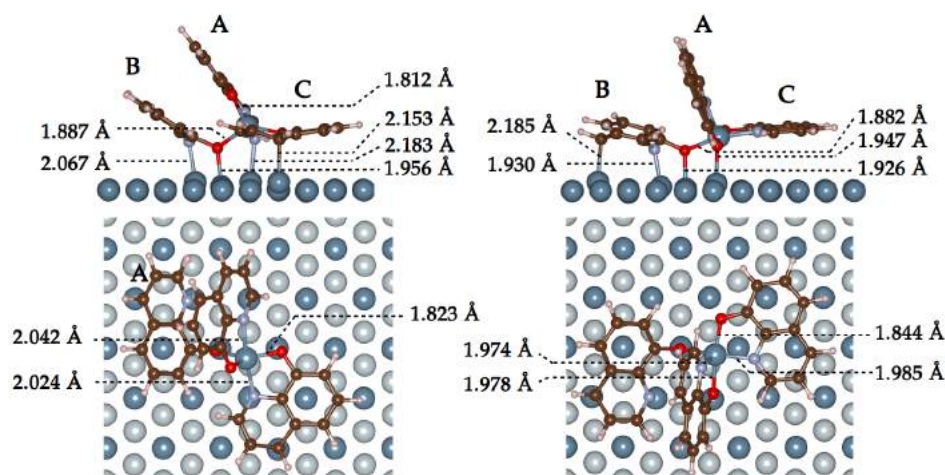


FIGURE 13: Trois molécules q adsorbées sur une surface Al-Al(111); A gauche : la géométrie 10 issue de la DM1; à droite : la géométrie 17 issue de la DM2 (la plus stable). En bleu : l'atome Al du complexe et les atomes Al de la couche supérieure. En gris : les atomes Al des couches inférieures.



0.5 Conclusions et Perspectives

Dans ce résumé, nous avons montré que pour la Hq et tous ses dérivés, les complexes formés avec l'aluminium ont une structure électronique similaire autour de Al. Cela a été montré par des analyses topologiques ELF et QTAIM, qui concluent à l'existence de liaisons ioniques à faible degré covalent entre les molécules et l'Al, et un ion Al à l'état d'oxydation Al^{III} dans tous les cas. Cela montre que le remplacement des H aux positions ortho et para ne modifient pas les propriétés de complexation de ces molécules. Ensuite, l'adsorption de molécules déprotonées, approximées par des formes déshydrogénées qX, sur une surface Al(111) dans le vide montre que toutes les molécules étudiées peuvent former des couches stables et compactes sur Al(111) (recouvrement θ_3). À faible taux de recouvrement θ_1 , les géométries d'adsorption les plus stables sont différentes entre la molécule q et ses dérivés. Des différences lors du début de la formation d'une couche (θ_1) pourraient avoir une influence sur le processus de formation d'une couche complète, et donc sur l'efficacité de l'inhibition de la corrosion. L'ajout d'un modèle de solvant simulant l'effet de l'eau n'a une influence significative que sur les molécules qS et qSH, et ne remet pas en cause nos conclusions. Enfin, l'adsorption ou la formation d'un complexe sur une surface Al(111) montre qu'un complexe peut bien s'adsorber fortement sur la surface d'aluminium, mais que la géométrie issue de la formation d'un complexe directement sur la surface à partir d'un adatome d'Al est la plus stable.

Par la suite, afin de se rapprocher encore plus des conditions expérimentales, d'autres systèmes pourraient être envisagés. Un agrandissement de la cellule de calcul permettrait de chercher des géométries de couches plus complexes car moins périodiques. Une surface d'oxyde d'aluminium pourrait nous donner des informations sur l'action des molécules sur les surfaces oxydées où se produisent les réactions cathodiques de la corrosion. Enfin, des défauts de surface plus réalistes que le cas d'un adatome isolé, tels que des marches et des dimères d'adatoms, pourraient être modélisés.

References

- (1) Albert, A.; Phillips, J. N. *J. Chem. Soc.* **1956**, 1294–1304.

- (2) Hollingshead, R. G. W., *Oxine and its Derivatives*; Butterworths Scientific Publications: 1956; Vol. 4.
- (3) Summers, K. L.; Pushie, M. J.; Sopasis, G. J.; James, A. K.; Dolgova, N. V.; Sokaras, D.; Kroll, T.; Harris, H. H.; Pickering, I. J.; George, G. N. *Inorganic Chemistry* **2020**, *59*, PMID: 32936627, 13858–13874.
- (4) Verma, C.; Quraishi, M.; Ebenso, E. E. *Surfaces and Interfaces* **2020**, *21*, 100634.
- (5) Baker, B. C.; Sawyer, D. T. *Analytical Chemistry* **1968**, *40*, 1945–1951.
- (6) Nghia, N. N.; Lee, Y.-I., et al. *Microchimica Acta* **2019**, *186*, 36.
- (7) Wang, J.; Li, Y.; Li, K.; Meng, X.; Hou, H. *Chemistry – A European Journal* **2017**, *23*, 5081–5089.
- (8) Soroka, K.; Vithanage, R. S.; Phillips, D. A.; Walker, B.; Dasgupta, P. K. *Analytical Chemistry* **1987**, *59*, 629–636.
- (9) Fukushima, T.; Kaji, H. *Organic Electronics* **2012**, *13*, 2985 –2990.
- (10) Cölle, M.; Dinnebier, R. E.; Brütting, W. *Chem. Commun.* **2002**, 2908–2909.
- (11) Singh, D.; Nishal, V.; Bhagwan, S.; Saini, R. K.; Singh, I. *Materials Design* **2018**, *156*, 215 –228.
- (12) Williams, E. S.; Panko, J.; Paustenbach, D. J. *Critical reviews in toxicology* **2009**, *39*, 553–575.
- (13) Garrigues, L.; Pebere, N.; Dabosi, F. *Electrochimica Acta* **1996**, *41*, 1209 –1215.
- (14) Lamaka, S.; Zheludkevich, M.; Yasakau, K.; Montemor, M.; Ferreira, M. *Electrochimica Acta* **2007**, *52*, 7231 –7247.
- (15) Mei LI, S.; rui ZHANG, H.; hua LIU, J. *Transactions of Nonferrous Metals Society of China* **2007**, *17*, 318 –325.
- (16) Chiter, F. Étude théorique d’inhibiteurs verts de corrosion : adsorption de la 8-hydroxyquinoléine sur surfaces d’aluminium, Ph.D. Thesis, 2015.
- (17) Chiter, F.; Lacaze-Dufaure, C.; Tang, H.; Pébère, N. *Phys. Chem. Chem. Phys.* **2015**, *17*.
- (18) Chiter, F.; Bonnet, M.-L.; Lacaze-Dufaure, C.; Tang, H.; Pébère, N. *Phys. Chem. Chem. Phys.* **2018**, *20*, 21474–21486.
- (19) Grimme, S. *Journal of Computational Chemistry* **2006**, *27*, 1787–1799.
- (20) Grimme, S.; Antony, J.; Ehrlich, S.; Krieg, H. *The Journal of Chemical Physics* **2010**, *132*, 154104.

- (21) Savin, A.; Jepsen, O.; Flad, J.; Andersen, O. K.; Preuss, H.; von Schnering, H. G. *Angewandte Chemie International Edition in English* **1992**, *31*, 187–188.
- (22) Silvi, B.; Savin, A. *Nature* **1994**, *371*, 683–686.
- (23) Li, H.; Zhang, F.; Wang, Y.; Zheng, D. *Mater. Sci. Eng.: B* **2003**, *100*, 40–46.
- (24) Saxena, A. K. *Synth. React. Inorg. Met. Org. Chem.* **1999**, *29*, 1747–1767.
- (25) Curioni, A.; Boero, M.; Andreoni, W. *Chemical Physics Letters* **1998**, *294*, 263–271.
- (26) Katakura, R.; Koide, Y. *Inorganic Chemistry* **2006**, *45*, PMID: 16841973, 5730–5732.
- (27) Bader, R. F. W.; Essen, H. *J. Chem. Phys.* **1984**, *80*, 1943–1960.
- (28) Bader, R. F. W.; Clarendon Press.
- (29) Contreras, R.; Domingo, L. R.; Silvi, B. In *Encyclopedia of Physical Organic Chemistry*; American Cancer Society: 2017, pp 1–114.
- (30) Murgich, J.; Franco, H. J. *Journal of Physical Chemistry A* **2009**, *113*, 5205–5211.
- (31) Costa, D.; Ribeiro, T.; Cornette, P.; Marcus, P. *The Journal of Physical Chemistry C* **2016**, *120*.
- (32) Kovačević, N.; Kokalj, A. *Corrosion Science* **2013**, *73*, 7–17.
- (33) Peljhan, S.; Koller, J.; Kokalj, A. *The Journal of Physical Chemistry C* **2014**, *118*, 933–943.
- (34) Kokalj, A.; Peljhan, S.; Koller, J. *The Journal of Physical Chemistry C* **2014**, *118*, 944–954.
- (35) Poberžnik, M.; Costa, D.; Hemeryck, A.; Kokalj, A. *The Journal of Physical Chemistry C* **2018**, *122*, 9417–9431.
- (36) Li, X.; Deng, S.; Xie, X. *Corrosion Science* **2014**, *81*, 162–175.
- (37) Chiter, F.; Costa, D.; Maurice, V.; Marcus, P. *Applied Surface Science* **2021**, *537*, 147802.
- (38) Poberžnik, M.; Chiter, F.; Milošev, I.; Marcus, P.; Costa, D.; Kokalj, A. *Applied Surface Science* **2020**, *525*, 146156.
- (39) Vernack, E.; Costa, D.; Tingaut, P.; Marcus, P. *Corrosion Science* **2020**, *174*, 108840.
- (40) Neugebauer, J.; Scheffler, M. *Phys. Rev. B* **1992**, *46*, 16067–16080.
- (41) Makov, G.; Payne, M. C. *Phys. Rev. B* **1995**, *51*, 4014–4022.
- (42) Mathew, K.; Kolluru, V. S. C.; Hennig, R. G. VASPsol: Implicit solvation and electrolyte model for density-functional theory, <https://github.com/henniggroup/VASPsol>, 2018.

-
- (43) Mathew, K.; Sundararaman, R.; Letchworth-Weaver, K.; Arias, T. A.; Hennig, R. G. J. *Chem. Phys.* **2014**, *140*, 084106.
- (44) Steinmann, S. N.; Sautet, P.; Michel, C. *Phys. Chem. Chem. Phys.* **2016**, *18*, 31850–31861.

General Introduction

The 8-hydroxyquinoline (Hq) molecule is composed of a phenol ring and a pyridine ring. Hq and its derivatives are first known for their chelating properties, i.e. their ability to chelate metallic cations, forming metal-organic complexes. Thus, in solution, Hq derivatives are used to detect metallic ions, by making use of the luminescent properties of the complex. Using this latter property, light emitting devices such as organic light emitting diodes (OLEDs) are obtained from films of complexes. Such devices are widely used in digital displays such as televisions and smartphone screens for their low energy consumption and large potential light emission spectrum. In the literature, OLEDs of different characteristics have been reported, obtained from complexes of various Hq derivatives and Al, B, Be, Ga, In, Li, Mg, Sn and Zn metallic ions. Hq is also known as an efficient corrosion inhibitor of aluminum and steel. In the case of aluminum, the corrosion process is slowed by the formation of a layer of molecules or complexes protecting the aluminum surface against the aggressive species present in the solution. This makes Hq and its derivatives good candidates for the replacement of toxic chromate-based corrosion inhibition treatments currently employed for aluminum.

In the present work, we study the 8-hydroxyquinoline (Hq) molecule and two of its derivatives: the 5,7-dibromo-8-hydroxyquinoline (HqBr) and the 8-hydroxyquinoline-5-sulfonic acid (HqSH). It was shown in the literature that chemical modifications of the Hq molecule, leading to Hq derivatives, modify its properties, such as the solubility of the complex, the wavelengths of its light emission, and the corrosion inhibition efficiency of the molecule. The HqBr and HqSH derivatives have been chosen because they differ in their efficiency as corrosion inhibitors. These molecules have different chemical groups at the ortho and para positions of the phenol ring, and are noted HqX (X = H, Br, SO₃H). The aim of this work is to carry out a theoretical study of the interactions of Hq and its derivatives with aluminum, and to quantify how the X groups influence these interactions. This is done both by the study of the complexes formed by deprotonated HqX species with Al³⁺ ions, and by

the study of the adsorption of dehydrogenated and deprotonated HqX molecules on an aluminum surface. All calculations are performed in the framework of the dispersion corrected Density Functional Theory (DFT).

This thesis manuscript is divided in six chapters.

In Chapter 1, we present the three molecules studied in this work, and provide a state of the art of the properties and applications of the molecules, in the field of light emission, depollution, medicine and corrosion inhibition. We then summarize the theoretical studies already carried out on the studied molecules.

In Chapter 2, we detail the theoretical background of our calculations, in the framework of the Density Functional Theory, and the different approximations and corrections used in our calculations, for both molecular and periodic approaches. Finally, the topological analyses used to characterise our systems are introduced.

The calculations performed on molecular systems presented in Chapter 3 concern the study of the influence of the X groups ($X = \text{H}, \text{Br}, \text{SO}_3\text{H}/\text{SO}_3^-$) on the chelating properties of the molecules, by characterizing the bonding of the deprotonated molecules with an Al^{3+} ion.

The Chapter 4 is dedicated to the presentation of the molecules, complexes, and surface models in the framework of periodic calculations, which are then used in Chapter 5 and 6 for adsorption of molecules and complexes on an aluminum surface. The geometries of the molecules and complexes are compared to those obtained by molecular calculations, and the different slab models are discussed.

In Chapter 5, the dehydrogenated Hq molecule and its derivatives are adsorbed on a flat Al(111) surface, at three surface coverage, from a single adsorbed molecule to a compact organic monolayer. We investigate how the X groups ($X = \text{H}, \text{Br}, \text{SO}_3\text{H}$) influence this adsorption at the different surface coverage. All calculations are first done in vacuum. Then, for some cases, a solvent model is added to simulate the interaction of the adsorbed molecules with an aqueous environment. Finally, the charged deprotonated species are adsorbed on Al(111) in presence of solvent in order to get closer to the experimental conditions and to validate the study of the adsorption of dehydrogenated molecules on Al(111) as a model of the adsorption of the deprotonated molecules on aluminum.

In Chapter 6, the hypothesis of the formation of a Alq_3 -like complex on an Al(111) surface is investigated. Two processes are considered: i) the adsorption of an Alq_3 complex pre-formed in vacuum on a flat Al(111) surface, ii) the adsorption of three q molecules on an Al adatom of an Al(111) surface. In order to explore the conformation space of such systems, we employ *ab initio* Molecular Dynamics. We identify stable geometries for both adsorbed complexes and complexes formed on the Aluminum surface.

Chapter 1

State of the art

In this Chapter, the molecules that are the subject of our studies are introduced, and the notations used throughout this work are given. The experimental data of the molecules and chelates, i.e. complexes formed from molecules and metallic ions, are exposed. A state of the art of the works carried out on several applications of these molecules is presented. Such applications include depollution, light emission, and corrosion inhibition, the last one being our main focus in this thesis. Finally, a list of theoretical works done on the interaction of 8-hydroxyquinoline with metal surfaces is given.

1.1 The Hq molecule and its derivatives

The molecules studied in this work are the 8-hydroxyquinoline (C_9H_7NO , noted Hq hereafter), the 5,7-dibromo-8-hydroxyquinoline ($C_9H_5Br_2NO$, noted HqBr hereafter) and the 8-hydroxyquinoline-5-sulfonic acid ($C_9H_7NO_4S$, noted HqSH hereafter). The structures of these molecules are presented in Figure 1.1, with the X1 and X2 groups indicated in Table 1.1 for each molecule. Hq is a bicyclic molecule composed of a pyridine ring fused with a phenol ring, with H atoms at the para (X1) and ortho (X2) positions relatively to the phenol ring. The HqBr and HqSH molecules are similar to Hq, with the H groups of the X1 and X2 positions replaced by Br atoms in the case of the HqBr, and the H atom of the X1 position replaced by a SO_3H group in the case of the HqSH molecule. The HqBr and HqSH molecules are chosen because of existing experimental data, detailed in Section 1.4.4, especially in relation to their effectiveness or not as aluminum corrosion inhibitors.

The Hq molecule is soluble in water, with a solubility of 556 mg/L at 20°C[1] and is

FIGURE 1.1: HqX molecules. X1 and X2 correspond to the groups presented in Table 1.1

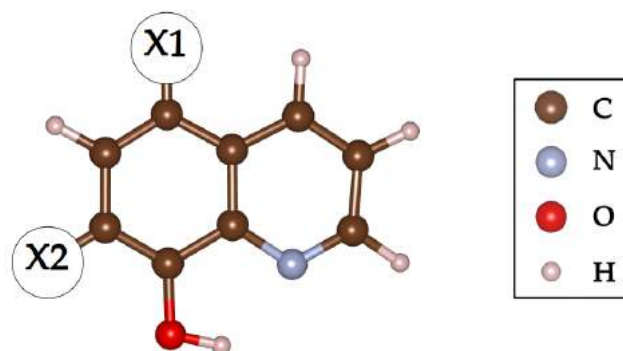


TABLE 1.1: Notation of the HqX molecules

Species	Hq	HqBr	HqSH
X1	H	Br	SO ₃ H
X2	H	Br	H

present simultaneously in several forms, in proportions depending on the pH of the solution. At 20 °C, the pKa of the OH/O⁻ group is 9.89, while the pKa of the NH⁺/N group is 5.13[2, 3]. For the HqSH molecule, also soluble in water, the pKa value of the NH⁺/N group is 4.09, while the pKa of the OH/O⁻ group has not been determined experimentally. In native form, the Hq molecule and its derivatives are noted HqX. In deprotonated form (N and O⁻), the molecules are noted qX⁻. The molecule can also exist in hydrogenated (NH⁺ and OH), and tautomeric (NH⁺ and O⁻) forms. The pKa associated to the SO₃H/SO₃⁻ group of the HqSH is very low, indicating that the SO₃H form is only present in extremely acidic environment[4], and the SO₃⁻ form is predominant in most solutions. Finally, the HqBr molecule is less soluble in water than the Hq molecule, with a solubility of 19 mg/L [5], while pKa values are not known. Solubilities of HqBr in various organic solvents have been studied experimentally, and high solubility was found for HqBr in 1-methyl-2-pyrrolidinone (NMP), N,N-dimethylaniline (DMA), N,N-dimethylformamide DMF and 1,4-dioxane[6].

The Hq crystal is an orthorhombic system of lattice parameters of $a = 29.18\text{\AA}$, $b = 25.36\text{\AA}$ and $c = 3.91\text{\AA}$ [7], with 16 molecules in the unit cell. To our knowledge, the crystal structures of HqBr and HqSH are not known.

1.2 Complexes formed between Hq and its derivatives and metallic ions

The Hq derivatives are known for their chelating properties, meaning they can form coordination complexes with metallic ions[8, 9], such as Cu^{2+} , Zn^{2+} , Co^{3+} and Al^{3+} . In this work, we focus on the interaction of HqX species with aluminum. First, the interaction between deprotonated Hq molecules, noted qX^- , with an Al cation is investigated. The structures of the formed complexes are shown in Figure 1.2, with the notation of the species with respect to the X1 and X2 groups given in Table 1.2. The complexes obtained from the q^- , HqBr^- and HqSH^- molecules are noted Alq_3 , $\text{Al}(\text{qBr})_3$ and $\text{Al}(\text{qSH})_3$. The complexes exist in two isomers, called meridional (*mer*) and facial (*fac*)[10]. In the *mer* isomer, the plane formed by the three O atoms is almost perpendicular to the plane formed by the N atoms. In the *fac* isomer, the three O atoms and the three N atoms are directed at two opposite faces of the complex.

FIGURE 1.2: $\text{Al}(\text{qX})_3$ complexes. X1 and X2 correspond to the groups presented in Table 1.2. On the left side: *mer* isomer. On the right side: *fac* isomer

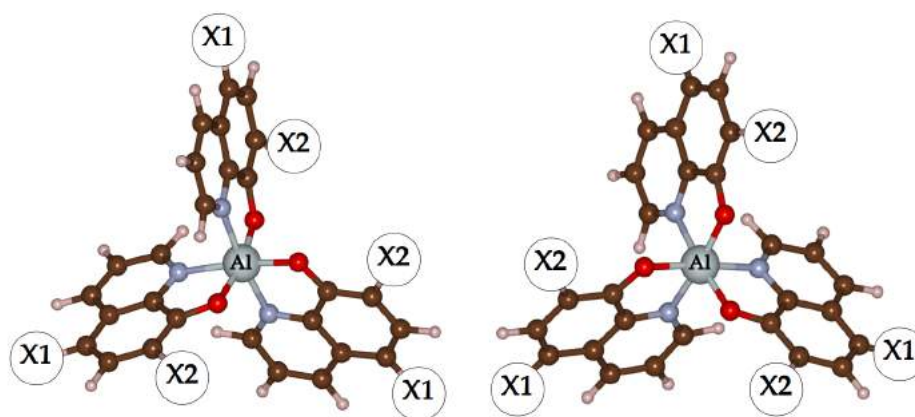


TABLE 1.2: Notation of the $\text{Al}(\text{qX})_3$ complexes

Species	Alq_3	$\text{Al}(\text{qBr})_3$	$\text{Al}(\text{qSH})_3$
X1	H	Br	SO_3H
X2	H	Br	H

While the Alq_3 complex has been reported to precipitate easily in water, the $\text{Al}(\text{qSH})_3$, due to the interaction of the $\text{SO}_3\text{H}/\text{SO}_3^-$ with water, is reported to be much more soluble than Alq_3 [11]. The solubility of the $\text{Al}(\text{qBr})_3$ has not been reported. The pKa of the

$\text{SO}_3\text{H}/\text{SO}_3^-$ group in the $\text{Al}(\text{qSH})_3$ complex has not been measured experimentally, but should be very similar to the one in the HqSH molecule.

The complexes formed between q^- and metallic ions can exist in amorphous state or as a crystal. The most well known structures are those of species used in Organic Light Emitting Diodes (OLEDs), mainly Alq_3 and Gaq_3 , both in amorphous or crystalline states[12]. For Alq_3 , five crystal phases have been recorded (α , β , γ , δ and ϵ)[13]. These phases differ in the arrangement of the complexes as well as in the proportions of *mer* and *fac* isomers. The different inter-molecular interactions and different isomers in the five phases lead to different properties, further discussed in Section 1.3.

1.3 The Hq molecule and its derivatives as chelating compounds

The Hq molecule and its derivatives are widely used in the field of metallic ion capture, detection, and removal, i.e. when they are present as contaminants in solutions[14, 15], and the use of Hq and HqSH molecules, bonded to a substrate, usually a porous solid, is still studied today in that perspective[16–18]. The HqBr molecule is also investigated for the removal or separation of metal ions in the field of hydrometallurgy [19]. The photoluminescent properties of the Hq derivatives are used both in solution and in solid state. The main application of these properties in solution is the detection of metal ions. In the case of Hq, the single molecule has only weak fluorescence, but the complex formed with various metal atoms is highly fluorescent[11]. In addition, the intensity and pH dependence of the fluorescence vary depending on the metallic element, which allows element specific detection[11]. The HqSH molecule, which have similar fluorescent properties (non fluorescent as a single molecule, fluorescent in a complex), is also much more soluble in water, making it even more convenient than Hq for detection[20]. Other derivatives of Hq are studied as complexes formed with Al^{3+} (5,7-dimethyl-8-hydroxyquinoline, 5-chloro-8-hydroxyquinoline), with the tuning of the molecule structure leading to a shift in emission peak wavelength of up to 56 nm and a decrease of the intensity of luminescence, compared to Alq_3 [21].

For Alq_3 crystalline thin films, light emission properties can be influenced by the packing of the complexes, as well as by the isomers present in the crystal[13, 22]. For example, the γ and δ phases are said to be composed solely of *fac* isomers, leading to a blue-shifted light emission compared to other phases[23]. Complexes of a variety of Hq derivatives have been

tested in view of the fabrication of light emitting devices, leading to OLEDs of different characteristics [24].

The chelating properties of the Hq molecule and derivatives are also used for medicinal applications[25, 26], acting as regulator of metal ion concentration in the human body by making use of their chelating abilities, with the tuning of their molecular structure influencing their interactions with the cells and therefore their biological effects. Various halogenated derivatives, including the HqBr molecule, are used to treat infections, and are candidates for the treatment of cancer and neurodegeneracy[25, 26].

1.4 The Hq molecule and its derivatives as aluminum corrosion inhibitors

1.4.1 Corrosion of aluminum

Aluminum and its alloys are used in a broad range of applications. In particular, the 2024 aluminum alloy (Cu: 4 to 5 %, Mg: 1 to 2 %) is currently used in the aeronautic industry for its low cost and good mechanical properties. The natural oxide layer of this metal, developed spontaneously in presence of oxygen, protects it to a certain degree from corrosion, and it is shown to be stable in a pH range of about 5 to 8.5 [27]. When exposed to alkaline, acidic, or chloride-containing solutions, it can be subject to corrosion, releasing Al^{3+} ions in the solution in the following process. In acidic solutions, the combination of both anodic and cathodic reactions gives the resulting reaction [28] :

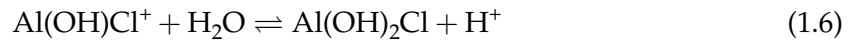
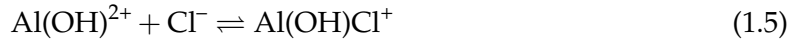
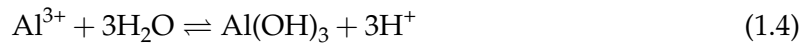


In alkaline solutions, combination of both anodic and cathodic reactions gives the resulting reaction [29]:



In these two cases, the presence of OH^- or H^+ species lead to the degradation of the aluminum matrix by releasing Al respectively as Al^{3+} and $\text{Al}(\text{OH})_4^-$ species.

In chloride solutions, pitting corrosion can occur. At some localized areas of the surface, the adsorption of Cl^- ions on the oxide layer and their subsequent migration to the oxide/metal leads to a local dissolution of the oxide film, and to the formation of cavities, or pits, in the surface. Anodic and cathodic reactions take place at different sites. Inside the pits, the anodic reaction given by Eq. 1.3 occurs [30]. The Al^{3+} ions released then react with water and Cl^- ions (Eq. 1.4, 1.7 and 1.8), resulting in the acidification of the local environment [31]:



The following cathodic reactions take place outside the pits [27, 30]:



This type of corrosion can be very destructive, as the pit is progressively propagated in the material. No stable oxide layer is formed inside the pit, due to the local acidity of the environment, as seen in Eq. 1.4.

1.4.2 Aluminum corrosion inhibition by chromates

In industry, the traditionally used method to protect aluminum alloys against corrosion is the use of $\text{Cr}_2\text{O}_7^{2-}$ chromates. This limits the diffusion of aggressive species inside the material, and repairs the weak parts of the passive layer. However, european directives, through

the REACH regulations [32], are imposing the replacement of chromium based corrosion inhibitors, due to their toxicity and carcinogenicity. Research is being carried out in order to find environment friendly replacements. The possibility of using organic inhibitors is investigated both experimentally[33] and by theoretical methods[34].

1.4.3 Aluminum corrosion inhibition by organic molecules

To be effective, an organic corrosion inhibitor has to contain an anchoring function, usually including heteroatoms such as N, O, S, and P atoms[35] allowing chemical bonding with the metal surface. The rest of the molecule separates the metal surface from the aggressive species of the solution. Finally, the surface of the organic layer formed by the adsorbed molecules can be functionalized in order to interact in a specific way with the environment, depending on the chemical groups oriented towards the environment.

The carboxylic acids bond with the surface by their COO^- group. In the case of linear carboxylic acids, the $\text{C}_n\text{H}_{2n+1}$ chain can lead to the formation of a thick organic layer of hydrophobic nature. These types of molecules have been shown to be potentially effective corrosion inhibitors of aluminum and other metals[36]. Molecules with heterocycle compounds, i.e. carbon cycles of various size containing heteroatoms capable of bonding with the surface, are widely studied for their corrosion inhibition properties. Species composed of one cycle of 5 atoms (ATAT)[37], and cycles of six and five atoms (BTA, MBT, Hq...) [38–40] are examples of such molecules. On aluminum,azole derivatives (BTA, MBT...) are mainly cathodic corrosion inhibitors [41], acting on the copper inter-metallic particles, while the Hq acts on the aluminum matrix, as has been shown by the joint use of BTA and Hq as corrosion inhibitors of 2024 aluminum alloy [38].

Prediction of corrosion inhibition efficiency by theoretical methods

In order to establish predictive models capable of orienting the choice of molecules to be used in experimental work, correlations have been searched between the known experimental corrosion inhibition efficiency of molecules and some calculated properties. The first and simplest attempt at building such a model was the MEPTIC approach, which made use of the properties of the molecules, calculated independently of the metal of interest, including

frontier orbital energies and dipole moment, and correlated them to experimentally determined inhibition efficiency. Although very used in the literature, it has been shown to have no predictive value as correlations are observed only on sets of a few very close molecules or molecules specifically chosen to validate the model (cherry-picking) [42, 43]. Although Machine Learning (ML) methods now find correlations on larger sets of molecules [44] leading to predictive models, it does not allow the identification of the underlying mechanisms of corrosion inhibition.

Explicit modeling of the interaction between the molecule and the metal using first-principles calculations is a method allowing a deeper insight in the mechanism behind corrosion inhibition. The studies involving such modeling methods using metal surface models allow to investigate how strongly the molecule is adsorbed, and if the formed organic layer is compact enough to prevent the interaction between the metal surface and the species of the solution. Once the layer formed, descriptors such as the work function and the dipole moment of the organic layer are directly related to some known corrosion mechanisms, as they influence on the possibility of the anodic and cathodic reactions to occur. Such studies have been carried out for various metal surfaces and molecules such as carboxylic acids [45, 46], triazole derivatives [43, 47–49], and Hq [50, 51]. The explicit calculation of the interaction of O_2 with the covered surface is used to determine the cathodic corrosion inhibition efficiency of molecules [45, 51]. This explicit modeling of both molecule and metal surface is used for our work on Hq derivatives.

1.4.4 Aluminum corrosion inhibition by Hq and its derivatives

In the case of Hq, studies by impedance spectroscopy showed that the surface of AA2024 aluminum alloy is much less subject to corrosion when immersed in a solution containing 0.5 M of NaCl and Hq than in a solution of only NaCl [40]. The presence of chelates on the surface protecting the aluminum against aggressive species was suggested. However, it is not known if Hq molecules are directly adsorbed on the Al surface or if Alq_3 complexes, pre-formed from Al^{3+} ions in the solution, are adsorbed on the surface. The corrosion inhibition synergy between Hq and BTA has also been demonstrated, with Hq acting mainly on the aluminum matrix and the BTA on the intermetallic particles [38]. In addition to its efficiency against aluminum corrosion, the Hq molecule has also been shown to be an effective corrosion inhibitor of X60 steel [34] and AZ91D magnesium alloy [52, 53].

The HqSH molecule has been compared to Hq in terms of AA2024 alloy corrosion inhibition in a 3.5% NaCl solution, and it has been shown that HqSH does not protect aluminum against corrosion, and could even accelerate the corrosion process[54]. This result was recently confirmed by works in our laboratory on a solution of 0.05 M NaCl with presence of HqSH. Considering the high solubility of the $\text{Al}(\text{qSH})_3$ complex, one possible explanation of this corrosion acceleration is that the HqSH molecule bonds with Al atoms from the substrate, leading to a highly soluble species, therefore decomposing even more the oxide layer.

S.V. Lamaka compared the inhibition effectiveness on a series of molecules, including HqBr[55]. The impedance spectroscopy measurements did not show any significant difference between the simple NaCl solution and the NaCl + HqBr solution, indicating no inhibition of the corrosion by HqBr. This could be due to the too low amount of HqBr in solution, as the solubility of the molecule is very low.

A theoretical study of Hq as corrosion inhibitor of aluminum has been carried out in F. Chiter's thesis[56]. Four forms of Hq (native, dehydrogenated, hydrogenated and tautomer) have been studied in regard to their adsorption on an Al(111) surface. It has been shown that the dehydrogenated molecule is the form that is adsorbed the most strongly. At maximum surface coverage, the dehydrogenated molecules form a compact chemisorbed organic layer, which has been shown to inhibit the O_2 reduction reaction[51], which is one of the cathodic reaction in chloride solutions (see Eq. 1.9).

The theoretical study of the interaction of HqSH and HqBr with aluminum is necessary to better understand their properties.

1.5 Conclusion

In this chapter, the molecules that are the focus of this work were presented. An overview of the application of the Hq molecule, as well as its derivatives, was given, with a special interest given on the different properties arising from the modification of the chemical structure of the Hq molecule. First, the tuning of Hq can result in different solubility of the molecules and $\text{Al}(\text{qX})_3$ complexes, making some derivatives efficient candidates for specific applications. For instance, the luminescent properties of the complexes vary with the tuning of the molecule, potentially leading to OLED emitting in various wavelengths. In the case

of aluminum corrosion inhibition, while the solubility of the molecules and complexes are measurable and can be correlated to the effectiveness of the molecules, it is not sufficient to explain how the tuning of the molecule modifies the corrosion inhibition efficiency. First principle calculations can provide valuable insights on the interaction of the molecules with aluminum at atomic scale. In the following chapter, the theoretical tools employed for our calculations, as well as the programs and parameters chosen, are introduced.

Chapter 2

Theoretical Methods & Calculation Parameters

In order to understand the interaction of Hq and its derivatives with aluminum, *ab initio* methods need to be employed. In this chapter, the formalism of density functional theory (DFT) is briefly presented, along with the different approximations and corrections used for the calculations. Then, the electron localization function (ELF) and the quantum theory of atoms in molecule (QTAIM) topological analyses are introduced. Finally, the codes used for both the DFT calculations and topological analyses are presented, along with the parameters that are kept constant in our calculations.

2.1 Theoretical Background

In this section, the basics of the first principles calculations within the frame of DFT are presented. Then, several approximations and corrections are detailed. Finally, the theoretical background of two topological analysis methods used in this work are given.

2.1.1 Ab-initio calculations

The Schrödinger equation for many-body systems

First principles of quantum mechanics are employed. For this, the time independent Schrödinger equation 2.1 must be solved.

$$H\psi(\mathbf{r}, \mathbf{R}) = E\psi(\mathbf{r}, \mathbf{R}) \quad (2.1)$$

Where H is the Hamiltonian of the system, detailed below, $\psi(\mathbf{r}, \mathbf{R})$ is the wave function, depending on the spatial coordinates of the electrons (\mathbf{r}) and nuclei (\mathbf{R}) and E is the total energy of the system.

The Hamiltonian of the system is defined by:

$$H = -\sum_i^{n_n} \frac{1}{2} \nabla_i^2 - \sum_i^{n_e} \frac{1}{2} \nabla_i^2 - \sum_i^{n_e} \sum_j^{n_n} \frac{Z_j}{|\mathbf{x}_i - \mathbf{R}_j|} + \frac{1}{2} \sum_i^{n_e} \sum_{j \neq i}^{n_e} \frac{1}{|\mathbf{x}_i - \mathbf{x}_j|} + \frac{1}{2} \sum_i^{n_n} \sum_{j \neq i}^{n_n} \frac{Z_i Z_j}{|\mathbf{R}_i - \mathbf{R}_j|} \quad (2.2)$$

The two first term of the Hamiltonian are the kinetic energy operators respectively of the nuclei and electrons, the third term is the term corresponding to the coulomb interactions between the nuclei and the electrons, and the fourth and fifth terms correspond to the electron-electron and nucleus-nucleus coulomb interactions respectively. n_n and n_e are respectively the number of nuclei and electrons of the system, and Z_i is the atomic number of the i atom.

Solving this equation means solving a many-body problem, which is not possible without a set of approximations. First, the Born and Oppenheimer approximation is employed. The movements of the nuclei are considered separated from the movements of the electrons, as they are indeed much slower[57]. The problem can now be simplified to one where the nuclei are fixed:

$$H_e = -\sum_i^{n_n} \frac{1}{2} \nabla_i^2 - \sum_i^{n_e} \sum_j^{n_n} \frac{Z_j}{|\mathbf{r}_i - \mathbf{R}_j|} + \frac{1}{2} \sum_i^{n_e} \sum_{j \neq i}^{n_e} \frac{1}{|\mathbf{r}_i - \mathbf{r}_j|} \quad (2.3)$$

With H_e the Hamiltonian associated to the energy of the electrons of the system. The equation to be solved for the electrons of the system is therefore:

$$H_e \psi_e(\mathbf{r}, \mathbf{R}) = E_e \psi_e(\mathbf{r}, \mathbf{R}) \quad (2.4)$$

The two main methods used to solve these equations are the Hartree-Fock (HF) and Density Functional Theory (DFT). In this work, because it includes electron correlation interactions, the DFT approach is the most convenient for large systems.

Density Functional Theory (DFT), Hohenberg and Kohn theorems

The DFT method relies on the Thomas-Fermi model[58, 59], which allowed a first approach of the calculation of the energy of a system of electrons in interaction with fixed nuclei based on the functional of the charge density. The Density Functional Theory goes further making use of two theorems, known as Hohenberg Kohn theorems[60]:

- i) For a system of electrons in an external potential $V_{ext}(\mathbf{r})$, the external potential is determined solely by the charge density of the ground state of the system $\rho_0(\mathbf{r})$.
- ii) For a given external potential, the energy of the ground state of the system is a unique functional of the charge density $\rho(\mathbf{r})$, and the obtained energy of the ground state is at its minimum only for the ground state charge density $\rho_0(\mathbf{r})$.

The energy of the ground state can therefore be calculated by minimizing the following energy functional:

$$E[\rho] = T[\rho] + E_{ee}[\rho] + \int V_{ext}(\mathbf{r})\rho(\mathbf{r})d\mathbf{r} \quad (2.5)$$

Where $T[\rho]$ is the kinetic energy of the electrons of the system and $E_{ee}[\rho]$ is the energy associated to the electron-electron interactions.

Kohn-Sham equations

Kohn and Sham proposed to replace Equation 2.5 by an equation describing a system of non-interacting electrons in a same potential[61]. The charge density associated to this system is identical to the one presented above, and the system can be reduced to a set of one-electron equations:

$$H_{KS}\psi_i = \epsilon_i\psi_i \quad (2.6)$$

Where ϵ_i is the energy of the Kohn-Sham orbital ψ_i and the one-electron Hamiltonian H_{KS} is defined as:

$$H_{KS} = T_{KS} + V_{ext} + V_H + V_{xc} \quad (2.7)$$

Where T_{KS} is the kinetic energy of the non interacting electrons, V_{ext} is the external potential due to the ions, V_H is the Hartree potential, i.e. the potential associated to the coulomb interaction between pairs of electrons, and V_{xc} is the exchange correlation potential, detailed further below.

$$V_{ext}(\mathbf{r}) = \frac{\delta E_{ext}}{\delta \rho(\mathbf{r})} = - \sum_i^{n_n} \frac{Z_i}{|\mathbf{r} - \mathbf{R}_i|} \quad (2.8)$$

$$V_H(\mathbf{r}) = \frac{\delta E_H}{\delta \rho(\mathbf{r})} = - \int \frac{\rho(\mathbf{r}')}{|\mathbf{r} - \mathbf{r}'|} d\mathbf{r}' \quad (2.9)$$

$$V_{xc}(\mathbf{r}) = \frac{\delta E_{xc}}{\delta \rho(\mathbf{r})} \quad (2.10)$$

Finally, the charge density is determined by the orbitals ψ_i :

$$\rho(\mathbf{r}) = \sum_i^{n_e} |\psi_i|^2 \quad (2.11)$$

This system can be solved iteratively, by choosing a arbitrary starting charge density $\rho(r)$ and solving the equations iteratively until convergence is reached.

Exchange-correlation energy

The reformulation proposed by Kohn and Sham features the exchange correlation term E_{xc} . This term contains the electron-electron interaction terms, other than the coulomb interaction between pairs, as well as the correction to the kinetic energy, needed to describe the real system with interacting electrons. The general form of this energy is not known, and approximations are therefore used for this energy in the frame of the density functional theory.

The localized density approximation is the simplest approximation, and assumes that at each point of the system, the exchange correlation energy density ϵ_{xc} is equal to the corresponding value for a free electron gas of same charge density[62]. The resulting energy, with spin polarization, is thus determined by:

$$E_{XC}^{LDA}[\rho(\mathbf{r})] = \int \epsilon_{xc}(\rho_{\uparrow}, \rho_{\downarrow})\rho(\mathbf{r})d^3\mathbf{r} \quad (2.12)$$

This approach is reliable for systems where the charge density ρ varies weakly in space. For other systems, the generalised gradient approximation (GGA) is preferred. For the GGA method, the exchange correlation energy density results not only from the charge density ρ , but also from its gradient $\nabla\rho$:

$$E_{XC}^{GGA}[\rho(\mathbf{r})] = \int \epsilon_{xc}(\rho_{\uparrow}, \rho_{\downarrow}, \nabla\rho_{\uparrow}, \nabla\rho_{\downarrow})\rho(\mathbf{r})d^3\mathbf{r} \quad (2.13)$$

In this case, the formulation of ϵ_{xc} can be defined by semi-empirical or theoretical methods. Such methods include wPW [63] B3LYP [64], and PBE [65, 66].

Basis sets

While we have the tools to find the ground charge density and associated electron wavefunction, we have the choice of the basis sets from which are built the wavefunctions injected in the Kohn-Sham equations. In this work, we use two codes, one mostly used for the study of free molecular systems (GAUSSIAN09[67]), and one for the study of periodic systems (VASP[68–70]). The basis sets are adapted to the type of system studied.

Molecular systems

In molecular systems, electrons are strongly localized in molecular orbitals, which share similarities with the atomic orbitals verifying the Schrödinger equations in hydrogen-like systems. One of the approximate solutions used for the atomic orbitals is the Slater Type Orbitals (STO), which is further approximated by a linear combination of Gaussian Type Orbitals (GTO). The approximated STO is defined as:

$$\phi_{ijk} = \sum_v^L c_{ijkv} g_{ijk} \quad (2.14)$$

Where L is the number of GTO in the STO, c_{ijkv} is the coefficient of each GTO, and g_{ijk} is the GTO of index i , j and k , which determine the spatial properties of the function in order to reproduce the s, p, d etc. type orbital shape:

$$g_{ijk} = Kx^i y^j z^k e^{-\alpha r^2} \quad (2.15)$$

Where K is the normalization constant and α is the parameter determining the gaussian part of the function.

The use of a single STO to approximate each orbital is called a minimal basis set. Exemple of these basis sets are the STO-3G and STO-6G [71, 72], which correspond to STOs composed by respectively 3 and 6 GTOs. In order to describe the orbitals in complex molecules, this type of basis set is not sufficient. The split valence (SV) basis sets consist in describing differently the core and valence electrons, typically with the valence electrons described with more than one STO, while the core electrons are described with a single STO. The accuracy of these basis sets are mainly determined by the number of STOs used for the valence electrons. Basis sets for which valence electrons are described by two, three and four STOs are respectively called double, triple, and quadruple zeta function or DZ, TZ and QZ. An exemple of DZ basis set is the 6-31G [73] where core electrons are described by one STO of 6 GTO and valence electrons are described by two STOs of 3 and 1 GTOs. An exemple of a TZ basis set is the def2-TZVP [74, 75], where the valence electrons are described by three STO.

Periodic systems

Some DFT calculation programs, such as VASP, are specially designed for the study of crystalline systems. The system is always periodic, and the user provides the geometry of the unit cell. This implies that the Kohn-Sham potential applied to the electrons is periodic:

$$V_{KS}(\mathbf{r}) = V_{KS}(\mathbf{r} + \mathbf{L}) \quad (2.16)$$

Where \mathbf{L} is the translation vector associated to the unit cell. Consequently, following the Bloch theorem[76], the electron wavefunctions are of the form:

$$\psi_i(\mathbf{r}, \mathbf{k}) = U_i(\mathbf{r}, \mathbf{k})e^{i\mathbf{k}\cdot\mathbf{r}} \quad (2.17)$$

k is a vector of the reciprocal space and $U_i(\mathbf{r}, \mathbf{k})$ is a function of same periodicity as ions of the system:

$$U_i(\mathbf{r}, \mathbf{k}) = U_i(\mathbf{r} + \mathbf{L}, \mathbf{k}) \quad (2.18)$$

Therefore, electron wavefunctions can be developed as combinations of plane waves.

Pseudopotentials

Pseudopotentials are used to save computational resources by making use of fact that core electrons are not involved in formation of bonds, and are very weakly affected by the environment. Therefore, only valence electrons are calculated explicitly by the Kohn-Sham equations, and a pseudopotential describes both the interactions between electrons of the core, and the interaction of the ions (nuclei and core electrons) with the valence electrons. The pseudopotential method used for periodic systems in this work is the plane augmented-wave (PAW) pseudopotential, which separates the space into two areas. The first is associated to the core electrons, which are described by the partial atomic wavefunctions, and the second is associated to the valence electrons, which are described by plane waves.

2.1.2 Van der Waals interactions

Because the LDA and GGA exchange correlation functionals only rely on the local properties of the charge density and its gradient, interactions induced by long range correlations between fluctuating electrons (dispersion interactions, commonly called van der Waals interactions) are not well described by DFT. Methods were developed to correct the energy calculated by DFT in order to better model the van der Waals interaction. In the case of the

D2 method developed by Grimme [77, 78], used in this work for periodic calculations, the term added to the exchange correlation energy is equal to:

$$E_{disp} = -S_6 \sum_{i=1}^N \sum_{j=1}^N \frac{C_{6ij}}{R_{ij}^6} f_d(R_{ij}) \quad (2.19)$$

The scale factor S_6 depends on the DFT functional used. The damping function f_d is defined by:

$$f_d(R_{ij}) = \frac{1}{1 - e^{-d\left(\frac{R_{ij}}{R_{0ij}} - 1\right)}} \quad (2.20)$$

Where d determines the steepness of the function and R_{ij} is the distance between the i and j atoms. The C_{6ij} and R_{0ij} parameters are determined by pairs of C_{6i} and R_{0i} :

$$C_{6ij} = \sqrt{C_{6i}C_{6j}} \quad (2.21)$$

$$R_{0ij} = R_{0i} + R_{0j} \quad (2.22)$$

Where the C_{6i} and R_{0i} parameters are values having been obtained empirically.

The more recent D3 version of Grimme's dispersion correction [78] also takes into account the coordination number of each atoms, deduced from the local geometry.

2.1.3 Molecular dynamics

The main use of the density functional theory, as detailed above, consists in determining the ground state of a system, without considering any temperature effect. In order to simulate the dynamics of a system, specific methods are used, coupled to DFT calculations or empirical data. In this work, we employ the ab-initio molecular dynamics, which uses DFT calculations to find the electronic ground state for each geometry, and an equation derived from Newton mechanics to treat the ion trajectories:

$$m_i \frac{\partial^2 \mathbf{r}_i}{\partial t^2} = \mathbf{F}_i - \gamma_i \frac{\partial \mathbf{r}_i}{\partial t} + \sqrt{2\gamma_i k_B T} R(t) \quad (2.23)$$

Where i is the index of the atom i , m_i is the mass of the atom, r_i is position of the atom, F_i is the force applied on the atoms by the system's potential, γ_i is the friction coefficient associated to the atom, T is the temperature of the system, $R(t)$ is a Gaussian process of mean value equal to 0 aiming to give random forces to the atoms. Together with the damping term $-\gamma_i \frac{\partial r_i}{\partial t}$, it maintains the agitation of the atoms close to a constant temperature T .

The use of the *ab initio* Molecular Dynamics for conformation space exploration was made possible thanks to the help of Nathalie Tarrat from CEMES, Toulouse.

2.1.4 Solvent model

In this work, we study systems that are generally in aqueous environment in experimental conditions. In order to include in the calculations the influence of the surrounding solvent, two methods can be used. The first is the use of an explicit solvent by the addition of water molecules in the system, treated at *ab-initio* level. In addition to being computationally costly, this method requires to carefully choose the number and positions of the water molecules. The second method, used in this work, is more straightforward and less costly. It consists in adding an implicit solvent, which is a continuum surrounding the system, based on the Poisson-Boltzmann equation rather than quantum mechanics. In the VASP-sol program[79–81], used in the frame of the program VASP, two terms are added to the Kohn-Sham potential:

The electrostatic term:

$$V_{el} = - \frac{\partial \epsilon(\rho(\mathbf{r}))}{\partial \rho(\mathbf{r})} \frac{|\nabla \phi|^2}{8\pi} \quad (2.24)$$

ϕ is the net electrostatic potential of the system.

$\epsilon(\rho)$ is the dielectric function, equal to:

$$\epsilon(\rho(\mathbf{r})) = 1 + (\epsilon_b - 1)S(\rho(\mathbf{r})) \quad (2.25)$$

The cavitation term, which is associated to the energy needed for the solvent to form a cavity around the main system:

$$V_{cav} = -\tau \frac{\partial |\nabla S|}{\partial \rho(\mathbf{r})} \quad (2.26)$$

At the interface between the main system (treated at ab-initio level) and the solvent, the properties of the solvent are modulated by the shape function:

$$S(\rho(r)) = \frac{1}{2} \operatorname{erfc}\left(\frac{\ln(\rho(\mathbf{r})/n_c)}{\sigma\sqrt{2}}\right) \quad (2.27)$$

Where $\operatorname{erfc}()$ is the error function.

The dielectric constant ϵ_b , the width of the dielectric constant σ , the cutoff charge density n_c and the effective cavity surface tension τ are parameters given by the user depending on the solvent.

2.1.5 Topological analysis

Electron Localization Functional (ELF)

The Electron Localization Function η (Eq. 2.28) gives a mapping of the spatial localization of the electrons in a molecule. The first formulation introduced by Becke and Edgecombe [82] made use of $D(\mathbf{r})$ (Eq. 2.29), the Laplacian of the conditional probability, i.e. the probability for $\mathbf{r}=\mathbf{r}'$, of finding in \mathbf{r}' one electron of same spin than the one already located in \mathbf{r} . Savin et al. [83, 84] developed an ELF formulation based on the contribution of the Pauli repulsion to kinetic energy.

$$\eta(\mathbf{r}) = \frac{1}{1 + \left(\frac{D(\mathbf{r})}{D_0}\right)^2} \quad (2.28)$$

$$D(\mathbf{r}) = \frac{1}{2} \sum_i |\nabla \psi_i|^2 - \frac{1}{8} \frac{|\nabla \rho|^2}{\rho} \quad (2.29)$$

These author remarked that $D(\mathbf{r})$ is the excess local kinetic energy due to the Pauli principle, corresponding to the total kinetic energy, from which is removed the von Weizsäcker

kinetic energy density[85]. This last term can be understood as the kinetic energy density for a system of bosonic particles (i.e. without Pauli repulsion) of density ρ . In the expression of the ELF function, $D(\mathbf{r})$ is divided by the same quantity, calculated for the homogeneous electron gas reference (Eq. 2.30).

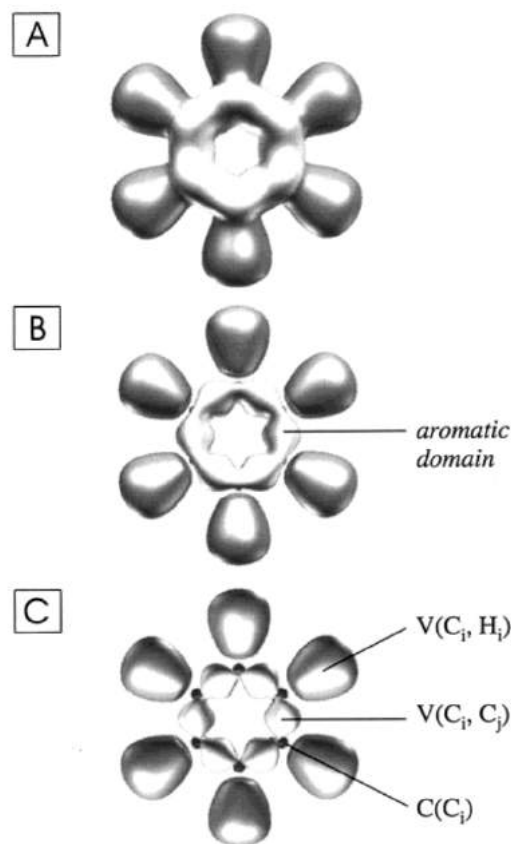
$$D_0 = C_F \cdot \rho^{5/3} \quad (2.30)$$

Where C_F is the Fermi constant.

The ELF function is therefore constructed to be confined between 0 and 1. The two extreme values of $\eta = 0$ and $\eta = 1$ are obtained respectively for maximum Pauli repulsion, and minimum Pauli repulsion. In the latter case ($\eta = 1$), electrons are similar to those of a hydrogen or helium atom (no same spin electrons, $D(\mathbf{r}) = 0$). Thus, high values of η are obtained for regions occupied by a single opposite spin pair such as cores or covalent bonds. The latter may be related to the corresponding electronic pairs in the Lewis's valence theory.

In our study, we use the topological analysis of the ELF function to partition the molecular space into basins, used for the integration of the charge density yielding their average population. These domains are obtained by the separation of the η isosurfaces as η increases. An attractor is a specific point where the ELF function is a local maximum. Each attractor is associated to an irreducible domain, or to a basin containing all the points that are part of the $\nabla\eta$ (gradient of η) trajectories converging towards the attractor. Basins associated to core electrons are noted $C(X)$ with X an atom. Basins associated to valence electrons can be either monosynaptic if they have a separating surface in common with one core basin only or multisynaptic if they have separating surfaces in common with more than one core basin. A n -synaptic basin is noted $V(X_i, \dots, X_n)$. As an example, three ELF isosurfaces of different values of η are presented for benzene in Figure 2.1.

FIGURE 2.1: Benzene molecule. ELF isosurfaces in benzene for (A) $\eta = 0.5$, (B) $\eta = 0.64$, (C) $\eta = 0.65$ (from ref. [86]).

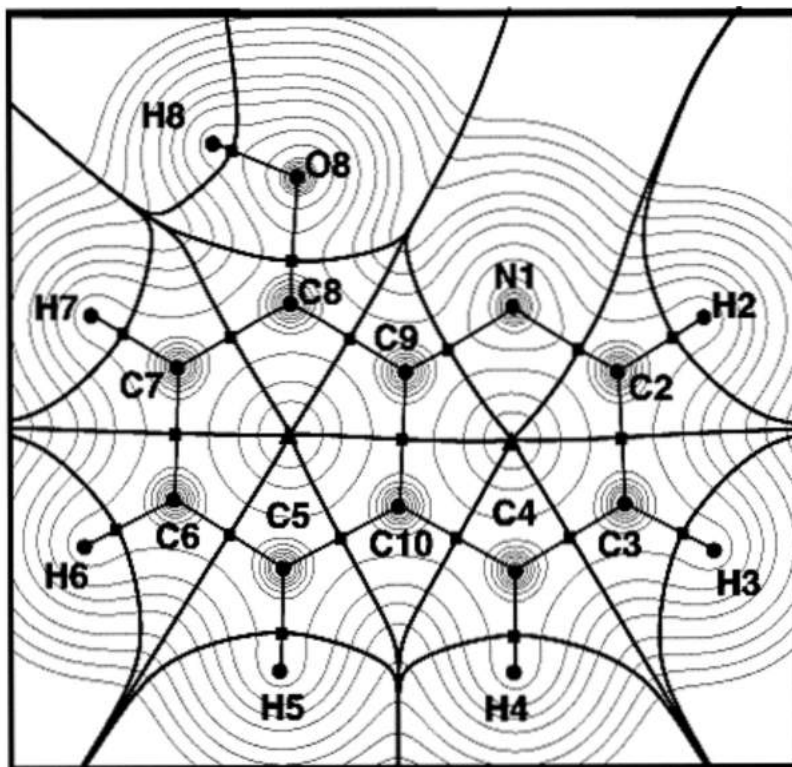


Quantum Theory of Atoms in Molecules (QTAIM)

The QTAIM (Quantum Theory of Atoms in Molecules) analysis is based on the charge density ρ . It makes use of the formalism developed by Richard Bader [87]. Atomic charges are determined by integrating the populations over domains determined by the mapping of the system with respect to the charge density ρ . The maximum of ρ are associated to the position of the ions, and the domains associated to the atoms are defined by the points of the $\nabla\rho$ trajectories concluding at the ion position. In QTAIM theory, bonds between atoms correspond to paths of maximum ρ , named bond paths (BP). It attains its minimum value of ρ at the bond critical point (BCP). The BCP is also part of the interatomic surface (IAS) containing the trajectories of $\nabla\rho$ concluding at the BCP. The curvature of ρ , which determines the bond nature, is therefore composed of a positive and a negative component, corresponding respectively to the BP and the IAS directions. The sign of the Laplacian of ρ at the BCP $\Delta\rho_{bcp}$ depends on which component is predominant. A negative Laplacian $\Delta\rho_{bcp} < 0$ corresponds to a local concentration of ρ , indicating an electron-sharing or open-shell bond, while a positive Laplacian $\Delta\rho_{bcp} > 0$ corresponds to a local depletion of ρ , indicating a closed-shell bond.

Figure 2.2 shows the isocontours of ρ , the IAS and critical points of the Hq molecule.

FIGURE 2.2: Hq molecule. ρ isocontours in Hq in grey, interatomic surfaces (IAS) in black, bond critical point as ■, ring critical point (minimum of ρ) as ▲ (from ref. [88]).



In addition, the $\frac{|V_{bcp}|}{G_{bcp}}$ indicator allows a more refined classification of the bonds by giving the relative contribution of potential energy V and kinetic energy G to the local energy density at the BCP. It distinguishes closed shell ($\frac{|V_{bcp}|}{G_{bcp}} < 1$), intermediate ($1 < \frac{|V_{bcp}|}{G_{bcp}} < 2$) and open shell ($2 < \frac{|V_{bcp}|}{G_{bcp}}$) bonding interactions.[89] Finally, the $\frac{H_{bcp}}{\rho_{bcp}}$ indicator, where $H_{bcp} = G_{bcp} + V_{bcp}$, gives information on the covalent contribution of the bond. If $\frac{H_{bcp}}{\rho_{bcp}} < 0$ ($|V_{bcp}| < G_{bcp}$), the bond has a covalent contribution. If $\frac{H_{bcp}}{\rho_{bcp}} > 0$ ($|V_{bcp}| > G_{bcp}$), the bond is purely ionic. Around $\frac{H_{bcp}}{\rho_{bcp}} = 0$, the bond is of intermediate nature. The exact form of V and G which are used for the analysis of the molecular systems (Chapter 3), are obtained from the values of the wavefunctions.

However, for the periodic systems, for practical reasons, we use the approximation proposed by Abramov[90] which allows us to calculate them exclusively from the charge density ρ :

$$G_{bcp} = \frac{3}{10} (3\pi^2)^{2/3} \rho_{bcp}^{5/3} + \frac{1}{6} \Delta\rho_{bcp} \quad (2.31)$$

$$\frac{1}{4}\Delta\rho_{bcp} = 2G_{bcp} + V_{bcp} \quad (2.32)$$

2.2 Computational details

In the following work, we use two codes. GAUSSIAN09[67] is needed in order to i) study charged molecular species in vacuum, ii) obtain an output containing the electronic structure that is compatible with the ELF analysis program TopMod[91]. VASP[68–70] is employed in order to model the adsorption of molecules on the aluminum surface, by taking advantage of the periodicity of the system. The calculations are performed using HPC resources from the regional computing center CALMIP and from the national computing center CINES.

2.2.1 GAUSSIAN09 calculation parameters

Molecular calculations are performed with the GAUSSIAN09 package[67] (version G09RevD.01), making use of the gradient corrected PBE functional[65, 66] with Grimme’s D3 dispersion correction[77, 78]. The orbitals are described by the def2TZVP basis set[74, 75]. The geometries of the studied molecules and complexes are optimized without constraints. Stable geometries are checked to be energy minima using vibrational analysis. Zero point corrections are included to the total energies. Most of the investigations are done in vacuum, but in order to approach the experimental conditions and to understand the effect of the solvent on the various species, the Truhlar and coworkers SMD solvation model[92] is used in part of the calculations.

2.2.2 VASP calculation parameters

Calculations are performed using the Vienna Ab-Initio Simulation Package (VASP) [68–70] (version 5.4.4), with the PBE exchange correlation functional[65]. To model the dispersion part of the van der Waals interactions in the system, which have a significant impact on the molecule-surface and molecule-molecule interactions [50, 93], Grimmes’s D2 dispersion correction is used [77, 78]. The newest D3 method is not compatible with the version of VASP used at the beginning of the thesis. Therefore the D2 method is employed for all our work for the sake of allowing the comparison of all our results. PAW pseudopotentials

are used [94, 95] for the description of the interactions between electrons and ions. Spin polarization is taken into account.

The Equation 2.17 in Section 2.1 shows that Kohn-Sham orbitals can be constructed in a plane wave basis, and are thus defined as:

$$\psi(\mathbf{r}, \mathbf{k}) = \frac{1}{\sqrt{\Omega}} \sum_{\mathbf{G}} C(\mathbf{G}, \mathbf{k}) e^{i(\mathbf{G}+\mathbf{k})\cdot\mathbf{r}} \quad (2.33)$$

Where Ω is the volume of the unit cell and \mathbf{G} is a reciprocal lattice vector verifying :

$$\mathbf{a}_n \cdot \mathbf{G}_m = 2\pi \delta_{nm} \quad (2.34)$$

The exact description of the orbitals would need an infinite number of \mathbf{G} vectors and plane waves. But as the value of the C coefficient decrease as $|\mathbf{k} + \mathbf{G}|$ increases, plane waves used for the wavefunction can be restricted to a finite number with the limit set by the cutoff energy, defined as:

$$\frac{1}{2} |\mathbf{k} + \mathbf{G}|^2 < E_{cut} \quad (2.35)$$

Where E_{cut} is the energy of the plane wave of highest energy.

Based on the optimization of calculation parameters carried out by F. Chiter [56], a cutoff energy of 450 eV is chosen.

The smearing is a parameter controlling the partial occupation of the electronic states around the Fermi energy. While the ground state of a system, obtained by DFT, is at $T = 0$ K, the discontinuity of occupation between completely occupied and completely unoccupied states causes convergence issues in the program. Therefore, it is necessary to "soften" the occupation distribution around the Fermi energy. Several functions can be used to this aim. In this work, the Methfessel-Paxton smearing [96] is employed, with a parameter of $\sigma = 0.1$.

The convergence criterion on the energy for the self-consistent calculation of the wavefunctions and charge density is set to EDIFF = 10^{-6} eV, and the PREC parameter, controlling the precision of the FFT grid, is set to PREC = Accurate, unless specified otherwise in the

chapters hereafter.

Geometry optimization is performed using a combination of conjugate gradient algorithm [97] and RMM-DIIS algorithm [98]. Optimization stopped after the forces on free atoms reached the value of $5.10^{-3} \text{ eV} \cdot \text{\AA}^{-1}$, unless specified otherwise in the chapters hereafter.

Most calculations are performed in vacuum. However, to model the interaction of water with the system, we use an implicit solvent model, provided by the VASPsol package [79, 80]. The solvent is given the relative permittivity of 78.4 (LSOL = T, EB_k = 78.4 in VASP), which is the relative permittivity of water. In addition to simulating the solvent environment and its effect on the molecule properties, this is also useful to shield the possible interactions, allowing unbiased calculations for the charged molecule on Al(111), in presence of a non-interacting counter-ion to compensate the anionic charge and get a neutral simulation cell (Chapter 4).

2.2.3 Topological analysis

The topological analysis by ELF and QTAIM was made possible thanks to the help of Christine Lepetit from LCC, Toulouse.

ELF analysis

The ELF analyses presented in this work are performed on electronic structure files obtained from GAUSSIAN09 calculations using the TopMod program[91].

QTAIM analysis

For molecular calculations, the charge density and Laplacian of the charge density at Bond Critical Points (BCP) ρ_{bcp} and $\Delta\rho_{bcp}$, as well as the kinetic and potential energy densities at Bond Critical Points G_{bcp} and V_{bcp} , are calculated from the GAUSSIAN09 output files using the AIMAll program[99]. The QTAIM atomic charges are calculated using the the TopMod program[91].

For periodic calculations, ρ_{bcpr} and $\Delta\rho_{bcpr}$ are calculated from the VASP output files using the AIM-UC program[100]. From these values are calculated the energy densities G_{bcpr} and V_{bcpr} , using the Abramov formulation (See Section 2.1). The QTAIM atomic charge are calculated using the executable developed by the Henkelman group[101].

Geometry visualization

The geometries presented in this work are obtained from the Molekel[102] and VESTA[103] visualization programs.

2.3 Conclusion

In this chapter, after presenting the basics of DFT, we detailed the different approximations used for the calculations: exchange correlation functional and pseudopotentials. We showed the two types of basis set used for our calculations, i.e. atomic orbitals for calculation of isolated species, and plane waves, preferred for calculation of periodic systems, in our case surfaces. While most of the calculations are done in vacuum, the use of an implicit solvent model, based on the Poisson-Boltzmann equation, allows us to simulate the aqueous environment of the studied systems. Moreover, *ab initio* molecular dynamics, employing the Langevin thermostat, was introduced to simulate thermal agitation, allowing us to explore the configuration space of a system. The two topological analyses used in this work on electronic structure determined by DFT calculations were presented and proved useful to determine the nature of the bonds in the systems. The ELF topological analysis makes use of the wavefunctions and charge density to map the electron pair localization, in correspondence with the Lewis model. The QTAIM analysis is based on the charge density value and curvature, and on energy density descriptors. For all these steps, the corresponding programs were presented, and the general parameters chosen. Throughout next chapters, parameters used only for given calculations will be specified. In the next chapter are presented the results of our work using molecular calculations.

Chapter 3

Study of the chelation of an aluminum cation by Hq derivatives

The solubility, light emission, and corrosion inhibition properties of the Hq and its derivatives, noted HqX and introduced in Chapter 1, are shown to be different depending on the groups located on the ortho and para sites of the phenol ring of the molecule (H, Br and $\text{SO}_3\text{H}/\text{SO}_3^-$). In this chapter, we use dispersion corrected Density Functional Theory calculations to investigate the interactions of the Hq and its derivatives with aluminum cations. To that aim, we first determine optimized geometries in vacuum and water of free Hq, HqBr and HqSH molecules with various forms of the hydroxyl group (native and deprotonated) and then perform ELF and QTAIM analysis of their electronic structures. In order to get a direct insight on the chelating properties of the molecules, a similar investigation is carried out for the complexes formed between three deprotonated molecules and an Al^{3+} ion.

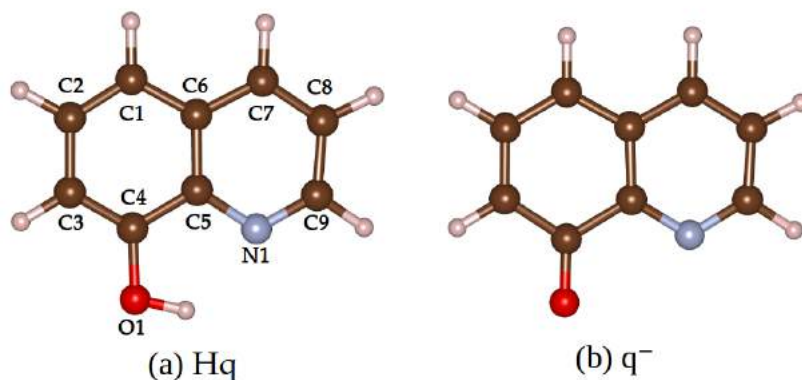
3.1 Computational Details

3.1.1 Presentation of the molecules

The molecules studied in this work are the 8-hydroxyquinoline (Hq), the 5,7-dibromo-8-hydroxyquinoline (HqBr) and the 8-hydroxyquinoline-5-sulfonic acid (HqSH) (See Figure 1.1 in Chapter 1. In solution, these molecules exist in several forms, depending on the pH of the solution. At neutral pH ($5.13 < \text{pH} < 9.89$ for the Hq molecule[2, 3]), the molecules are in their native form. In this case, the hydroxyl group on the phenol ring is in its OH form (native Hq is shown Figure 3.1(a)). At basic pH ($\text{pH} > 9.89$ for the Hq molecule), the

hydroxyle group on the phenol ring is in its phenolate O^- form. The sulfonic acid group (SO_3H/SO_3^-) of the HqSH molecule has a negative pK_a [4, 104, 105], indicating that the SO_3H form is predominant only in extremely acidic solutions. While such a form of the HqSH only exists at extreme conditions, this molecule is nevertheless studied in this work with sulfonic acid groups in both SO_3H and SO_3^- forms, for two reasons: i) The SO_3H form can be seen as a model of a SO_3^- group interacting with a counter ion of charge +1. ii) It is necessary in order to obtain a molecule model of neutral charge, which is needed in later periodic calculations (Chapter 4 and 5). The forms of the 8-hydroxyquinoline-5-sulfonic acid containing a SO_3H group are noted HqSH in the following work, while the forms containing a SO_3^- group are noted HqS. To sum up, the native molecules are noted Hq, HqBr, HqS and HqSH, and the deprotonated molecules are noted q^- , qBr^- , qS^{2-} and qSH^- . The notations HqX and qX^{n-} ($n = 1$ or 2) are used to designate all four molecules, respectively in native, dehydrogenated and deprotonated forms ($X = H, Br, SO_3^-, SO_3H$).

FIGURE 3.1: Hq molecule with atom labels. (a) Native Hq molecule. (b) Deprotonated q^- anion.



3.1.2 DFT calculations

The results presented in this chapter are obtained using molecular DFT calculations, performed with the GAUSSIAN09 package [67], using the PBE functional [65, 66] with Grimme's D3 dispersion correction [77, 78], and the def2TZVP basis set [74, 75]. In specific cases, the SMD solvation model [92] is employed.

The complex formation energies are calculated in vacuum and in water from the total energies of the $Al(qX)_3^{n-}$ ($n = 0$ or 3) complexes, Al^{3+} ion and deprotonated $(qX)^{n-}$ ($n = 1$ or 2) molecules:

$$E_{form}^{cx} = E^{cx} - 3E^{deprot\ mol} - E^{Al^{3+}} \quad (3.1)$$

Where $E^{deprot\ mol}$ is the total energy of the free deprotonated molecule and $E^{Al^{3+}}$ is the total energy of the free Al^{3+} cation.

3.2 Free molecules and anions

3.2.1 Geometries of the molecules

We first present the geometries of the native and deprotonated forms of Hq, to show the influence of the deprotonation on the geometry of the molecule. The effect of solvent on the geometry is discussed, and the geometries are compared to the one measured experimentally. Then, the geometries of the Hq derivatives are presented and compared in their deprotonated form in order to obtain a first insight on the influence of the X groups.

Comparison of the geometries of the Hq forms

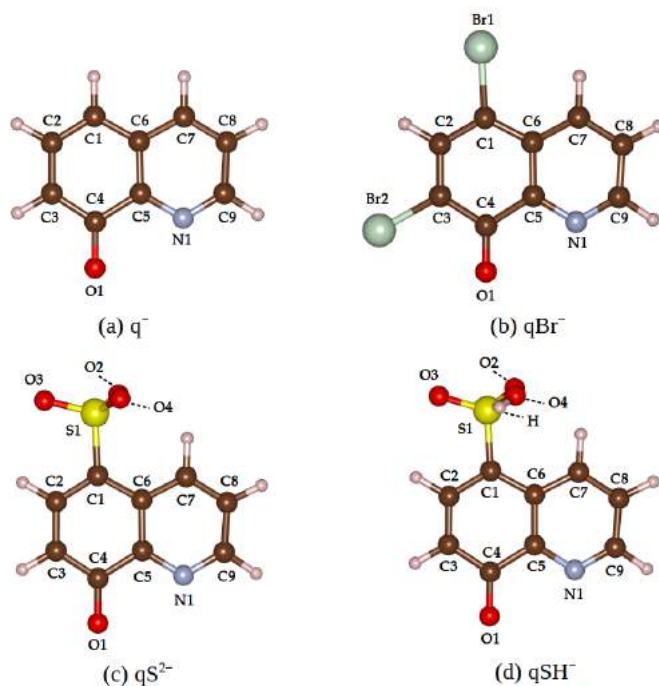
The bond lengths in native (Hq) and deprotonated (q^-) forms are presented in Table 3.1. The geometries of the native Hq molecule in vacuum and in water are close to the experimentally determined geometry of the Hq native form in crystal state[106], with a maximum difference of $\Delta d_{C4-C5} = 0.038 \text{ \AA}$. The comparison between the Hq species in vacuum versus in water shows very close bond lengths, with highest differences obtained for the C4-O1 bond, which is 0.017 \AA longer in water than in vacuum. This shows a slight influence of the presence of the solvent on the geometry of the molecule. In vacuum, we first notice that the C4-O1 bond is shorter for the deprotonated form, compared to the native form ($\Delta d_{C4-O1} = 0.094 \text{ \AA}$). The removal of H^+ also affects the C-C bonds close to the O1 atom, with differences of up to $\Delta d_{C4-C5} = 0.064 \text{ \AA}$. The similarity between the Hq geometry obtained from our calculations and the experimental geometry indicates that the calculation parameters are sufficient to model the Hq. As the deprotonated form (q^-) is the chelating species leading to the formation of Alq_3 complexes, this form will be used for the comparisons of HqX species carried out below.

TABLE 3.1: Bond lengths (in Å) in native Hq and deprotonated q^- forms optimized in vacuum and in water.

Species	Hq			q^-	
	Vacuum	Water	Exp.[106]	Vacuum	Water
d_{C1-C2}	1.383	1.382	1.365	1.396	1.388
d_{C2-C3}	1.418	1.414	1.427	1.394	1.404
d_{C3-C4}	1.384	1.383	1.371	1.442	1.421
d_{C4-C5}	1.431	1.428	1.393	1.495	1.473
d_{C5-C6}	1.429	1.429	1.428	1.451	1.441
d_{C6-C7}	1.418	1.418	1.402	1.420	1.420
d_{C7-C8}	1.380	1.379	1.357	1.380	1.378
d_{C8-C9}	1.415	1.414	1.389	1.412	1.411
d_{C1-C6}	1.418	1.419	1.410	1.413	1.418
d_{C4-O1}	1.351	1.368	1.367	1.257	1.295
d_{C5-N1}	1.360	1.364	1.374	1.353	1.364
d_{C9-N1}	1.324	1.327	1.331	1.327	1.328
d_{O1-H}	0.991	0.988	1.00		

Comparison of the geometries of the qX^{n-} ($n = 1$ or 2) anions

The geometries of the q^- , qBr^- , qS^{2-} and qSH^- molecules are presented in Figure 3.2. Corresponding bond lengths are summarized in Table 3.2. By comparing the three fully deprotonated species (q^- , qBr^- , qS^{2-}), we notice few differences in bond lengths. The highest differences are obtained for the C4-O1 bond, with values of d_{C4-O1} of 1.257 Å, 1.246 Å and 1.267 Å respectively for q^- , qBr^- and qS^{2-} . The qSH^- species stands out from the other species in term of geometry, with variations of geometry between qS^{2-} and qSH^- around the O1 and N1 atoms ($\Delta d_{C4-O1} = 0.019$ Å, $\Delta d_{C5-N1} = 0.031$ and $\Delta d_{C9-N1} = 0.023$ Å). The substitution of the ortho and para H atoms by Br and SO_3^- groups only slightly impact the geometries of the molecules. The neutralization of the SO_3^- group of qS^{2-} to give qSH^- modifies the geometry around the atoms implicated in chelation, possibly modifying the chelating properties.

FIGURE 3.2: Deprotonated qX^{n-} ($n = 1$ or 2) species optimized in vacuum.TABLE 3.2: Bond lengths (in Å) in the q^- , qBr^- , qS^{2-} and qSH^- anions.

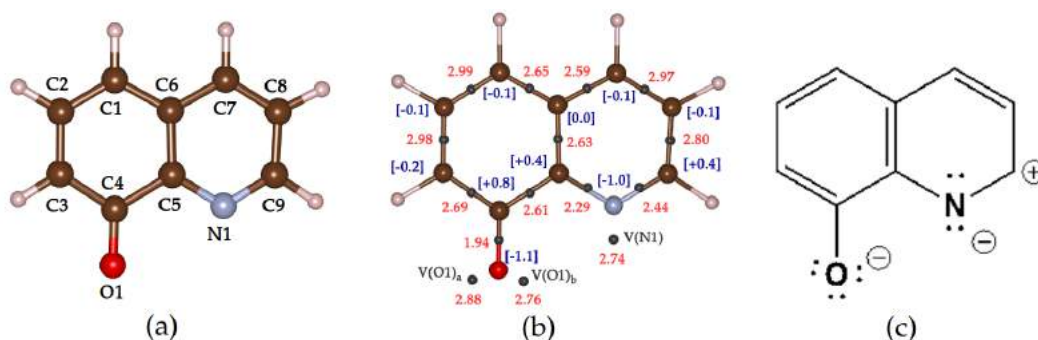
Species	q^-	qBr^-	qS^{2-}	qSH^-
d_{C1-C2}	1.396	1.389	1.393	1.409
d_{C2-C3}	1.394	1.391	1.397	1.379
d_{C3-C4}	1.442	1.444	1.433	1.443
d_{C4-C5}	1.495	1.498	1.493	1.501
d_{C5-C6}	1.451	1.452	1.454	1.444
d_{C6-C7}	1.420	1.418	1.423	1.421
d_{C7-C8}	1.380	1.380	1.380	1.382
d_{C8-C9}	1.412	1.409	1.410	1.404
d_{C1-C6}	1.413	1.411	1.424	1.434
d_{C4-O1}	1.257	1.246	1.267	1.248
d_{C5-N1}	1.353	1.349	1.358	1.327
d_{C9-N1}	1.327	1.326	1.326	1.349
d_{C1-Br1}		1.935		
d_{C3-Br2}		1.921		
d_{C1-S1}			1.810	1.731
d_{S1-O2}			1.486	1.460
d_{S1-O3}			1.483	1.451
d_{S1-O4}			1.486	1.667

3.2.2 Topological analyses of qX^{n-} ($n = 1$ or 2) anions

ELF analysis

The ELF attractors of the q^- species and the electron populations in their associated basins are shown in Figure 3.3 (b). Population values in the $V(C,C)$ basins of the aromatic cycles are of about $2.5 e^-$ to $3 e^-$ for each basin related to a C-C bond, which is to be expected for bonds in aromatic cycles. More globally, the populations are consistent to what has been found with topological analysis on naphthalene derivatives[86, 107, 108]. As the qX^{n-} ($n = 1$ or 2) molecules interact with the aluminum cation by the O1 and N1 atoms, special interest is given to the ELF basins close to these atoms. As this work as well as previous work[50, 51] shows that the q^- molecule interacts with the Al(111) surface by the C7 atom, ELF basins close to this atom is also investigated. The populations in the $V(C7,C6)$ and $V(C7,C8)$ basins are respectively of $2.59 e^-$ and $2.97 e^-$, expected values for aromatic rings. In addition to the $V(C4,O1)$ basin associated to the C4-O1 bond, two monosynaptic basins $V(O1)_a$ and $V(O1)_b$ are found, corresponding to the lone pairs on O1. Population in the $V(C4,O1)$ basin is of $1.94 e^-$, while $V(O1)_a$ and $V(O1)_b$ have populations of $2.88 e^-$ and $2.76 e^-$ respectively. The values on the two monosynaptic basins, summing to up to almost $6 e^-$, are consistent with the mesomeric form of the q^- species shown Figure 3.3 (c). The difference between the two populations is the result of the asymmetry of the molecule. On the N1 atom, population of the monosynaptic basin $V(N1)$ is of $2.74 e^-$, which is higher than the expected population of a lone pair ($2 e^-$). This suggests a significant contribution of the pyridine mesomeric form (Figure 3.3 (c)).

FIGURE 3.3: Deprotonated q^- molecule. (a) Atom labels. (b) Map of ELF attractors and their associated electron populations (in e^-) in red; QTAIM atomic charges (in e) in blue. (c) Phenolate and pyridine mesomeric forms.



Populations of interest in the q^- , qBr^- , qS^{2-} and qSH^- are summarized in Table 3.3. Only very slight differences between species are found, indicating no significant change in

electronic structure in the proximity of the O1, N1 and C7 atoms when the H atoms on C1 and C3 atoms are substituted by Br, SO_3^- and SO_3H groups.

TABLE 3.3: Comparison of the population (in e^-) of selected ELF basins of the q^- , qBr^- , qS^{2-} and qSH^- species.

Species	q^-	qBr^-	qS^{2-}	qSH^-
V(C4,O1)	1.94	2.00	1.88	2.02
V(O1) _a	2.88	2.83	2.92	2.82
V(O1) _b	2.76	2.76	2.79	2.79
V(N1)	2.74	2.72	2.76	2.73
V(C5,N1)	2.29	2.30	2.31	2.27
V(C9,N1)	2.44	2.44	2.43	2.45
V(C7,C6)	2.59	2.60	2.57	2.63
V(C7,C8)	2.97	2.94	2.96	2.91

QTAIM analysis

The QTAIM atomic charges are also indicated in Figure 3.3 (a) for the q^- species, and in Table 3.4 for q^- , qBr^- , qS^{2-} and qSH^- for all C, O, N Br, and S atoms. We focus our analysis on the known reactive atoms i.e. the O1 and N1 atoms. Strong negative net charges are found on O1 and N1 atoms, with values of -1.10 e to -1.16 e for q_{O1} and -1.02 e to -1.04 e for q_{N1} . This is also consistent with the mesomeric form presented in Figure 3.3 (c), and confirms that the electronic structure at the O1 and N1 atoms is not significantly impacted by the substitution of the H atoms of the cycles by the Br, SO_3^- and SO_3H groups.

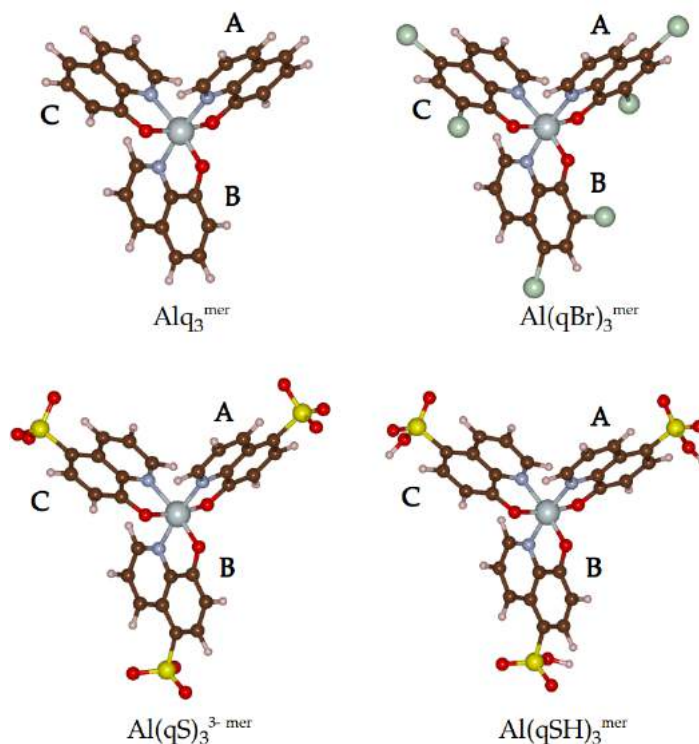
TABLE 3.4: QTAIM atomic (in e) charges on the deprotonated q^- , qBr^- , qS^{2-} and qSH^- species.

Species	q^-	qBr^-	qS^{2-}	qSH^-
q_{C1}	-0.14	-0.12	-0.16	-0.22
q_{C2}	-0.09	-0.03	-0.09	-0.07
q_{C3}	-0.17	-0.14	-0.17	-0.14
q_{C4}	+0.84	+0.89	+0.81	+0.87
q_{C5}	+0.39	+0.40	+0.37	+0.40
q_{C6}	-0.02	+0.01	-0.02	+0.00
q_{C7}	-0.10	-0.08	-0.08	-0.10
q_{C8}	-0.12	-0.10	-0.12	-0.10
q_{C9}	+0.42	+0.43	+0.40	+0.43
q_{O1}	-1.13	-1.10	-1.16	-1.10
q_{N1}	-1.03	-1.02	-1.04	-1.02
q_{Br1}		-0.18		
q_{Br2}		-0.15		
q_{S1}			+3.02	+2.77
q_{O2}			-1.31	-1.26
q_{O2}			-1.31	-1.26
q_{O3}			-1.31	-1.13

3.3 $Al(qX)_3^{n-}$ ($n = 0$ or 3) complexes

The Hq, HqBr and HqSH molecules are known to have chelating properties, meaning they can bind metal atoms, forming complexes. A maximum of 3 deprotonated molecules qX^{n-} ($n = 1$ or 2) can bind to the aluminum ion, leading in that case to a complex noted $Al(qX)_3^{n-}$ ($n = 0$ or 3). As explained in Chapter 1, this species exists in two isomers, called meridional and facial, noted *mer* and *fac* in this work. For Alq_3 in vacuum, the *mer* isomer is found to be 138 meV more stable than the *fac* isomer (173 meV in literature [109]). In water at 0 K the *fac* isomer is more stable than the *mer* isomer by 11 meV. Experimentally, the *mer* isomer is the one mainly observed in solution at room temperature [110–113]. Therefore, the following study is restricted to the *mer* isomer of each complex: The *mer* complexes studied in this work are noted Alq_3^{mer} , $Al(qBr)_3^{mer}$, $Al(qS)_3^{3-mer}$ and $Al(qSH)_3^{mer}$ (see Figure 3.4), respectively obtained by the bonding of three q^- , qBr^- , qS^{2-} or qSH^- molecules with an aluminum cation.

FIGURE 3.4: Geometries of the Alq_3^{mer} , $Al(qBr)_3^{mer}$, $Al(qS)_3^{3-mer}$ and $Al(qSH)_3^{mer}$ complexes optimized in vacuum. The three molecules in a complex are noted from A to C.



3.3.1 Formation energies of $Al(qX)_3^{n-}$ ($n = 0$ or 3) in vacuum and in water

The formation energies in vacuum of all complexes are compared in Table 3.5. The formation energy is lower in magnitude for the $Al(qBr)_3^{mer}$ and $Al(qSH)_3^{mer}$ complexes (-58.19 eV and -57.77 eV respectively) than for the Alq_3^{mer} complex (-59.71 eV), and the $Al(qS)_3^{3-mer}$ has the strongest formation energy in magnitude (-63.97 eV). These energies indicate in all cases strong interactions of the molecules with the aluminum ion. The same calculations were performed in the presence of solvent (SMD solvation model[92] proposed by Truhlar *et al.*), leading to lower differences between formation energies of the complexes (-24.30 ± 0.29 eV), which shows similar strength of interactions between all qX^{n-} ($n = 1$ or 2) species with the Al cation in aqueous environment.

TABLE 3.5: Complex formation energy E_{form}^{cx} (in eV) of the four complexes in vacuum. For ΔE_{form}^{cx} the reference is the energy of the Alq_3^{mer} complex.

Species	Alq_3^{mer}	$Al(qBr)_3^{mer}$	$Al(qS)_3^{3-mer}$	$Al(qSH)_3^{mer}$
E_{form}^{cx}	-59.71	-58.19	-63.97	-57.77
ΔE_{form}^{cx}	0	1.52	-4.26	1.94

3.3.2 Geometries of the $\text{Al}(\text{qX})_3^{n-}$ ($n = 0$ or 3) complexes

The O1-Al and N1-Al bond lengths in the complexes are summarized in Table 3.6. They are of 1.875 ± 0.015 Å for O1-Al and 2.072 ± 0.030 Å for N1-Al, showing no significant difference between complexes, meaning that the substitution of the H atoms on the phenol ring by the Br atoms or by $\text{SO}_3\text{H}/\text{SO}_3^-$ groups does not influence the geometry of the complex around the Al atom. The length of the O1-Al bond and N1-Al bond are respectively very close to the sum of the ionic radii of the Al and O atoms (~ 1.9 Å), and to the sum of the ionic radii of the Al and N atoms (~ 2.0 Å). This is a first indication of the ionic nature of the bonds.

TABLE 3.6: Bond lengths (in Å) in the $\text{Alq}_3^{\text{mer}}$, $\text{Al}(\text{qBr})_3^{\text{mer}}$, $\text{Al}(\text{qS})_3^{3-\text{mer}}$ and $\text{Al}(\text{qSH})_3^{\text{mer}}$ complexes, in molecules **A**, **B** and **C** of the complexes (see Figure 3.4).

Species	$\text{Alq}_3^{\text{mer}}$	$\text{Al}(\text{qBr})_3^{\text{mer}}$	$\text{Al}(\text{qS})_3^{3-\text{mer}}$	$\text{Al}(\text{qSH})_3^{\text{mer}}$
A				
$d_{\text{O1-Al}}$	1.894	1.888	1.899	1.892
$d_{\text{N1-Al}}$	2.045	2.045	2.053	2.042
B				
$d_{\text{O1-Al}}$	1.863	1.860	1.871	1.867
$d_{\text{N1-Al}}$	2.058	2.057	2.066	2.056
C				
$d_{\text{O1-Al}}$	1.891	1.886	1.896	1.890
$d_{\text{N1-Al}}$	2.101	2.100	2.100	2.088

3.3.3 Topological analysis of $\text{Al}(\text{qX})_3^{n-}$ ($n = 0$ or 3) complexes

ELF analysis

In Table 3.7 are presented the average ELF populations of the valence basins associated to the O1-Al and N1-Al bonds $V(\text{O1})_a$, $V(\text{O1})_b$ and $V(\text{N1})$ for the four complexes. Values for the **C** molecule of the complex and the Al^{3+} ion are shown in red in Figure 3.5. First, it is worth noting that no disynaptic $V(\text{Al},\text{O1})$ or $V(\text{Al},\text{N1})$ basins is found, indicating that the O1-Al and N1-Al bonds are not strongly covalent. In the $\text{Alq}_3^{\text{mer}}$ complex, a reorganisation of the ELF populations takes place on O1 and N1 atoms upon formation of the complex. The dissymmetry between the monosynaptic $V(\text{O1})_a$ and $V(\text{O1})_b$ basins is stronger in the complex (average values of $V(\text{O1})_a = 2.31 e^-$ and $V(\text{O1})_b = 3.70 e^-$) than in the free q^- molecule ($V(\text{O1})_a = 2.88 e^-$ and $V(\text{O1})_b = 2.76 e^-$), reflecting the strong reduction of symmetry of the

TABLE 3.8: Relevant QTAIM descriptors (in a.u.) related to the O1-Al and N1-Al bonds in $\text{Alq}_3^{\text{mer}}$ complexes. Descriptors are averaged over the three O1-Al and N1-Al bonds.

Species	$\text{Alq}_3^{\text{mer}}$	$\text{Al}(\text{qBr})_3^{\text{mer}}$	$\text{Al}(\text{qS})_3^{3-\text{mer}}$	$\text{Al}(\text{qSH})_3^{\text{mer}}$
BCP O1-Al				
ρ_{bcp}	0.071	0.072	0.070	0.071
$\Delta\rho_{\text{bcp}}$	0.397	0.403	0.388	0.397
$\frac{ V_{\text{bcp}} }{G_{\text{bcp}}}$	1.06	1.06	1.06	1.06
$\frac{H_{\text{bcp}}}{\rho_{\text{bcp}}}$	-0.09	-0.08	-0.09	-0.08
BCP N1-Al				
ρ_{bcp}	0.053	0.053	0.053	0.054
$\Delta\rho_{\text{bcp}}$	0.223	0.223	0.219	0.227
$\frac{ V_{\text{bcp}} }{G_{\text{bcp}}}$	1.09	1.09	1.09	1.09
$\frac{H_{\text{bcp}}}{\rho_{\text{bcp}}}$	-0.10	-0.11	-0.11	-0.11

where the charge density is concentrated near the atoms rather than in the neighbourhood of the BCP. The $\frac{|V_{\text{bcp}}|}{G_{\text{bcp}}}$ indicator allows to locate the bond on a scale containing ionic, intermediate and covalent bonds. For instance, the value of 1.06, obtained for the O1-Al bond, indicates a bond of intermediate nature, almost purely ionic, as the limit between ionic and intermediate region is 1. This is also true for the N1-Al bond ($\frac{|V_{\text{bcp}}|}{G_{\text{bcp}}} = 1.09$). The covalent domain corresponds to values of $\frac{|V_{\text{bcp}}|}{G_{\text{bcp}}}$ higher than 2. For instance, the C1-C2 bond of the phenol ring has a $\frac{|V_{\text{bcp}}|}{G_{\text{bcp}}}$ value of 3.98. Finally, the small negative value of $\frac{H_{\text{bcp}}}{\rho_{\text{bcp}}}$ for both O1-Al and N1-Al shows a slight covalent contribution to the bond, which is consistent with what suggested the $\frac{|V_{\text{bcp}}|}{G_{\text{bcp}}}$ indicator. In addition to this, the QTAIM atomic charge on the aluminum atom has a value of $+2.49 \pm 0.01$ e in all four complexes, indicating very similar Al^{III} oxidation state of the ion in all complexes.

QTAIM analysis performed by Murgich *et al.* on Feq_3 , Mnq_3 and Coq_3 [88] shows close values for Feq_3 ($\frac{|V_{\text{bcp}}|}{G_{\text{bcp}}} = 1.07$ for O-Fe and $\frac{|V_{\text{bcp}}|}{G_{\text{bcp}}} = 1.08$ for N-Fe), while Mn_3 and Co_3 have a higher covalence contribution to the bonds (up to $\frac{|V_{\text{bcp}}|}{G_{\text{bcp}}} = 1.19$).

The comparison of these indicators for the four complexes shows once again very similar values, meaning that O1-Al and N1-Al bonds are similar in all complexes.

3.4 Conclusion

In this chapter, we investigated the influence of the X groups at para and ortho positions of the phenol ring of the qX^{n-} ($n = 1$ or 2) anions on the geometrical, electronic, and aluminum chelating properties of these anions. For the free qX^{n-} ($n = 1$ or 2) anions and $Al(qX)_3^{n-}$ ($n = 0$ or 3) complexes, the X substituents (H, Br, SO_3^- , SO_3H) influence only locally the geometry and electronic structures of the species, and thus do not change the metal-ligands interaction. In all complexes, ionic bonding of the qX^{n-} ($n = 1$ or 2) anions with the aluminum cation was shown to be very similar, with only a slight covalent contribution to the bonding. The charge on the aluminum ion was determined to be the same for all complexes, i.e. $+2.49 e$. The complex formation energies were found to be different between complexes, when calculated in vacuum, but much closer when calculated in water, i.e. closer to experimental conditions (-24.30 ± 0.29 eV). These results show that the differences in experimentally determined properties between these species do not originate in a modification of the electronic structure of the qX^{n-} anions or $Al(qX)_3^{n-}$ complexes by the influence of the X groups, but on other factors such as the interaction of the the X groups with the environment (solvent, surface). In the following chapters, to get a better understanding of the interaction of the X groups with the surfaces, focusing on the corrosion inhibition properties of the studied species, periodic calculations of the adsorption of the molecules on an aluminum surface are presented.

Chapter 4

Periodic calculations: Free molecules and complexes, bare surfaces

Starting from this chapter, periodic calculations are employed (Chapter 4 to 6). This allows an accurate description of metallic surfaces, which are used for the study of the adsorption of the molecules on an Al(111) surface. In this chapter, the free molecules, complexes and surface models employed in Chapters 5 and 6 are detailed. Their properties are studied with respect to the calculation parameters, and are compared to experimental data in order to evaluate the validity of the models. In the case of the complexes, a systematic study of systems composed of n ($n = 1, 2$ or 3) dehydrogenated Hq molecules with an Al atom is carried out in order to better understand the interactions responsible for the stability of the complex.

4.1 Free molecules and complexes

4.1.1 Computational details

Periodic DFT calculation are performed using VASP[68–70], with the PBE-D2 functional[65, 77, 78] and the PAW pseudopotentials[94, 95].

Molecules

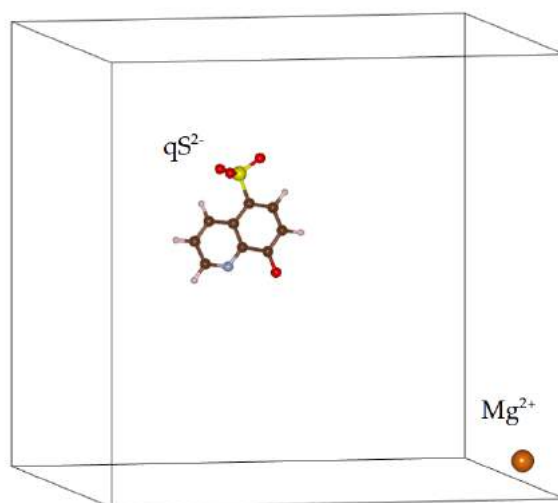
For the modeling of the deprotonated species, two different models are used to : a neutral dehydrogenated form and a charged deprotonated form. Dehydrogenated forms are neutral radicals obtained from the homolytic dissociation of the OH group from the native form. They are noted q, qBr, qS and qSH. The notation qX is used to designate all four of these dehydrogenated species. Deprotonated forms (q^- , qBr^- , qS^{2-} and qSH^-) are charged species obtained from the removal of H^+ protons from the hydroxyl group of the native form. Although the deprotonated form is closer to the molecule found in experimental conditions at basic pH, the dehydrogenated form is used in molecule adsorption studies, because it is more convenient to work on neutral systems for periodic systems. The validity of this approximation is discussed in Chapter 5.

Simulation cells are set to be of $20 \times 21 \times 22 \text{ \AA}^3$ for neutral species, i.e. native and dehydrogenated forms, which is enough to make interactions between images insignificant. Calculations are performed at gamma point of the reciprocal space.

In order to simulate the solvent environment and its effect on the molecule properties, we use an implicit solvent model, provided by the VASPsol package [79, 80]. In the presence of solvent, we also achieve to study deprotonated forms, therefore charged species qX^{n-} ($n = 1$ or 2).

In the case of isolated charged species, the VASP calculations can be challenging, as convergence is difficult to reach when the total system in the cell is charged. To avoid this problem, we keep the total charge of the cell neutral by adding a cation in the cell, with the adequate charge to obtain the desired negative charge on the molecule. For example, the addition of a Mg^{2+} cation in the cell allows us to obtain a molecule of charge $-2 e$. This was checked by QTAIM analysis in all calculations. In that case, we use an implicit solvent model which shields interactions between the molecule and the counter-ion, as well as interactions between periodic images. In order to obtain a high enough distance between the molecule and the ion, $25 \times 26 \times 27 \text{ \AA}^3$ simulation cells are chosen for the charged species. The molecule and ion were proved to be isolated as a larger cell and longer molecule-ion distance led to similar total energy. An example of such a cell is shown in Figure 4.1.

FIGURE 4.1: qS^{2-} and Mg^{2+} simulation cell used for periodic calculations. In orange : Mg^{2+} ion. Shortest distance between qS^{2-} anion and Mg^{2+} is of 18 Å.



Complexes formed from n q molecules (n = 1, 2 or 3) and an Al atom

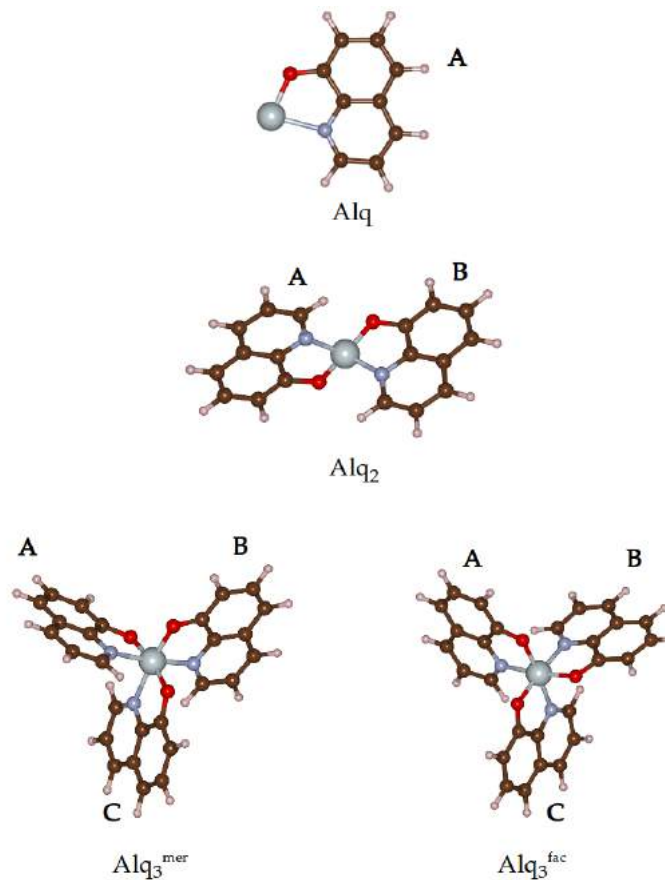
The complexes formed by an Al atom and one to three dehydrogenated q molecules, i.e. the Alq , Alq_2 and Alq_3 are presented in Figure 4.2. For Alq_3 , both free isomers Alq_3^{mer} and Alq_3^{fac} are studied in this chapter.

All complexes are optimized in $32 \times 31 \times 30 \text{ \AA}^3$ cells, except for Alq which is optimized in a $22 \times 21 \times 20 \text{ \AA}^3$ cell. The reciprocal space is sampled by a gamma point. All calculations are performed in vacuum. Due to steric hindrance, it is not possible to add a fourth q molecule. The n molecules are denoted from **A** to **C** (see Figure 4.2).

The complex formation energy is the energy associated to the formation of an Alq_n (n = 1, 2 or 3) complex from one Al atom and n q molecules and is defined by:

$$E_{form}^{cx} = E^{cx} - nE^{mol} - E^{Al\ atom} \quad (4.1)$$

Where E^{cx} is the total energy of the free optimized Alq_n complex, n is the number of q molecules in the complex, E^{mol} is the total energy of the free optimized q molecule and $E^{Al\ atom}$ is the energy of the free Al atom. Because we use a periodic approach, the references are neutral species (q molecule and Al atom), unlike in Chapter 3 where the references are charged species (q^- anion and Al^{3+} cation), therefore the complex formation energies calculated below and those calculated in Chapter 3 are not to be compared directly. In this

FIGURE 4.2: Alq_n ($n = 1, 2$ or 3) complex geometries.

work, the energy of the deprotonated molecule will be noted $E^{deprot\ mol}$ while the energy of the dehydrogenated molecule will be noted E^{mol} .

Interaction energies allow to quantify the interaction between several parts of a system. The interaction energy between the n q molecules and the Al atom in the Alq_n complex is defined by:

$$E_{int}^{n\ mol/Al} = E^{cx} - E_{SP}^{n\ mol} - E^{Al\ atom} \quad (4.2)$$

Where $E_{SP}^{n\ mol}$ is the total energy of the n q molecules at the geometry of the Alq_n complex, without the Al atom.

The inter-molecular interaction energy is the interaction energy between the n q molecules of the complex and is defined by:

$$E_{int}^{inter-mol} = E_{SP}^{n\ mol} - \sum_{i=A,\dots} E_{SP}^{moli} \quad (4.3)$$

Where $\sum_{i=A,\dots} E_{SP}^{moli}$ is the sum of the energies of the isolated n molecules calculated separately at the geometry of the Alq_n complex.

For example, the inter-molecular energy in Alq_3 is equal to:

$$E_{int}^{inter-mol} = E_{SP}^{3\ mol} - E_{SP}^{molA} - E_{SP}^{molB} - E_{SP}^{molC} \quad (4.4)$$

The deformation energy of the n molecules in the Alq_n ($n = 1, 2$ or 3) complex is defined as :

$$E_{def}^{n\ mol} = \sum_{i=A,\dots} E_{SP}^{moli} - nE^{mol} \quad (4.5)$$

As an example, the deformation energy of the 3 q molecules in Alq_3 is equal to:

$$E_{def}^{3\ mol} = E_{SP}^{molA} + E_{SP}^{molB} + E_{SP}^{molC} - 3E^{mol} \quad (4.6)$$

4.1.2 Free Hq molecules, dehydrogenated and deprotonated species

Geometries of the free native Hq, dehydrogenated q and deprotonated q^- molecules are presented in Table 4.1. The q^- anion is only calculated in water so as to screen the interactions between periodic images, as well as interactions between q^- and Na^+ . Geometries are similar to those calculated with the molecular approach (GAUSSIAN09, PBE-D3/def2TZVP) in Chapter 3, also reported in Table 4.1 for the q molecule and q^- anion. Variations between species are consistent, with for example a longer C4-O1 bond in q^- than in q. The solvent model used for the molecular approach and for the periodic approach also lead to similar molecule geometries in water. Geometries HqBr, HqS and HqSH in native, dehydrogenated and deprotonated forms are given in Appendix A. The results validate our calculation parameters (PBE-D2/PAW, $E_{cut} = 450$ eV, $\sigma = 0.1$ MP smearing), and these molecule models will be used in the work presented in Chapter 5 and 6.

TABLE 4.1: Bond lengths (in Å) in native Hq, dehydrogenated q and deprotonated q⁻ forms in vacuum and in water.

Species	Hq		q			q ⁻	
	Vacuum	Exp.[106]	Vacuum	Vacuum†	Water	Water	Water†
d_{C1-C2}	1.384	1.365	1.400	1.398	1.401	1.391	1.388
d_{C2-C3}	1.415	1.427	1.387	1.386	1.387	1.403	1.404
d_{C3-C4}	1.385	1.371	1.457	1.454	1.451	1.428	1.421
d_{C4-C5}	1.431	1.393	1.497	1.495	1.490	1.481	1.473
d_{C5-C6}	1.431	1.428	1.430	1.429	1.427	1.445	1.441
d_{C6-C7}	1.418	1.402	1.414	1.413	1.414	1.421	1.420
d_{C7-C8}	1.381	1.357	1.384	1.382	1.384	1.380	1.378
d_{C8-C9}	1.417	1.389	1.409	1.412	1.408	1.415	1.411
d_{C1-C6}	1.419	1.410	1.426	1.424	1.426	1.417	1.418
d_{C4-O1}	1.355	1.367	1.249	1.243	1.259	1.284	1.295
d_{C5-N1}	1.361	1.374	1.344	1.342	1.347	1.363	1.364
d_{C9-N1}	1.325	1.331	1.334	1.332	1.338	1.330	1.328
d_{O1-H}	0.990	1.00					

† Molecular calculation from Chapter 3.

4.1.3 Free Alq_n (n = 1, 2 or 3) complexes

The formation, interaction and deformation energies as well as van der Waals contributions are presented in Table 4.2. The lengths of the O1-Al and N1-Al bonds in the complexes are presented in Table 4.3, and the charges on the Al, O1 and N1 atoms are summarized in Table 4.4. The dipole moments of the Alq₃ complexes are given in Figure A.1 of Appendix A, and discussed in Chapter 6.

The complex formation energy E_{form}^{cx} values show that the complex is highly stabilized by each addition of a q molecule. Van der Waals interactions only weakly contribute to this energy, with values ranging from -0.07 eV for Alq to -0.71 eV for Alq₃^{fac}, on a total formation energy ranging from -4.99 eV for Alq to -13.74 eV for Alq₃^{mer}. For n = 3, the *mer* isomer is found to be 125 meV more stable than the *fac* isomer. The formation energy per molecule becomes smaller as n increases, with values ranging from -4.99 eV for Alq to -4.54 eV for Alq₃^{fac}. The interaction energy between the molecules and the Al atom $E_{int}^{n mol/Al}$ shows a very strong bonding, with values of interaction energy per molecule $E_{int}^{n mol/Al}/n$ ranging from -5.02 eV to -5.39 eV. The van der Waals contribution to $E_{int}^{n mol/Al}$ is very low, with values ranging from -0.07 eV for the Alq to -0.22 eV for the Alq₃^{mer} and Alq₃^{fac} complexes. The interaction between molecules, quantified by the $E_{int}^{inter-mol}$ energy, are repulsive as the energy values are positive (0.24 eV to 0.61 eV). The stabilizing contributions of the van der Waals interactions to this energy are especially strong for the Alq₃ species (-0.45 eV and -0.52 eV).

TABLE 4.2: Alq_n ($n = 1, 2$ or 3) formation energies and their van der Waals contributions, formation energy per molecule, interaction energies and their van der Waals contributions, interaction energies per molecule and deformation energies (in eV).

Species	Alq	Alq ₂	Alq ₃ ^{mer}	Alq ₃ ^{fac}
E_{form}^{cx}	-4.99	-9.51	-13.74	-13.61
$E_{form}^{cx}(vdW)$	-0.07	-0.21	-0.64	-0.71
E_{form}^{cx}/n	-4.99	-4.75	-4.58	-4.54
$E_{int}^{n\ mol/Al}$	-5.35	-10.79	-15.20	-15.06
$E_{int}^{n\ mol/Al}(vdW)$	-0.07	-0.14	-0.22	-0.22
$E_{int}^{n\ mol/Al}/n$	-5.35	-5.39	-5.07	-5.02
$E_{int}^{inter-mol}$		+0.24	+0.56	+0.61
$E_{int}^{inter-mol}(vdW)$		-0.09	-0.45	-0.52
$E_{def}^{n\ mol}$		+1.04	+0.90	+0.83

TABLE 4.3: Bond lengths (in Å) in the **A**, **B** and **C** parts of the Alq_n ($n = 1, 2$ or 3) complexes.

Species	Alq	Alq ₂	Alq ₃ ^{mer}	Alq ₃ ^{fac}	
A	d_{O1-Al}	1.848	1.770	1.891	1.856
	d_{N1-Al}	2.187	1.897	2.039	2.097
B	d_{O1-Al}		1.770	1.860	1.855
	d_{N1-Al}		1.897	2.052	2.099
C	d_{O1-Al}			1.888	1.856
	d_{N1-Al}			2.092	2.103

The lengths of the O1-Al (1.844 ± 0.074 Å) and N1-Al (2.051 ± 0.154 Å) bonds indicate chemical bonding between the molecules and the Al atom, which is in accordance with the high energy values. In the geometrically symmetrical Alq_2 complex are found the shortest bonds, as well as the highest molecule deformation energy (+1.04 eV for two molecules versus +0.90 eV and +0.83 eV for three molecules in the $\text{Alq}_3^{\text{mer}}$ and $\text{Alq}_3^{\text{fac}}$ complexes respectively). The bond lengths found for the $\text{Alq}_3^{\text{mer}}$ and $\text{Alq}_3^{\text{fac}}$ complexes are in accordance with experimental[23, 114] and theoretical[109, 115, 116] studies.

The charge on the Al atom is +0.86 e for Alq and ranges from +2.41 e to +2.45 e for Alq_2 , $\text{Alq}_3^{\text{mer}}$ and $\text{Alq}_3^{\text{fac}}$. The Al atom is close to the Al^I oxidation state in the case of Alq, and close to the Al^{III} oxidation state in the case of other complexes, which is consistent with the electronic structure of the Al atom ($3s^23p^1$). It is clear that the addition of a molecule leading to the transition of an Al^I state to an Al^{III} state (Alq to Alq_2) is more stabilizing ($\Delta E_{int}^{n\ mol/Al}$

TABLE 4.4: QTAIM atomic charges (in e) on the Al, O1 and N1 atoms of the Alq_n ($n = 1, 2$ or 3) complexes.

Species	q	Alq	Alq ₂	Alq ₃ ^{mer}	Alq ₃ ^{fac}	
q_{Al}		+0.86	+2.41	+2.45	+2.45	
A	q_{O1}	-0.96	-1.31	-1.30	-1.35	-1.25
	q_{N1}	-1.15	-1.37	-1.42	-1.33	-1.34
B	q_{O1}		-1.30	-1.35	-1.25	
	q_{N1}		-1.42	-1.27	-1.36	
C	q_{O1}			-1.26	-1.26	
	q_{N1}			-1.27	-1.36	

= -5.44 eV) than the addition of a molecule that does not change the oxidation state (Alq_2 to Alq_3 , $\Delta E_{int}^{n\text{ mol}/Al} = -4.27$ for the *mer* isomer and $\Delta E_{int}^{n\text{ mol}/Al} = -4.41$ eV for the *fac* isomer). For all complexes, the O1 and N1 atoms receive electrons upon complex formation.

Overall, our calculations show that all complexes display strong bonding between the Al atom and the n molecules, associated with high charge transfers leading to Al^I or Al^{III} oxidation states. Up to three q molecules can form bonds with the Al atom, and the most stable complex formed with three q molecules is the $\text{Alq}_3^{\text{mer}}$ isomer, which is in accordance with experimental studies [110–113]. Distances and atomic charges obtained for the $\text{Alq}_3^{\text{mer}}$ are consistent with the values calculated with Gaussian in Chapter 3. Having obtained a better understanding of the interactions taking place in the complexes and having verified the consistency of our complex model with experimental and theoretical data, we used it for the calculations presented in Chapter 6.

4.2 Bare aluminum surface

Periodic DFT calculations allow us to model extended metal surfaces by using slabs, i.e. stacks of atom layers. However, in order to accurately model the geometric, energetic and electronic properties of the surface, the surface model employed and the calculation parameters need to allow a fine description of the electronic structure. The calculation parameters, such as the k-point grid for the sampling of the reciprocal space and the cutoff energy (Chapter 2), have a computational cost, making necessary the optimization of such parameters, in order to obtain accurate modeling at the lowest computational cost possible. A first optimization of the parameters was carried out in Fatah Chiter's PhD Thesis, as well as in other

works.[56, 117, 118] Calculations performed in this work use higher precision in the FFT grid (PREC = Accurate), as well as a different version of VASP and a more recent version of the dispersion correction to the exchange correlation functional (Grimme’s D2[77, 78]). Thus, the number of layers in the slab, as well as the k-point grids had to be reoptimized. An overview of the properties of the surface model used in this work, and their comparison with experimental data are therefore necessary. In the following, bulk aluminum is first studied in order to obtain the lattice parameter corresponding to our calculation parameters, as well as the cohesive energy E_{coh} , which is needed for the calculations of surface properties in this chapter.

4.2.1 Bulk aluminum

The Al atom has three electrons in its outer electronic shell ($3s^23p^1$), and core electrons are described by the PAW pseudopotential[94, 95]. The solid state aluminum has a face centered cubic crystal structure. It is therefore modeled by a rhombohedral elementary cell containing one Al atom at the origin. It is important for the modeling of bulk metal electronic structure to use a high enough k-point grid. A $15 \times 15 \times 15$ k-point grid is the best choice for the bulk aluminum, as any increase above this k-point density induces variations smaller than the numerical errors. Calculated and experimental values of the conventional lattice constant a_0 and cohesive energy E_{coh} are presented in Table 4.5. The cohesive energy is the energy associated to the interaction between Al atoms in bulk and is defined by :

$$E_{coh} = E^{Al\ bulk} - E_{free}^{Al\ atom} \quad (4.7)$$

With $E^{Al\ bulk}$ the energy of one Al atom in bulk and $E_{free}^{Al\ atom}$ the energy of a free Al atom.

TABLE 4.5: Lattice constant (in Å) and cohesive energy (in eV) of bulk aluminum.

Functional	PBE	PBE-D2	exp.[76]
a_0	4.037	4.008	4.05
E_{coh}	-3.55	-3.81	-3.39

Results for both PBE and PBE-D2 functionals show underestimated lattice constant and overestimated cohesive energy magnitude compared to the experimental values. Results show that the standard PBE functional better models the properties of bulk aluminum,

which is to be expected as the van der Waals forces have no role in bulk metals, and thus the D2 correction introduces errors.

4.2.2 Aluminum surface model

In periodic calculation method, surfaces are modelled by constructing slabs, i.e. a stack of atomic layers separated from its periodic image by vacuum in one dimension (z). In the two other dimensions, the periodic conditions properly simulate the infinite character of the surface. The accuracy with which the slab models the surface depends on the number of atomic layers it is composed of. Finally, the vacuum height must be large enough to avoid interactions between the top of a slab and the bottom of the image slab. In the specific case of a polarized slab, a dipole correction can be employed to correct long-range interaction between image slabs. The two main slab construction methods are detailed below.

Symmetric slab

The symmetric slab approach consists in fixing a number of central layers of the slab and letting layers of both sides of the slab free to relax, leading to two relaxed surfaces (top and bottom of the slab) in one simulation cell. This approach is useful to determine the number of layers required so that the surface properties are no longer affected by the variation of number of layers. A symmetric slab of 5 layers is shown in Figure 4.3 (a).

The surface energy is the excess energy at the surface of a material compared to the bulk. It can be seen as the work associated to the breaking of the bonds between atoms to form the surface and subsequent relaxation of the surface atoms. This value can be calculated for symmetric slabs using the following expression:

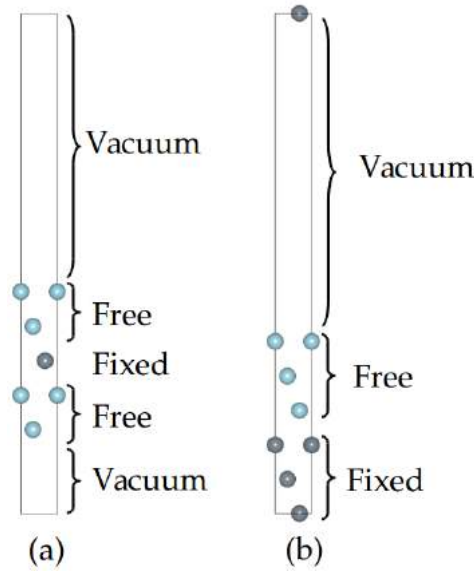
$$\sigma^S = \frac{1}{2}(E_{rlx}^{slab} - nE^{bulk/atom}) \quad (4.8)$$

Where E_{rlx}^{slab} is the total energy of the relaxed slab, $E^{bulk/atom}$ is the total energy of an atom in bulk and n is the number of atoms in the slab. The $\frac{1}{2}$ factor is necessary to take into account only one of the slab surface.

Asymmetric slab

The asymmetric slab approach consists in fixing a given number of bottom layers and letting the top layers free to relax. It is less costly in term of computational resources than the symmetric slab approach, even if more layers are usually needed to get accurate values of the surface energy, and is especially adapted to the case of molecule adsorption, where species is adsorbed only on one side of the slab. An asymmetric slab of 6 layers is shown in Figure 4.3 (b).

FIGURE 4.3: (a) Symmetric Al(111) 5 layer slab. (b) Asymmetric Al(111) 6 layer slab. Blue atoms are set free to relax. Dark grey atoms are fixed.



For an asymmetric slab, the two surfaces of the slab are not equivalent. To calculate the surface energy, the following expressions are thus employed:

$$\sigma^{AS} = \sigma_{urlx}^{AS} - \Delta E_{rlx}^{slab} \quad (4.9)$$

Where σ_{urlx}^{AS} is surface energy of the unrelaxed slab obtained from:

$$\sigma_{urlx}^{SA} = \frac{1}{2}(E_{urlx}^{slab} - nE^{bulk/atom}) \quad (4.10)$$

And ΔE_{rlx}^{slab} is the energy associated to the relaxation of the asymmetric slab given by the following equation:

$$\Delta E_{rlx}^{slab} = E_{rlx}^{slab} - E_{urlx}^{slab} \quad (4.11)$$

Where E_{rlx}^{slab} and E_{urlx}^{slab} are respectively the total energies of the relaxed and unrelaxed slabs.

Interlayer distance variation

The interlayer distance is the distance between two atomic layers. In the case of the Al(111) surface, the creation of surfaces induces a relaxation of the layers near the surface, i.e. a local variation of the interlayer distances compared to the one of the bulk. This variation is quantified by :

$$\Delta d_{i,j} = 100 \times \frac{d_{i,j}^{slab} - d^{bulk}}{d^{bulk}} \quad (4.12)$$

Where $d_{i,j}^{slab}$ is the interlayer distance between the i and j atomic layers after relaxation and d^{bulk} is the bulk interlayer distance.

4.2.3 Flat Al(111) surface

The "flat" surface designates a perfect surface, i.e. without any adatom, vacancies or steps. In Table 4.6 are summarized the different slabs calculated either for testing purposes or to be used as surface model on which molecules or complexes are adsorbed in the following chapters. Because an asymmetric slab is more suitable for the study of adsorption, we focus our tests on asymmetric slabs. Slabs of various dimensions are needed for the work presented in following chapters. Although we adapt the k-point grid in order to keep the k-point density as constant as possible, this density varies slightly depending on the dimensions of the slabs. This allows us to investigate the variations of the calculated properties associated with the variations of the k-point density. All slabs are separated from their images by at least 22 Å of vacuum.

When using the PBE functional, same surface energy is found for the 6 layer slab and the 21 layer slab (0.35 eV/atom). The surface energy of the 4 layer slab is 9 % away from

the one calculated from a 6 layer slab. When using the PBE-D2 functional, a surface energy of 0.48 eV/atom is found for the 3 layer slab, while a value of 0.51 eV/atom is found for a 4 layer slab, even with slightly different k-point densities. The absence of σ variations between them shows that convergence of surface energy with respect to the k-point densities is reached. Globally, the use of dispersion correction better reproduces the experimental value. However, this does not mean that van der Waals forces have any role in such a system, but the dispersion correction could compensate some errors inherent to the model, leading to values closer to the experimental values[117].

The interlayer distance variations are between -1% and 2% and vary highly depending on the parameters, and the comparison of the interlayer distance variations of the different 4 layer slabs shows that small variations of k-point density can modify the interlayer distance variation by up to 0.64 %.

In order to save computational resources and because it leads to surface properties close enough to the experimental properties, slabs of a total of 4 layers including 2 free layers are chosen for Chapter 5. In Chapter 6, where a large calculation cell and costly calculation method (*ab initio* Molecular Dynamics) are employed, a smaller slab has to be used, with a total of 3 layers including 2 free layers.

TABLE 4.6: Al(111) surface properties depending on the number of layers (between parenthesis : number of free layers), the slab size, the k-point grid and the functional. σ the surface energy (in eV/atom and J/m²), $\Delta d_{i,j}$ the change of the interlayer distance between the layers i and j induced by relaxation in % . The top layer is noted 1. Unless indicated otherwise, all slabs are asymmetric.

Functional	PBE			PBE-D2				Exp.
Total Al layers	4	6	21*	3	4	4	4	
Free Al layers	2	3	20*	2	2	2	2	
Slab size	1×1	1×1	1×1	8×8	2×3	3×3	5×6	
k-points grid	15×15×1	15×15×1	12×12×1	2×2×1	7×5×1	5×5×1	3×3×1	
Used in Chap.	test	test	test	6	5	5	5	
σ (eV/atom)	0.38	0.35	0.35	0.48	0.51	0.51	0.51	0.50 ± 0.01 [119]
σ (J/m ²)	0.85	0.80	0.79	1.09	1.15	1.15	1.15	1.15 ± 0.01 [119]
$\Delta d_{1,2}$	+0.70	+1.39	+1.40	+0.48	+1.99	+1.45	+1.35	+1.7 ± 0.3 [120]
$\Delta d_{2,3}$	-0.47	+0.04	+0.56	+0.48	-0.48	-0.51	-0.93	+0.5 ± 0.7 [121]

*Symmetric slab

4.2.4 Defective Al(111) surface: Al-Al(111)

In Chapter 6, we study the adsorption of molecules and complexes on a defective Al surface, in our case an Al(111) surface with an Al adatom, noted Al-Al(111). The Al adatom on the Al(111) surface is located at fcc or hcp threefold sites (Figure 4.4), as it is not stable on other sites (top, bridge). When on an hcp site, the Al atom directly under the adatom is part of the s-1 layer (s being the top surface layer), while on an fcc site, the Al atom directly under the adatom is part of the s-2 layer. The distance between the adatom and the first layer of the Al(111) surface is defined by :

$$\Delta z_{Al\ adatom} = z_{Al\ adatom} - z_{1st\ layer} \quad (4.13)$$

Where $z_{Al\ adatom}$ is the z coordinate of the Al adatom, and $z_{1st\ layer}$ is the average coordinate of the first Al layer under the Al adatom.

The desorption energy of the adatom characterizes the strength of the bonding of the adatom on the surface and is defined by :

$$E_{desorp}^{Al/Al(111)} = E^{Al\ atom} + E^{Al(111)} - E^{Al-Al(111)} \quad (4.14)$$

Where $E^{Al\ atom}$ is the total energy of the free Al atom, $E^{Al(111)}$ is the total energy of the optimized Al(111) slab (without adatom), and $E^{Al-Al(111)}$ is the total energy of the optimized Al(111) slab with adatom.

The QTAIM atomic charge on the adatom $q_{Al\ adatom}$ is calculated from the VASP output by the program developed by the Henkelman group[101].

FIGURE 4.4: Al(111) surface sites. Dark blue atoms are the atoms of the top layer.

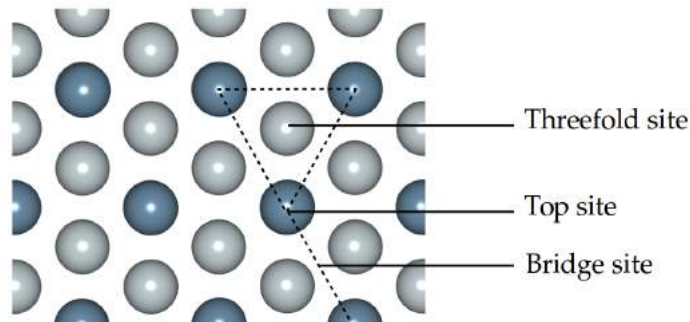


TABLE 4.7: Desorption energy (in eV), QTAIM atomic charge (in e) on the Al adatom, distance of the Al adatom from the Al(111) surface (in Å) depending on the number of layers, the slab size, the k-point grid.

Functional	PBE-D2		
Total Al layers	6	6	3
Free Al layers	2	2	2
Al(111) site	fcc	hcp	hcp
Slab size	5x5	5x5	8x8
k-points grid	3x3x1	3x3x1	2x2x1
Used in Chap.	test	test	6
E_{desorp}	+2.71	+2.75	+2.99
$q_{Al\ adatom}$	+0.11	+0.14	+0.12
$\Delta z_{Al\ adatom}$	+ 2.109	+ 2.072	+ 2.034

Al(111) slabs of 6 layers were used to determine the most stable adsorption site for the Al adatom. This is used for the sole purpose of the subsequent adsorption of qX molecules in Chapter 6, as the Al adatom is very mobile even at low temperature and should not be observed experimentally without being in interaction with at least one other Al adatom (as a dimer) [122, 123]. Desorption energy, atomic charge on the Al adatom and distance between the adatom and the Al(111) surface of tested Al-Al(111) slabs are presented in Table 4.7. The hcp site is determined to be 0.04 eV more stable than the fcc site. The same value was calculated by Chang *et al.* in another DFT study [124]. No stable state with the Al adatom on a top or bridge site is found. The 3 layer slab including two free layers and an adatom at hcp site, later used in Chapter 6, also shows a very strong adsorption of the Al adatom on the Al(111) surface. The QTAIM charge variation on the adatom between the different slabs is not significant, showing a small positive charge in all cases. In all cases distance from Al(111) to the Al adatom is less than the Al(111) bulk interlayer distance calculated with PBE-D2 (2.314 Å).

4.3 Conclusion

In this Chapter, we presented the variations between the properties calculated by our models and the properties determined experimentally or by computationally more costly models. In the case of the complexes and surfaces, we quantified the electronic charges and the interactions taking place in the systems, giving us a better understanding of the origin of their stability. We validated the molecule and complexes models, and chose slabs of 3

to 4 layers to model the Al surface. In the next chapters, the adsorption of molecules and complexes on the Al surface models presented in this chapter will be investigated.

Chapter 5

Adsorption of Hq derivatives on an Al(111) surface

In previous theoretical works on organic corrosion inhibitors, studies of molecules adsorbed on metallic surfaces have been carried out in order to obtain a better understanding of what determines the inhibition corrosion efficiency of molecules, showing that strong chemisorption of the molecule on the surface and the possibility of forming a compact organic monolayer correlate with experimental data showing high inhibition efficiency [45–48, 50, 51, 125–129]. In this chapter, properties of molecules adsorbed on an Al(111) surface, at different surface coverage, are investigated and compared for Hq, HqBr, HqS and HqSH derivatives. Previous works on the Hq molecule [50, 51] have shown that among the neutral forms of the Hq (native, dehydrogenated, hydrogenated and tautomer), the dehydrogenated form leads to the strongest adsorption on the Al(111) surface. Thus, we chose to compare the adsorption of the dehydrogenated forms of all the HqX molecules, i.e. the q, qBr, qS and qSH species, both in vacuum and water. These investigations are carried out in order to determine if and how the X1 and X2 groups at the ortho and para positions relatively to the phenol ring, influence the interaction of the molecules with the Al(111) surface, from low to high coverage (up to full coverage of the surface). The method, consisting in absorbing radical species (dehydrogenated molecules) instead of charged species (deprotonated molecules), is based on the assumption that a metallic surface model acts as a reservoir of electrons, and that the addition or not of an electron does not impact the geometry and charge of the adsorbed molecule. This method is widely used in other works on molecule adsorption on metallic surfaces [45–48, 50, 51, 125–129]. To validate this assumption for our systems, adsorption is also investigated in water using the charged species q^- , qBr^- and qS^{2-} , such as they exist in

solution at basic pH. Geometrical, energetic and electronic properties of the molecules adsorbed on Al(111) are presented and discussed. Special effort is dedicated in investigating the nature of bonds formed between the molecules and the Al(111) surface, using QTAIM topological analysis. This has rarely been applied to such systems, and provides a more accurate description of the bonding of the molecules on the aluminum surface.

5.1 Computational Details

In all the calculations of this chapter, the periodic DFT calculation program VASP [68–70] is employed, with the PBE-D2 functional[65, 66, 77, 78] and PAW pseudopotentials[94, 95].

5.1.1 Calculation parameters for qX species on Al(111) in vacuum

Adsorption modes of the dehydrogenated molecules q, qBr, qS and qSH are obtained at three coverage. The coverage θ_1 ($4.72 \cdot 10^{-3}$ molecule $\cdot \text{\AA}^{-2}$) corresponds to the case of a single molecule adsorbed on an Al(111) surface, with almost no interaction between the qX molecule and its periodic images. The coverage θ_2 ($1.57 \cdot 10^{-2}$ molecule $\cdot \text{\AA}^{-2}$) corresponds to the case of a layer of molecules adsorbed on a Al(111) surface, with interactions between neighbouring qX molecules. Finally, the coverage θ_3 ($2.36 \cdot 10^{-2}$ molecule $\cdot \text{\AA}^{-2}$) is the highest possible coverage of an Al(111) surface by qX molecules (at periodic constraints leading to one molecule per calculation cell). Asymmetric slabs of 4 layers are used, with the two top layers free to relax, and the two bottom layers fixed at the geometry of the 2 middle layers of an optimized 6 layer slab containing 3 free layers. The slabs are obtained from $5 \times 6 \times 1$, $3 \times 3 \times 1$ and $2 \times 3 \times 1$ supercells obtained from the replication of the Al(111) slab unit cell, respectively for θ_1 , θ_2 and θ_3 . About 22.5 \AA separate aluminium slabs from their periodic images, with a minimum of 14.72 \AA vacuum between the adsorbed molecule and the bottom of the above Al(111) slab. The k-point grids are chosen as to keep the k-point density as similar as possible between systems, and close to the one used for bulk Al. To this aim, Monkhorst-Pack grids [130] of $3 \times 3 \times 1$ k-points, $5 \times 5 \times 1$ k-points and $7 \times 5 \times 1$ k-points are chosen for respective coverage of $\theta_1 = 4.72 \cdot 10^{-3}$ molecule $\cdot \text{\AA}^{-2}$, $\theta_2 = 1.57 \cdot 10^{-2}$ molecule $\cdot \text{\AA}^{-2}$ and $\theta_3 = 2.36 \cdot 10^{-2}$ molecule $\cdot \text{\AA}^{-2}$. For each system, optimizations are performed starting from various initial geometries, with molecules parallel and perpendicular to the surface, with the O1 and N1 atoms on different sites of the surface (top, bridge, threefold). A dipole correction

on energy and forces in the direction perpendicular to the surface (IDIPOL = 3, LDIPOL = T) is employed to avoid dipole-dipole interactions between slabs [131, 132]. The local potential with respect to the direction normal to the surface is given for the q and qS molecules at θ_3 coverage respectively in Figure B.1 and B.2 of Appendix B, showing a flat potential in the vacuum region, with a step that is due to the dipole correction. This shows that there is no interactions between the molecule and the bottom layer of the image slab.

5.1.2 Calculation parameters for qX species on Al(111) in water

Adsorption of q and qS molecules on Al(111) is studied for the θ_1 and θ_3 coverage, described above. The implicit solvent model VASPsol[79, 80] is employed to simulate the effect of water, as described in Chapter 2. The geometries optimized in vacuum are used as initial geometries for calculation in solvent, as recommended in the VASPsol documentation [79]. The dipole correction is not included.

5.1.3 Calculation parameters for qX^{n-} ($n = 1$ or 2) species on Al(111) in water

In the case of the calculations in presence of a solvent, in addition to the adsorption of the radical qX species on Al(111), we study the adsorption of qX^{n-} ($n = 1$ or 2) anions on Al(111). To model the charged species, we use the method described in Section 4.1.1 of Chapter 4. As the simulation cell has to be neutral, Na^+ and Mg^{2+} ions are used to compensate the negative charge of the anions. To avoid interactions between the ions and the rest of the system, the ions are positioned at about equal distance between the molecule and the bottom layer of the above slab. The distance between the top layer of a slab and the bottom layer of the above slab is set to about 33 Å, as the ion has to be as isolated from the rest of the system as possible. The geometries optimized in vacuum are used as initial geometries.

5.1.4 Adsorption, interaction, and deformation energies

For qX species

The energy associated to the adsorption of a molecule on a Al(111) slab is the adsorption energy, defined as:

$$E_{ads}^{mol/Al(111)} = E^{mol/Al(111)} - E^{mol} - E^{Al(111)} \quad (5.1)$$

Where $E^{mol/Al(111)}$ is the total energy of the optimized molecule and slab after adsorption, E^{mol} is the total energy of the free molecule and $E^{Al(111)}$ is the total energy of the free optimized Al(111) slab.

The energy associated to the interaction between a molecule and the Al(111) slab is the interaction energy, defined as:

$$E_{int}^{mol/Al(111)} = E^{mol/Al(111)} - E_{SP}^{mol} - E_{SP}^{Al(111)} \quad (5.2)$$

Where E_{SP}^{mol} is the total energy of the molecule layer at the geometry after adsorption and $E_{SP}^{Al(111)}$ is the total energy of the Al(111) slab at the geometry after adsorption.

The molecule deformation energy is defined as:

$$E_{def}^{mol} = E_{SP}^{mol, isolated} - E^{mol} \quad (5.3)$$

Where $E_{SP}^{mol, isolated}$ is the total energy of the isolated molecule at the geometry after adsorption.

The energy associated to the deformation of the molecule is the molecule deformation energy, defined as:

$$E_{def}^{Al(111)} = E_{SP}^{Al(111)} - E^{Al(111)} \quad (5.4)$$

The inter-molecular interaction energy is the interaction of the molecules inside a layer, and is calculated as:

$$E_{int}^{inter-mol} = E_{SP}^{mol} - E_{SP}^{mol\ isolated} \quad (5.5)$$

For qXⁿ⁻ (n = 1 or 2) species

The energy associated to the adsorption of a charged species on a Al(111) slab is the adsorption energy, defined as:

$$E_{ads}^{deprot\ mol/Al(111)} = E^{deprot\ mol/Al(111)+ion} - E^{deprot\ mol+ion} - E^{Al(111)} \quad (5.6)$$

Where $E^{deprot\ mol/Al(111)+ion}$ is the total energy in solvent of the system containing the optimized molecule and slab after adsorption, and the Na⁺ or Mg²⁺ ion; $E^{deprot\ mol+ion}$ is the total energy in solvent of the system composed of the optimized molecule and Na⁺ or Mg²⁺ ion (without the slab); $E^{Al(111)}$ is the total energy in solvent of the free optimized Al(111) slab.

5.2 qX molecules adsorbed on Al(111) in vacuum

Adsorption, interaction, and deformation energies of the adsorbed qX molecules are given for the θ_1 , θ_2 and θ_3 coverage respectively in Table 5.1, 5.3 and 5.5. Adsorption geometries are presented in Figure 5.2, 5.3 and 5.4 and are noted *tilt_{bridge}*, *tilt_{top}*, *paral* and *down*. A *tilt_{bridge}* mode corresponds to the adsorption of the qX molecule on the Al(111) surface by the O1 and N1 atoms, with the O1 atom located on a bridge site of the Al(111) surface, and the N1 atom on a top site, while for a *tilt_{top}* mode, O1 and N1 atoms are both adsorbed on different top sites of the Al(111) surface. In a *paral* mode, the qX molecule is close to parallel to the Al(111) surface, and the molecule is bound to the Al(111) surface by the O1 and N1 atoms, as well as by the C7 atom. In the case of the qS and qSH molecules, the SO₃/SO₃H groups are also bound to the Al(111) surface in *paral* modes. Finally, a *down* mode is found for the qS molecule (not shown in Figure 5.2), which is oriented perpendicularly to the Al(111) surface and is adsorbed solely by the SO₃ group, with each O atoms of the SO₃ group (O2,O3,O4) located on top of the Al atoms constituting a threefold site of Al(111). Corresponding bond lengths of interest are summarized in Table 5.2, 5.4, 5.6, together with the angle formed by

the molecule with the aluminum surface (defined in Figure 5.1). Electronic density properties at the BCPs are shown in Table 5.7 and 5.8 respectively for the extreme cases of the single adsorbed molecule (θ_1) and the compact monolayer (θ_3). For θ_2 , only the *tilt* modes determined to be the most stable for θ_1 was tested. For θ_3 , only *tilt_{bridge}* modes are obtained, due to steric hindrance. Due to the impossibility of finding a stable geometry for the free qS molecule, no adsorption or interaction energies is presented for this molecule.

5.2.1 qX molecules adsorbed on Al(111) at θ_1 coverage in vacuum

For the q molecule, *tilt_{bridge}*, *tilt_{top}* and *paral* adsorption modes are found. The *tilt_{bridge}* mode is the most stable one, with *tilt_{top}* and *paral* modes respectively 0.08 eV and 0.11 eV less stable than the *tilt_{bridge}* mode.

The *tilt_{bridge}* mode adsorption energy ($E_{ads}^{mol/Al(111)} = -3.59$ eV) and interaction energy ($E_{int}^{mol/Al(111)} = -4.57$ eV) show a strong bonding of the molecule with the Al(111) surface, with short bond lengths ($d_{O1-Al1} = 1.909$ Å, $d_{O1-Al2} = 2.034$ Å, $d_{N1-Al2} = 2.043$ Å) and high net charge on the molecule ($Q_{mol} = -1.14$ e). This suggests chemisorption, i.e. formation of chemical bonds between the molecule and the Al(111) surface. The van der Waals interactions also contribute highly to the total interaction of the molecule with the Al(111) surface, with a value of $E_{int}^{mol/Al(111)}(VdW) = -0.66$ eV. Upon adsorption, the molecule is deformed ($E_{def}^{mol} = 0.54$ eV), as well as the Al(111) surface ($E_{def}^{Al(111)} = 0.43$ eV) as an Al atom is slightly pulled out (see Figure 5.2) of the surface.

TABLE 5.1: Total energy difference (the reference is the energy of the $tilt_{bridge}$ mode), adsorption energy, deformation energies, interaction energies, van der Waals contribution to the interaction energy (in eV) and net charge on the molecule (in e) at $\theta_1 = 4.72 \cdot 10^{-3}$ molecule $\cdot \text{\AA}^{-2}$ coverage. All modes are optimized in vacuum. For the qS and qSH molecules, only the most stable $tilt$ and $paral$ modes are presented.

Species	q		qBr		qS		qSH	
	$tilt_{bridge}$	$tilt_{top}$	$tilt_{bridge}$	$tilt_{top}$	$tilt_{bridge}$	$paral$	$tilt_{bridge}$	$paral$
ΔE	0	+0.08	0	-0.03	0	-0.19	0	-0.21
$E_{ads}^{mol}/Al(111)$	-3.59	-3.51	-3.48	-3.51	-3.48	-3.67	-3.70	-3.91
E_{def}^{mol}	+0.54	+0.32	+1.69	+0.35	+0.51	+1.84	+0.51	+2.04
$E_{def}^{Al(111)}$	+0.43	+0.19	+0.27	+0.19	+0.39	+0.28	+0.42	+0.32
$E_{int}^{mol}/Al(111)$	-4.57	-4.01	-5.43	-4.04	-4.39	-5.78	-4.63	-6.29
$E_{int}^{mol}/Al(111)$ (VdW)	(-0.66)	(-0.78)	(-1.26)	(-0.96)	(-0.78)	(-1.50)	(-0.74)	(-1.39)
$E_{int}^{inter-mol}$	+0.02	+0.00	-0.01	+0.00	+0.00	-0.01	+0.00	0.02
Q_{mol}	-1.14	-1.01	-2.02	-1.09	-1.21	-2.13	-1.69	-2.26

In $tilt_{top}$ mode, the bonding of both O1 and N1 atoms on top sites of the Al(111) surface ($d_{O1-Al1} = 1.807 \text{ \AA}$, $d_{N1-Al2} = 2.080 \text{ \AA}$) leads to a weaker interaction energy between the molecule and the Al(111) surface ($E_{int}^{mol/Al(111)} = -4.01 \text{ eV}$) than in the $tilt_{bridge}$ mode ($E_{int}^{mol/Al(111)} = -4.57 \text{ eV}$). There is a lower net charge on the molecule in $tilt_{top}$ ($Q_{mol} = -1.01$) than in $tilt_{bridge}$ ($Q_{mol} = -1.14$). Weaker deformation of the molecule and slab is found in the $tilt_{top}$ mode than in the $tilt_{bridge}$ mode, with values of $E_{def}^{mol} = 0.32 \text{ eV}$ and $E_{def}^{Al(111)} = 0.19 \text{ eV}$ for the $tilt_{top}$ mode. Overall, the molecule is closer to the Al(111) surface in $tilt_{top}$ mode than in $tilt_{bridge}$ mode (see Figure 5.2), leading to stronger van der Waals interaction in $tilt_{top}$ mode ($E_{int}^{mol/Al(111)}(VdW) = -0.78 \text{ eV}$) than in $tilt_{bridge}$ mode ($E_{int}^{mol/Al(111)}(VdW) = -0.66 \text{ eV}$).

The $para$ mode of the q molecule shows stronger interaction energy ($E_{int}^{mol/Al(111)} = -5.43 \text{ eV}$) and stronger deformation of the molecule ($E_{def}^{mol} = 1.69 \text{ eV}$) than for the two $tilt$ modes, as the molecule is bound to the Al(111) surface by three atoms ($d_{O1-Al1} = 1.800 \text{ \AA}$, $d_{N1-Al2} = 1.916 \text{ \AA}$, $d_{C7-Al4} = 2.192 \text{ \AA}$), inducing a high deformation of the pyridine ring (See Figure 5.2). As the molecule is globally closer to the Al(111) surface in the $para$ mode than in the $tilt$ modes, the van der Waals contribution to the adsorption energy is higher in the $para$ mode ($E_{int}^{mol/Al(111)}(VdW) = -1.26 \text{ eV}$) than in the $tilt_{bridge}$ and $tilt_{top}$ modes. The $para$ mode is the mode where the higher net charge is found on the molecule ($Q_{mol} = -2.02 \text{ e}$).

In all three adsorption modes of the q at θ_1 coverage, almost no interaction is found between molecules, which are separated by at least 8 \AA , with values of $E_{int}^{inter-mol}$ ranging from -0.01 eV to $+0.02 \text{ eV}$.

It is clear that for the three adsorption modes described above, the more bonds are formed between the molecule and the Al(111) surface, the strongest is the interaction between the molecule and the Al(111) surface, and the highest is the charge on the molecule. This could evidence an ionic nature of the Al-O and Al-N bonds. To get more insights, topological analysis is presented in Section 5.2.4.

TABLE 5.2: Shortest bond lengths (in Å) between the qX molecules and atoms of the Al(111) surface and angles (α_{mol} in $^\circ$) between the qX molecules and the Al(111) surface. at $\theta_1 = 4.72 \cdot 10^{-3}$ molecule $\cdot \text{Å}^{-2}$. Bonds between atoms At1 and At2 are listed in this table if $d_{At1-At2} < 2.5$ Å. Atom numbers are indicated in Figure 3.1 and 5.2. The angle α_{mol} is formed between the C5-C6 bond and its projection on the Al(111) surface (See Figure 5.1)

Species	q		qBr		qS		qSH	
	<i>tilt_{bridge}</i>	<i>tilt_{top}</i>	<i>tilt_{bridge}</i>	<i>tilt_{top}</i>	<i>tilt_{bridge}</i>	<i>paral</i>	<i>tilt_{bridge}</i>	<i>paral</i>
dO1-Al1	1.909	1.807	1.936	1.818	1.892	1.818	2.057	1.814
dO1-Al2	2.034		2.091		1.977		1.916	
dN1-Al2	2.043	2.080	2.039	2.085	2.002	1.909	2.038	1.919
dC7-Al4		2.192		2.174		2.202		1.919
dO2-Al5						1.930	1.892	2.059
dO3-Al6						1.935	1.923	
dO4-Al						1.895		
α_{mol}	68.5	42.4	79.0	41.3	87.8	10.5	56.6	13.0

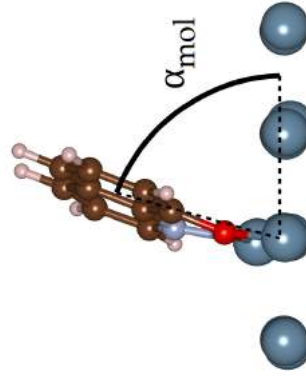
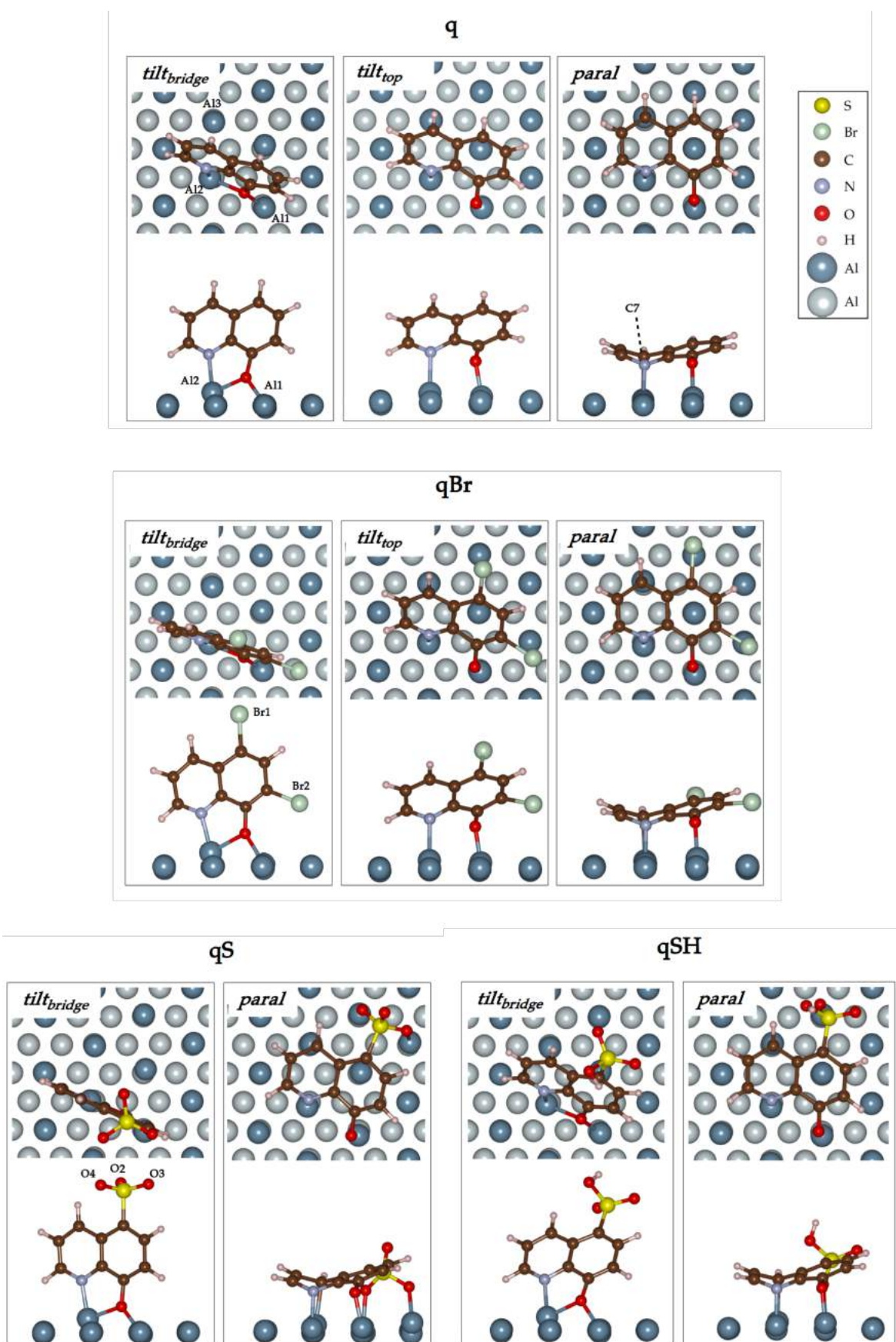


FIGURE 5.1: Angle α_{mol} between the C5-C6 bond (See Figure 3.1) and its projection on the Al(111) surface.

For the qBr molecule, the *paral* mode is 0.16 eV more stable than the *tilt_{top}* mode, and 0.19 eV more stable than the *tilt_{bridge}* mode. The difference compared to the case of the q molecule is due to the higher van der Waals interactions between the molecule and the slab for the qBr molecule compared to the q molecule. The van der Waals interactions contribute highly to the adsorption for modes where the molecule is close to the Al(111) surface, which is the case for the *paral* mode ($\alpha_{mol} = 11.4^\circ$) and to a lesser extent for the *tilt_{top}* mode ($\alpha_{mol} = 41.3^\circ$). Therefore the van der Waals interactions between the Br atoms and the Al(111) surface favors the *paral* and *tilt_{top}* compared to the *tilt_{bridge}* mode, as is shown by the values of the van der Waals contribution to the interaction energy. For the qBr molecule, the van der Waals part of the interaction energy is -0.72 eV stronger in the *paral* mode than in the *tilt_{bridge}* mode. By comparison, for the q molecule, the van der Waals part of the interaction energy is only -0.50 eV stronger in the *paral* mode than in the *tilt_{bridge}* mode.

For the qS and qSH molecules, the *paral* adsorption modes are the most stable. In the case of the qS, the bonding of the O2 and O3 atoms with the Al(111) surface in the *paral* mode ($d_{O2-Al5} = 1.930 \text{ \AA}$, $d_{O3-Al6} = 1.935 \text{ \AA}$) leads to a very high energy difference between the two modes, with a *paral* mode 1.82 eV more stable than the *tilt_{bridge}* mode. As can be seen in (Figure 5.2), the latter is found only with the molecule almost normal to the Al(111) surface, as initial positions with the molecule further tilted converged to the *paral* mode. In the case of the qSH molecule, the *paral* mode is found 0.21 eV more stable than the *tilt_{bridge}* mode, with the bonding of the O2 atom on the Al(111) surface ($d_{O2-Al5} = 2.059 \text{ \AA}$). The *down* mode shows chemical bonds formed by the three O atoms of the SO₃ group of the molecule with the Al atoms of the surface, but the molecule is more weakly adsorbed than the other two modes, and this mode is not investigated further.

FIGURE 5.2: Adsorption geometries of the qX molecules on an Al(111) surface in vacuum for a coverage of $\theta_1 = 4.72 \cdot 10^{-3}$ molecule $\cdot \text{\AA}^{-2}$. Al atoms of the top layer are in blue and Al atoms of the other layers are in grey.



5.2.2 qX molecules adsorbed on Al(111) at θ_2 coverage in vacuum

The θ_2 coverage is chosen because it is the highest coverage where *para* geometries can be obtained. At θ_2 coverage (Tables 5.3 and 5.4, Figure 5.3), the *para* modes are the most stable for all molecules, with energy differences between the *para* and *tilt* modes of 0.08 eV, 0.09 eV, 1.73 eV and 0.11 eV respectively for the q, qBr, qS and qSH molecules. Unlike for the low coverage θ_1 , the q has a more stable *para* mode than *tilt* mode. This could be explained by stabilizing inter-molecular interactions, present at θ_2 but not at θ_1 : the $E_{int}^{inter-mol}$ value quantifies this interaction, and is of -0.21 eV for the *para* mode versus +0.03 eV for the *tilt_{bridge}* mode for the q molecule at θ_2 .

The *para* mode of the qS molecule shows different bonding with the Al(111) surface than for the θ_1 coverage. While the C7-Al bond does not exist at θ_2 ($d_{Al3-C7} = 3.190 \text{ \AA}$), a C9-Al bond is formed ($d_{Al5-C9} = 2.143 \text{ \AA}$). The O1 atom is adsorbed on a bridge site ($d_{O1-Al1} = 1.918 \text{ \AA}$, $d_{O1-Al2} = 2.037 \text{ \AA}$) rather than on a top site like other *para* modes found.

Globally, compared to the θ_1 coverage, while inter-molecular interactions are much higher, with an average difference in $E_{int}^{inter-mol}$ of 0.14 eV, weaker interactions are found between the molecules and the Al(111) surface, with a average difference in $E_{int}^{mol/Al(111)}$ of 0.06 eV.

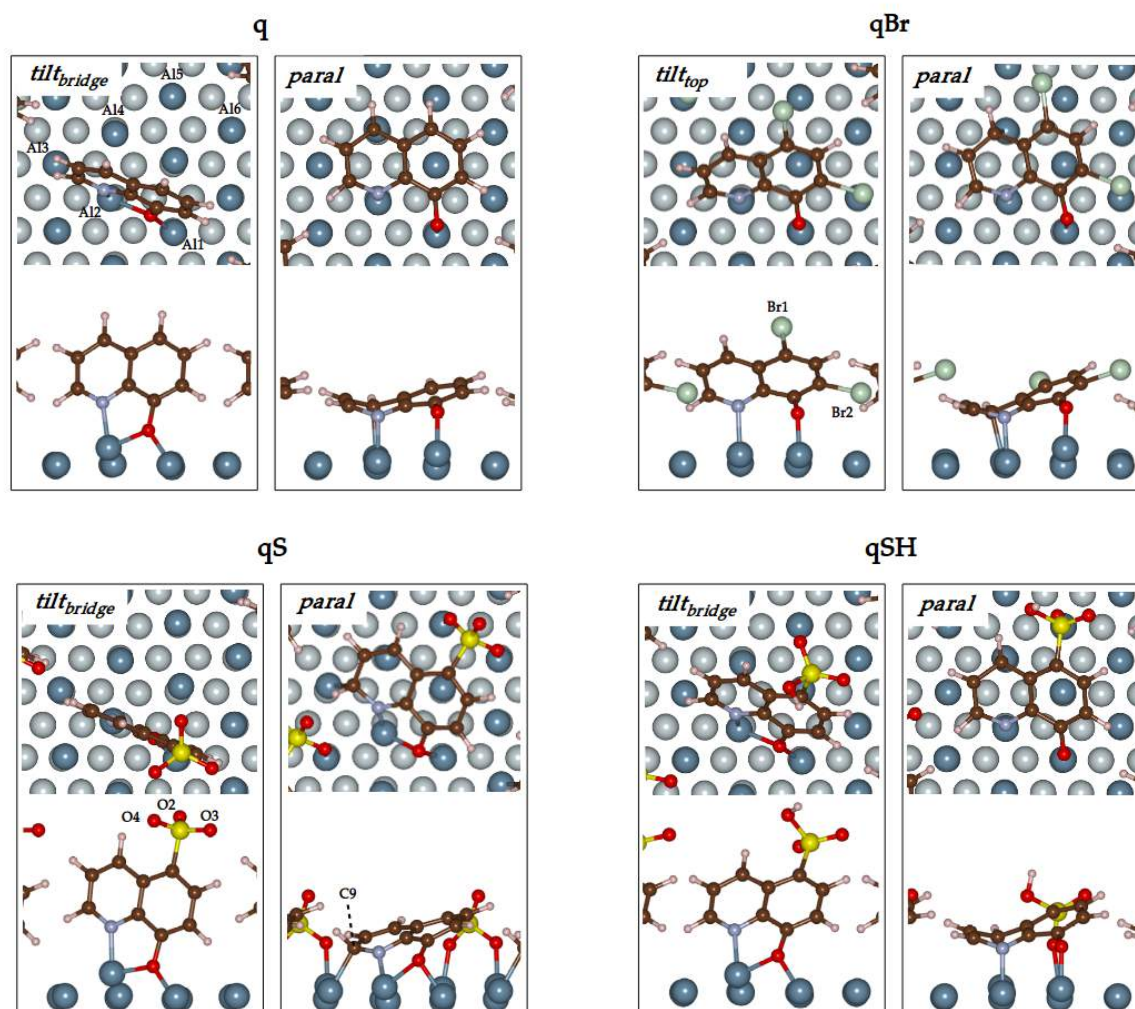
TABLE 5.3: Total energy difference (the reference is the energy of the *tilt_{bridge}* mode), adsorption energy, deformation energies, interaction energies, Van de Waals contribution to the interaction energy (in eV) and net charge on the molecule (in e) at $\theta_2 = 1.57 \cdot 10^{-2} \text{ molecule} \cdot \text{\AA}^{-2}$ coverage. All modes are optimized in vacuum. For the qS and qSH molecules, only the most stable *tilt* and *para* modes are presented.

Species	q		qBr		qS		qSH	
	<i>tilt_{bridge}</i>	<i>para</i>	<i>tilt_{top}</i>	<i>para</i>	<i>tilt_{bridge}</i>	<i>para</i>	<i>tilt_{bridge}</i>	<i>para</i>
ΔE	0	-0.08	0	-0.09	0	-1.73	0	-0.11
$E_{ads}^{mol/Al(111)}$	-3.54	-3.62	-3.54	-3.63			-3.75	-3.86
E_{def}^{mol}	+0.55	+1.69	+0.38	+2.07			+0.53	+2.26
$E_{def}^{Al(111)}$	+0.42	+0.26	+0.20	+0.32			+0.41	+0.25
$E_{int}^{mol/Al(111)}$	-4.54	-5.37	-3.94	-5.66			-4.59	-6.31
$E_{int}^{mol/Al(111)}(VdW)$	-0.64	-1.24	-0.97	-1.46			-0.73	-1.36
$E_{int}^{inter-mol}$	+0.03	-0.21	-0.17	-0.36			-0.09	-0.06
Q_{mol}	-1.14	-2.02	-1.17	-2.18	-1.56	-3.21	-1.31	-2.26

TABLE 5.4: Shortest bond lengths (in Å) between the qX molecules and the Al(111) surface and angles (α_{mol} in °) between the qX molecules and the Al(111) surface at $\theta_2 = 1.57 \cdot 10^{-2}$ molecule \cdot Å $^{-2}$ coverage. Bonds between atoms At1 and At2 are listed in this table if $d_{At1-At2} < 2.5$ Å. Atom numbers are indicated in Figures 3.1 and 5.3. The angle α_{mol} is formed between the C5-C6 bond and its projection on the Al(111) surface (See Figure 5.1)

Species	q		qBr		qS		qSH	
	$tilt_{bridge}$	$paral$	$tilt_{top}$	$paral$	$tilt_{bridge}$	$paral$	$tilt_{bridge}$	$paral$
d_{O1-Al1}	1.911	1.807	1.821	1.824	1.902	1.918	1.914	1.822
d_{O1-Al2}	2.017				1.942	2.037	2.045	
d_{N1-Al2}	2.025	1.919	2.076	1.928	1.996	1.889	2.026	1.923
d_{C9-Al3}						2.143		
d_{C7-Al4}		2.186		2.137				2.180
d_{O2-Al5}						1.964		2.023
d_{O3-Al6}						1.924		
α_{mol}	73.6	11.8	43.3	8.84	80.4	19.7	56.5	14.9

FIGURE 5.3: Adsorption geometries of the qX molecules on an Al(111) surface in vacuum for a coverage of $\theta_2 = 1.57 \cdot 10^{-2}$ molecule \cdot Å $^{-2}$. Al atoms of the top layer are in blue and Al atoms of the other layers are in grey.



5.2.3 qX molecules adsorbed on Al(111) at θ_3 coverage in vacuum

The θ_3 coverage is the maximum possible coverage, i.e. corresponds to the smallest simulation cell in which a qX molecule can fit. At coverage $\theta_3 = 2.36 \cdot 10^{-2}$ molecule $\cdot \text{\AA}^{-2}$, all four qX molecules show only $tilt_{bridge}$ modes. It is clear on Figure 5.4 that the geometrical restrictions due to the high coverage do not allow *para* modes. The coverage also affects the $tilt$ modes, as only a $tilt_{bridge}$ mode is found for the qBr molecule, even when using as initial geometry the $tilt_{top}$ mode from θ_1 coverage. All molecules show strong adsorption energies, with values of $E_{ads}^{mol/Al(111)}$ ranging from -3.52 eV to -4.12 eV. The energetic and charge values are very close for all molecules, which is consistent with the similar geometries found for all molecules (Table 5.6). The inter-molecular interactions for the qSH ($E_{int}^{inter-mol} = -0.40$ eV) molecule are significantly stronger than those of the q ($E_{int}^{inter-mol} = -0.06$ eV) and qBr ($E_{int}^{inter-mol} = -0.01$ eV) molecules. This can be explained by the interaction between the O2 atom of the SO₃H group and the H atom of the SO₃H group of the neighbouring molecule. Negative ($q_{O_2} = -1.27$ e) and positive ($q_H = +0.65$ e) charges are found respectively on the O and H atoms, and the corresponding O-H distance ($d_{O_2-H} = 2.738$ \AA) is in the range of a typical hydrogen bond. QTAIM analysis performed in Section 5.2.4 also suggests the existence of a hydrogen bond. This seems to be also true for the qS molecule at θ_3 , where a O-H distance of 2.373 \AA is found.

TABLE 5.5: Adsorption energy, deformation energies, interaction energies (in eV) and net charge on the molecule (in e) at $\theta_3 = 2.36 \cdot 10^{-2}$ molecule $\cdot \text{\AA}^{-2}$ coverage. All modes are optimized in vacuum.

Species	q $tilt_{bridge}$	qBr $tilt_{bridge}$	qS $tilt_{bridge}$	qSH $tilt_{bridge}$
$E_{ads}^{mol/Al(111)}$	-3.71	-3.52		-4.12
E_{def}^{mol}	+0.56	+0.54		+0.58
$E_{def}^{Al(111)}$	+0.42	+0.44		+0.43
$E_{int}^{mol/Al(111)}$	-4.63	-4.50		-4.72
$E_{int}^{mol/Al(111)}(VdW)$	-0.66	-0.78		-0.70
$E_{int}^{inter-mol}$	-0.06	-0.01		-0.40
Q_{mol}	-1.31	-1.33	-1.70	-1.31

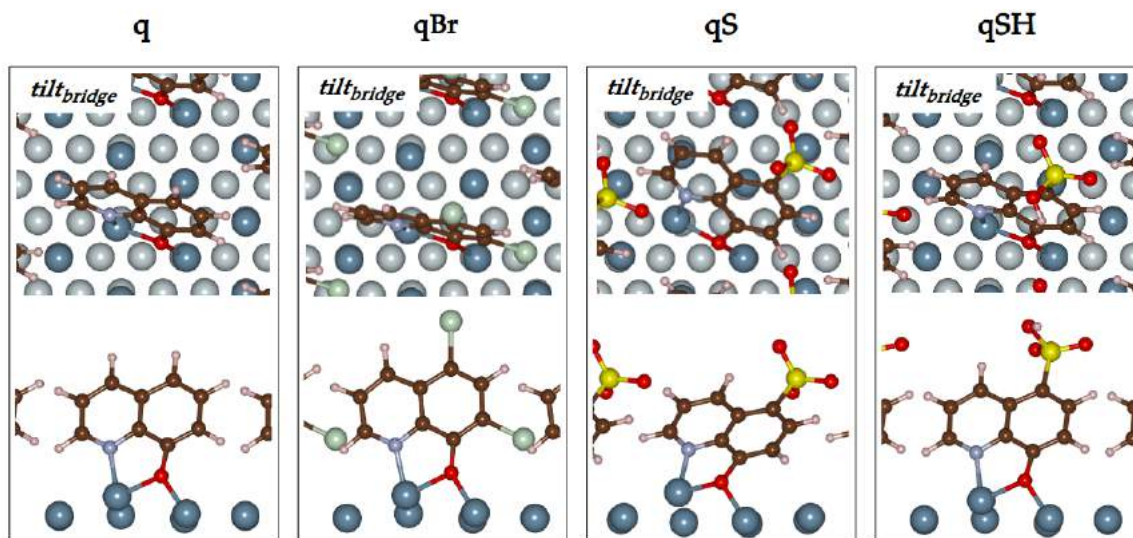
Overall, the interactions between the molecules of the organic layer contribute very weakly to the global stability of the compact monolayer for the q and qBr molecules, with the $E_{int}^{inter-mol}$ term being at most equal to 1% of the total interaction energy $E_{int} = E_{int}^{mol/Al(111)} + E_{int}^{inter-mol}$. For the qSH molecule, the inter-molecular interactions correspond to 8% of the

total interaction energy, due to the hydrogen bonds between molecules

TABLE 5.6: Length of bonds (in Å) between the qX molecules and the Al(111) surface and angles (α_{mol} in $^\circ$) between the qX molecules and the Al(111) surface at $\theta_3 = 2.36 \cdot 10^{-2}$ molecule $\cdot \text{Å}^{-2}$. Bonds between atoms At1 and At2 are listed in this table if $d_{At1-At2} < 2.5 \text{ Å}$. Atom numbers are indicated in Figure 3.1 and 5.2. The angle α_{mol} is formed between the C5-C6 bond and its projection on the Al(111) surface (See Figure 5.1)

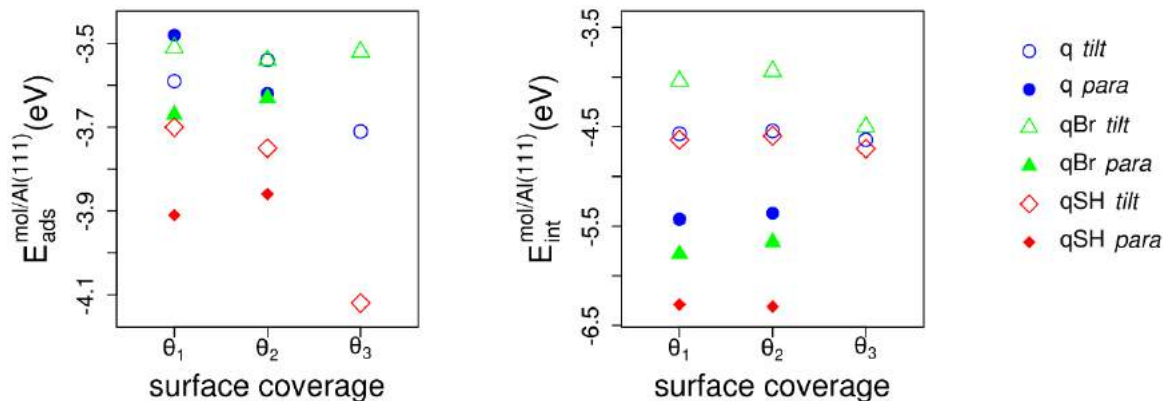
Species	q <i>tilt_{bridge}</i>	qBr <i>tilt_{bridge}</i>	qS <i>tilt_{bridge}</i>	qSH <i>tilt_{bridge}</i>
d_{O1-Al1}	1.902	1.933	1.909	1.908
d_{O1-Al2}	2.028	2.056	1.962	2.033
d_{N1-Al2}	2.018	2.021	1.984	2.021
α_{mol}	66.3	79.2	44.7	61.3

FIGURE 5.4: Adsorption geometries of the qX molecules on an Al(111) surface in vacuum for a coverage of $\theta_3 = 2.36 \cdot 10^{-2}$ molecule $\cdot \text{Å}^{-2}$. Al atoms of the top layers are in blue and Al atoms of the other layers are in grey.



The study of the adsorption of the q, qBr, qS and qSH molecules in vacuum shows that all four molecules adsorb strongly on Al(111) whatever the coverage and form stable compact layers (θ_3 coverage). The adsorption and interaction energies $E_{ads}^{mol/Al(111)}$ and $E_{int}^{mol/Al(111)}$ for the q, qBr and qSH molecules for θ_1 , θ_2 and θ_3 coverage are summarized in Figure 5.5. In the case of the adsorption energy, it is clear that the *para* geometry is more stable than the *tilt* geometry for all case, except for q at θ_1 coverage, where the most stable mode corresponds to a *tilt* geometry. It is also clear that at θ_3 coverage, the inter-molecular interactions leads to a much stronger adsorption of the qSH than the q and qBr molecules. These differences are due to the X groups at ortho and para positions of the phenol ring influence the structure of the organic layer, both by interacting with the surface and with neighbouring molecules.

FIGURE 5.5: Adsorption of the qX molecules on Al(111). On the left: adsorption energies. On the right: interaction energies. Energies in eV.



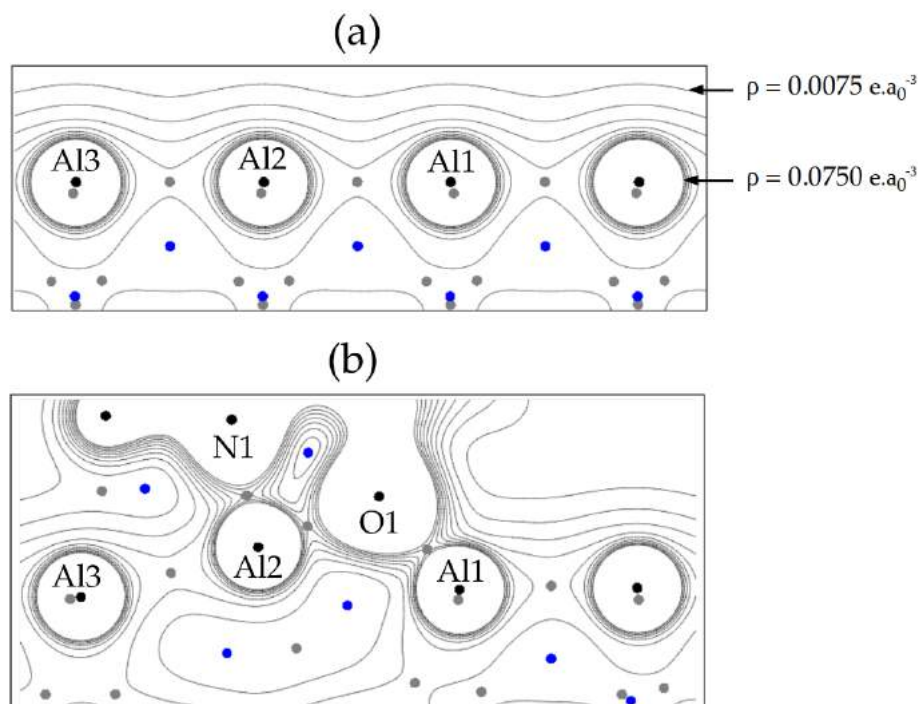
5.2.4 QTAIM analysis of the bonding of qX molecules on Al(111) in vacuum

In the work of Wang *et al.* [133], QTAIM analysis on bonds formed between molecules and an aluminum surface was employed to discuss the nature of the bonding. In this work, QTAIM analysis is performed on the most stable tilted and parallel modes of the adsorbed qX molecules at θ_1 and θ_3 coverage. A cross section of the charge density of the $\text{tilt}_{\text{bridge}}$ mode of the q molecule at θ_1 coverage is shown in Figure 5.6.

The adsorption of the molecule induces a reorganisation of the charge density around the Al atoms, with saddle points of the charge density between Al atoms and O1 and N1 atoms corresponding to BCPs of the Al-O and Al-N bonds. At these points, the values of charge density ($0.066 \text{ e} \cdot a_0^{-3}$ for O1-Al1) are higher than the values at saddle points between two adjacent Al atoms ($\rho < 0.038 \cdot a_0^{-3}$), but much lower than values between two atoms of the molecules i.e. covalent bonds. As an example, the charge density at BCP of the C1-C2 bond is equal to $0.321 \text{ e} \cdot a_0^{-3}$.

Charge density properties at BCPs (Bond Critical Points) of the bonds of interest are summarized in Table 5.7 for θ_1 and in Table 5.8 for θ_3 . At BCP of O1-Al1, O1-Al2, N1-Al2 and C7-Al4 bonds, low values of the charge density ρ_{bcp} are found, ranging from 0.048 to $0.086 \text{ e} \cdot a_0^{-3}$, the Laplacian of the charge density is always positive, with values of $\Delta\rho_{\text{bcp}}$ ranging from 0.100 to $0.550 \text{ e} \cdot a_0^{-5}$. These values indicate closed shell interactions, and are close to those found for the free complexes (Chapter 3). High positive charges are calculated on the Al atoms bound to the molecules (For example: $q_{\text{Al2}} = +0.95 \text{ e}$ for the $\text{tilt}_{\text{bridge}}$ mode of the q at θ_3), which is consistent with a strong ionic nature of the O-Al and N-Al bonds.

FIGURE 5.6: Charge density (in $e \cdot a_0^{-3}$) isocontours of a cross section of (a) the top layer of the free Al(111) surface (b) the q molecule adsorbed on an Al(111) surface ($tilt_{bridge}$ mode) for a coverage of $\theta_1 = 4.72 \cdot 10^{-3}$ molecule $\cdot \text{\AA}^{-2}$. Maxima, saddle points and minima of the charge density are shown respectively as black, grey and blue points. Isocontours correspond to charge density values of 0.0075 to $0.0750 e \cdot a_0^{-3}$, with steps of $0.0075 e \cdot a_0^{-3}$, from the vacuum to the nuclei. a_0 is the Bohr radius ($a_0 = 0.529 \text{\AA}$)



The nature of the bond can be further investigated using the $\frac{|V_{bcp}|}{G_{bcp}}$ and $\frac{H_{bcp}}{\rho_{bcp}}$ descriptors. For the O-Al and N-Al bonds, the $\frac{|V_{bcp}|}{G_{bcp}}$ descriptor is very close to 1, and $\frac{H_{bcp}}{\rho_{bcp}}$ close to 0. This indicates that these bonds are at the limit between purely ionic bonding and intermediate bonding, which includes dative bonding.[89, 134] With the exception of some of the O1-Al2 bonds, the values of the descriptors show a slight covalent contribution to the bonding ($\frac{|V_{bcp}|}{G_{bcp}} > 1, \frac{H_{bcp}}{\rho_{bcp}} < 0$). The C7-Al4 bonds show higher covalent contribution than the other bonds, suggesting that the nature of these bonds is intermediate between ionic and covalent.

TABLE 5.7: Charge density (in $e \cdot a_0^{-3}$), Laplacian of Charge Density (in $e \cdot a_0^{-5}$), $\frac{|V|}{G}$ and $\frac{H}{\rho}$ (in hartree $\cdot a_0^{-3}$) QTAIM descriptors at BCPs of the O-Al, N-Al and C-Al bonds in qX adsorption modes on the Al(111) surface at $\theta_1 = 4.72 \cdot 10^{-3}$ molecule $\cdot \text{\AA}^{-2}$ coverage

Species	q		qBr		qS		qSH	
	<i>tilt_{bridge}</i>	<i>paral</i>	<i>tilt_{top}</i>	<i>paral</i>	<i>tilt_{bridge}</i>	<i>paral</i>	<i>tilt_{bridge}</i>	<i>paral</i>
BCP O1-Al1								
ρ_{bcp}	0.066	0.089	0.082	0.086	0.070	0.086	0.065	0.085
$\Delta\rho_{bcp}$	0.336	0.526	0.530	0.550	0.353	0.537	0.327	0.533
$\frac{ V_{bcp} }{G_{bcp}}$	1.032	1.050	1.001	1.019	1.050	1.022	1.034	1.020
$\frac{H_{bcp}}{\rho_{bcp}}$	-0.043	-0.078	-0.002	-0.031	-0.066	-0.035	-0.044	-0.033
BCP O1-Al2								
ρ_{bcp}	0.051				0.058		0.049	
$\Delta\rho_{bcp}$	0.253				0.295		0.213	
$\frac{ V_{bcp} }{G_{bcp}}$	0.985				1.007		1.016	
$\frac{H_{bcp}}{\rho_{bcp}}$	0.018				-0.009		-0.017	
BCP N1-Al2								
ρ_{bcp}	0.060	0.079	0.055	0.078	0.067	0.080	0.061	0.078
$\Delta\rho_{bcp}$	0.256	0.377	0.205	0.373	0.270	0.391	0.248	0.381
$\frac{ V_{bcp} }{G_{bcp}}$	1.073	1.097	1.097	1.094	1.118	1.092	1.093	1.088
$\frac{H_{bcp}}{\rho_{bcp}}$	-0.074	-0.128	-0.100	-0.124	-0.135	-0.125	-0.075	-0.117
BCP C7-Al4								
ρ_{bcp}		0.057		0.058		0.055		0.056
$\Delta\rho_{bcp}$		0.111		0.129		0.100		0.116
$\frac{ V_{bcp} }{G_{bcp}}$		1.345		1.309		1.370		1.318
$\frac{H_{bcp}}{\rho_{bcp}}$		-0.259		-0.248		-0.266		-0.243

In addition to the O-Al, N-Al and C-Al bonds presented in Table 5.7 and 5.8, bond paths of lower ρ_{bcp} are found between the molecule and the Al(111) surface with a maximum ρ_{bcp} of $0.021 e \cdot a_0^{-3}$, involving the C, H and Br atoms. The very low net charges on these atoms exclude the possibility of ionic bonding, suggesting van der Waals bonding. At θ_3 coverage, bond paths between neighbouring molecules are also found, with a ρ_{bcp} maximum of $0.017 e \cdot a_0^{-3}$, involving C, O, H and Br atoms. In the case of qSH at θ_3 , a bond formed between the SO_3H groups of neighbouring molecules bond was discussed in Section 5.2.3 and associated to a hydrogen bond. The energy associated to this hydrogen bond can be calculated [135] ($E_{HB} = \frac{1}{2}V_{bcp}$). The energy of the bond is found to be of $E_{HB} = -0.23$ eV, which is close to the upper limit associated to such hydrogen bonds (-0.21 eV) [136].

TABLE 5.8: Charge density (in $e \cdot a_0^{-3}$), Laplacian of Charge Density (in $e \cdot a_0^{-5}$), $\frac{|V|}{G}$ and $\frac{H}{\rho}$ (in hartree $\cdot a_0^{-3}$) QTAIM descriptors at BCPs of the O-Al, N-Al and C-Al bonds in qX adsorption modes on the Al(111) surface at $\theta_3 = 2.36 \cdot 10^{-2}$ molecule $\cdot \text{\AA}^{-2}$ coverage

Species	q $tilt_{bridge}$	qBr $tilt_{bridge}$	qS $tilt_{bridge}$	qSH $tilt_{bridge}$
BCP O1-Al1				
ρ_{bcp}	0.066	0.060	0.069	0.051
$\Delta\rho_{bcp}$	0.348	0.318	0.338	0.335
$\frac{ V_{bcp} }{G_{bcp}}$	1.026	1.000	1.055	1.033
$\frac{H_{bcp}}{\rho_{bcp}}$	-0.035	0.000	-0.071	-0.044
BCP O1-Al2				
ρ_{bcp}	0.052	0.048	0.061	0.051
$\Delta\rho_{bcp}$	0.249	0.230	0.313	0.234
$\frac{ V_{bcp} }{G_{bcp}}$	0.997	0.988	1.014	1.013
$\frac{H_{bcp}}{\rho_{bcp}}$	0.004	0.014	-0.019	-0.015
BCP N1-Al2				
ρ_{bcp}	0.063	0.063	0.070	0.063
$\Delta\rho_{bcp}$	0.256	0.270	0.281	0.268
$\frac{ V_{bcp} }{G_{bcp}}$	1.104	1.083	1.132	1.086
$\frac{H_{bcp}}{\rho_{bcp}}$	-0.118	-0.097	-0.153	-0.100

5.3 qX and qX^{n-} ($n = 1$ or 2) species adsorbed on Al(111) in water

The adsorption modes of the q , qS , q^- , qBr^- and qS^{2-} species on Al(111) are calculated in water. Unlike the case of the qS molecule, the free qS^{2-} molecule energy could be calculated, allowing us to obtain adsorption, interaction, and deformation energies of the adsorbed qS^{2-} molecule. Adsorption, interaction, and deformation energies of the adsorption modes, as well as the net charge on the molecule for the adsorbed q and qS molecules in water are presented in Table 5.9, and corresponding bond lengths are given in Table 5.10. Energy properties of the adsorption modes as well as the total charge on the molecule for the adsorbed q^- , qBr^- and qS^{2-} anions in water are presented in Table 5.11 and 5.13 respectively for the θ_1 and θ_3 coverage. The length of the bonds formed between the molecules and the Al(111) surface are given in Table 5.2 and 5.6 respectively for θ_1 and θ_3 coverage. Corresponding geometries are presented in Figure 5.7 and 5.8 respectively.

5.3.1 qX molecules adsorbed on Al(111) at θ_1 and θ_3 coverage in water

For the q molecule at θ_1 coverage, the energy difference between the two modes is found similar to the one in vacuum (0.12 eV in water and 0.11 eV in vacuum), with the *tilt_{bridge}* mode more stable in both cases (Table 5.9). The adsorption energy is found lower in magnitude in water than in vacuum by 0.28 ± 0.01 eV for both *tilt_{bridge}* and *paral* modes. This is the consequence of the free q molecule being more stabilized by the presence of water (by about -0.4 eV) than the total system (stabilized by about -0.1 eV). The charge on the molecule is slightly lower in water (-1.00 e) than in vacuum (-1.14 e) for the *tilt_{bridge}* mode and is similar in both cases (-2.02 e and -2.06 e) for the *paral* mode. For the *tilt_{bridge}* mode, slightly shorter bond lengths are found in water compared to in vacuum, while in the *paral* mode, slightly longer bond lengths are found in water compared to in vacuum. For the qS molecule at θ_1 coverage, the *paral* mode is found 0.47 eV more stable than the *tilt_{bridge}* mode. The difference is much smaller than in vacuum ($\Delta E = -1.82$ eV), due to the stabilization of the *tilt_{bridge}* mode by water (about 1.6 eV versus about 0.2 eV for the *paral* mode). For the *tilt* mode, higher net charge is found on the qS molecule in water (-1.95 e) than in vacuum (-1.69 e), while for the *paral* mode, similar charges are found (-3.11 e and -3.03 e). The qS molecule is found globally further away from the surface when in water than in vacuum, with a maximum difference in bond lengths of 0.028 Å for the *tilt_{bridge}* mode and 0.034 Å for the *paral* mode (Table 5.10). For the *paral* mode of this molecule, the bonds lengths show that the SO₃ group is less strongly adsorbed on the Al(111) surface in the presence of water than in vacuum, which is consistent with the hydrophilicity of this group [137].

TABLE 5.9: Total energy difference (the reference is the energy of the *tilt_{bridge}* mode), adsorption energy (in eV) and net charge on the molecule (in e) at $\theta_1 = 4.72 \cdot 10^{-3}$ molecule \cdot Å⁻² and $\theta_3 = 2.36 \cdot 10^{-2}$ molecule \cdot Å⁻² coverage. All modes are optimized in water.

Coverage	θ_1				θ_3	
	q		qS		q	qS
Species	<i>tilt_{bridge}</i>	<i>paral</i>	<i>tilt_{bridge}</i>	<i>paral</i>	<i>tilt_{bridge}</i>	<i>tilt_{bridge}</i>
ΔE	0	+0.12	0	-0.47		
$E_{ads}^{mol/Al(111)}$	-3.31	-3.19			-3.40	
Q_{mol}	-1.00	-2.06	-1.95	-3.11	-1.16	-1.89

At θ_3 coverage, the adsorption energy of the q molecule is 0.31 lower in magnitude in water than in vacuum. Much like for θ_1 the charge on the molecule in water is lower than

in vacuum for q (respectively -1.16 e and -1.31 e) and higher than in vacuum for qS (respectively -1.89 e and -1.70 e). The geometry of the q molecule is very similar between the vacuum and water cases (maximum variation of 0.011 Å). The qS molecule is oriented slightly differently in water ($\alpha_{mol} = 58.7^\circ$), compared to its orientation in vacuum ($\alpha_{mol} = 44.7^\circ$), with the SO_3 group directed towards the water, whereas is the case of vacuum, the SO_3 group is closer to the image molecule. This again is due to the stabilizing effect of the solvent on the SO_3 group. These results show that the addition of a solvant model simulating the effect of water has few effect on the q molecule, but higher effect on the qS , which includes a group interacting strongly with water (SO_3).

TABLE 5.10: Length of bonds (in Å) between the qX molecules and the Al(111) surface and the Al(111) surface and angles (α_{mol} in °) between the qX molecules and the Al(111) surface at $\theta_1 = 4.72 \cdot 10^{-3}$ molecule \cdot Å $^{-2}$ and $\theta_3 = 2.36 \cdot 10^{-2}$ molecule \cdot Å $^{-2}$. Geometries optimized in water. Bonds between atoms At1 and At2 are listed in this table if $d_{At1-At2} < 2.5$ Å. Atom numbers are indicated in Figure 3.1 and 5.2. The angle α_{mol} is formed between the C5-C6 bond and its projection on the Al(111) surface (See Figure 5.1)

Coverage	θ_1				θ_3	
	q		qS		q	qS
Species	$tilt_{bridge}$	$paral$	$tilt_{bridge}$	$paral$	$tilt_{bridge}$	$tilt_{bridge}$
d_{O1-Al1}	1.901	1.813	1.903	1.831	1.900	1.890
d_{O1-Al2}	2.020		2.005		2.029	1.991
d_{N1-Al2}	2.036	1.923	2.027	1.918	2.029	2.011
d_{C7-Al4}		2.188		2.203		
d_{O2-Al5}				1.954		
d_{O3-Al6}				1.969		
α_{mol}	68.8	10.8	69.6	9.7	59.2	58.7

5.3.2 qX^{n-} ($n = 1$ or 2) species adsorbed on Al(111) at θ_1 coverage in water

First the distance between the molecule, the ion, and the image slab is checked to be sufficient as only small total energy variation (0.01 eV) is found when increasing these distances (Appendix B, Table B.2). For the q^- molecule in water, a strong adsorption is found for both $tilt_{bridge}$ and $paral$ modes, with respective adsorption energies of -2.45 eV and -2.43 eV (Table 5.11). In the $tilt_{bridge}$ mode, the value of the net charge on the molecules (-1.06 e) indicates that almost no charge transfer takes place between the Al(111) surface and the deprotonated molecule ($\Delta Q_{mol} = -0.06$ e). The charge transfer corresponds to the charge variation on the molecule upon adsorption, with the reference being the net charge on the free anion (-1 e or

-2 e). In the *paral* mode, a high net charge is found on the molecule, with a value of $Q_{mol} = -2.11 e$ ($\Delta Q_{mol} = -1.11 e$).

TABLE 5.11: Total energy difference (the reference is the energy of the *tilt_{bridge}* mode), adsorption energy (in eV), net charge on the molecule and charge transfer from the Al(111) surface to the molecule (in e) at $\theta_1 = 4.72 \cdot 10^{-3} \text{ molecule} \cdot \text{\AA}^{-2}$ coverage. All modes are optimized in water.

Species	q^-		qBr^-	qS^{2-}	
	<i>tilt_{bridge}</i>	<i>paral</i>	<i>paral</i>	<i>tilt_{bridge}</i>	<i>paral</i>
ΔE	0	+0.02		0	-0.26
$E_{ads}^{deprot\ mol / Al(111)}$	-2.45	-2.43	-2.50	-2.38	-2.64
Q_{mol}	-1.06	-2.11	-2.23	-2.07	-3.22
ΔQ_{mol}	-0.06	-1.11	-1.23	-0.07	-1.22

TABLE 5.12: Length of bonds (in \AA) between the qX^{n-} ($n = 1$ or 2) molecules and the Al(111) surface and angles (α_{mol} in $^\circ$) between the qX molecules and the Al(111) surface at $\theta_1 = 4.72 \cdot 10^{-3} \text{ molecule} \cdot \text{\AA}^{-2}$ in water. Bonds between atoms At1 and At2 are listed in this table if $d_{At1-At2} < 2.5 \text{\AA}$. Atom numbers are indicated in Figure 3.1 and 5.7. The angle α_{mol} is formed between the C5-C6 bond and its projection on the Al(111) surface (See Figure 5.1)

Species	q^-		qBr^-	qS^{2-}	
	<i>tilt_{bridge}</i>	<i>paral</i>	<i>paral</i>	<i>tilt_{bridge}</i>	<i>paral</i>
d_{O1-Al1}	1.903	1.818	1.828	1.908	1.838
d_{O1-Al2}	2.024			2.020	
d_{N1-Al2}	2.041	1.927	1.933	2.039	1.926
d_{C7-Al4}		2.187	2.174		2.208
d_{O2-Al5}					1.977
d_{O3-Al6}					2.000
α_{mol}	72.2	10.5	10.5	69.6	9.7

For the qBr^- molecule, an optimized geometry of a *tilt* mode could not be obtained. In the *paral* mode, a high net charge on the molecule (-2.23 e) is found.

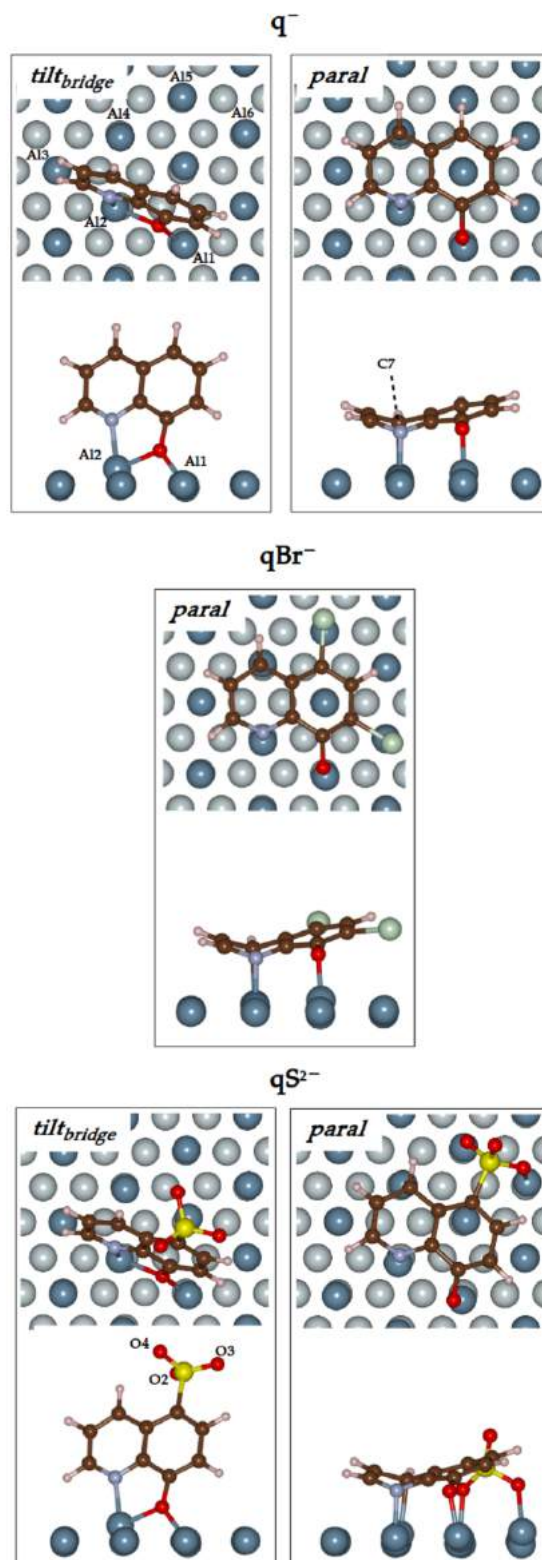
For the qS^{2-} molecule, the *paral* mode is found -0.26 eV more stable than the *tilt_{bridge}* mode, with respective adsorption energy values of -2.64 eV and -2.38 eV. Similarly to the q^- molecule, a very weak charge transfer is found in the *tilt_{bridge}* mode (-0.07 e), while a strong charge transfer is found for the *paral* mode (-1.22 e).

Globally, the comparison of these results with the ones obtained for the q and qS radicals (Table 5.1 and Table 5.9) shows less energy difference between the *tilt* and *paral* modes for both the q^- ($\Delta E = +0.02$ eV for q^- versus $\Delta E = +0.11$ eV for q) and qS^{2-} ($\Delta E = -0.26$ eV for qS^{2-} versus $\Delta E = -0.47$ eV for qS) molecules. The values of adsorption energies shows weaker adsorption than for the qX molecules, but still shows overall strong adsorption. The

net charge on the molecule is found to be similar from the case of qX to the case of qX^{n-} ($n = 1$ or 2), with the maximum variation being obtained for the $tilt_{bridge}$ mode of the qS^{2-} molecule, where the molecule is 0.12 e more charged for qS^{2-} than for qS . Finally, similar bond lengths are found for qX^{n-} ($n = 1$ or 2) and qX , with the exception of the bonds formed between the SO_3 group and Al(111), which are slightly longer for qS^{2-} than for qS (up to 0.031 Å).

Overall, the adsorption geometries and charges on the molecules shows very weak differences with the case of the neutral qX species, indicating that the adsorption of neutral species qX is a good approximation of the adsorption of charged qX^{n-} ($n = 1$ or 2) species. The adsorption energy, however, is different in both cases. The study of the adsorption of the anion is thus useful to verify if the adsorption is a stabilizing process.

FIGURE 5.7: Adsorption modes of the $q\chi^{n-}$ ($n = 1$ or 2) molecules on an Al(111) surface in water for a coverage of $\theta_1 = 4.72 \cdot 10^{-3}$ molecule $\cdot \text{\AA}^{-2}$. Al atoms of the top layers are shown in blue and Al atoms of the other layers are shown in grey.



5.3.3 qX^{n-} ($n = 1$ or 2) species adsorbed on Al(111) at θ_3 coverage in water

Before discussing the results, we check the validity of the model. The charges on Na^+ and Mg^{2+} ions were verified, allowing negative charges on the slab/molecule systems. Moreover, the number of layers in the slab was increased to six, and no significant difference in net charge on the molecules were found, meaning that the four layer slab is still a good reservoir of electron at θ_3 coverage in case of the adsorption of a charged species. The local potential in the direction normal to the surface for the adsorbed q^- and qS^{2-} is presented in Figure B.3 of Appendix B. It shows slight curves between the ion and the molecule on one side, as well as between the ion and the bottom of the image slab on the other side. This is not present for q in water (Appendix B, Figure B.1). This suggests interactions between the ion and the rest of the system, which could introduce errors in our results. To better quantify this interaction, the distance between the top of the molecule and the image slab was increased (See Table B.1 in Appendix B), leading to significant total energy variation (up to 0.18 eV for 5 Å distance increase for qS^{2-}), which was not the case at θ_1 coverage (Appendix B, Table B.2). The results therefore contain errors, and at the time of the writing of the manuscript, calculations with higher distance between the ion and the rest of the system are in progress. However, we discuss qualitatively the adsorption energies and net charge on

TABLE 5.13: Adsorption energies (in eV), net charge on the molecule and charge transfer from the Al(111) surface to the molecule (in e) at $\theta_3 = 2.36 \cdot 10^{-2}$ molecule $\cdot \text{Å}^{-2}$ coverage. All modes are optimized in water.

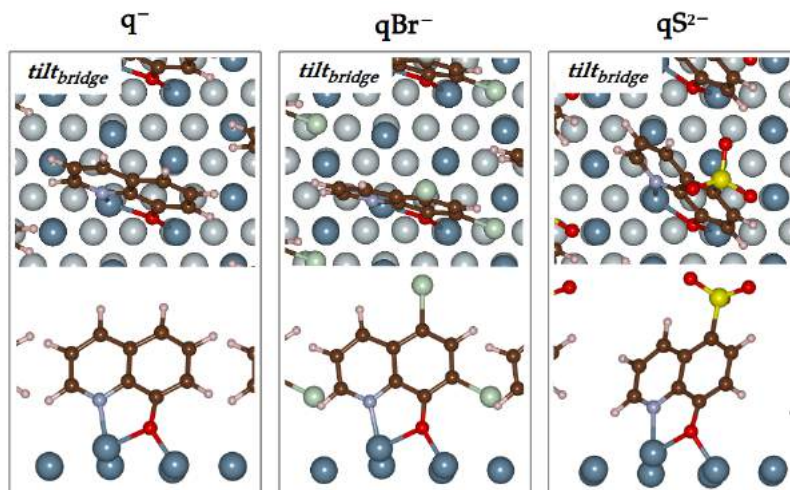
Species	q^- <i>tilt</i> _{bridge}	qBr^- <i>tilt</i> _{bridge}	qS^{2-} <i>tilt</i> _{bridge}
$E_{ads}^{deprot\ mol / Al(111)}$	-1.65	-1.38	-1.10
Q_{mol}	-1.66	-1.74	-2.48
ΔQ_{mol}	-0.66	-0.74	-0.48

the molecules for qX^{n-} ($n = 1$ or 2) in water that are presented in Table 5.13. At θ_3 coverage, adsorption energies are lower in magnitude than for the θ_1 coverage, but still show strong adsorption of the molecules on the Al(111) surface. The net charges on the adsorbed species are found much higher than for the *tilt* modes at θ_1 coverage, with a difference of 0.60 e for q^- and 0.67 e for qS^{2-} . The charges are also higher than for the θ_3 coverage for the neutral qX molecules (-0.50 e more charge on q^- than on q , and -0.59 e more charge on the qS^{2-} than on qS). However, for reasons pointed out previously, these results should not lead to extensive interpretations before less biased calculations are done.

TABLE 5.14: Length of bonds (in Å) between the qX^{n-} ($n = 1$ or 2) molecules and the Al(111) surface and angles (α_{mol} in $^\circ$) between the qX molecules and the Al(111) surface at $\theta_3 = 2.36 \cdot 10^{-2} \text{ molecule} \cdot \text{Å}^{-2}$ in water. Bonds between atoms At1 and At2 are listed in this table if $d_{At1-At2} < 2.5 \text{ Å}$. Atom numbers are indicated in Figure 3.1 and 5.7. The angle α_{mol} is formed between the C5-C6 bond and its projection on the Al(111) surface (See Figure 5.1)

Species	q^- $tilt_{bridge}$	qBr^- $tilt_{bridge}$	qS^{2-} $tilt_{bridge}$
d_{O1-Al1}	1.898	1.930	1.914
d_{O1-Al2}	2.032	2.054	2.088
d_{N1-Al2}	1.997	1.996	2.028
α_{mol}	61.5	75.6	58.2

FIGURE 5.8: Adsorption modes of the qX^{n-} ($n = 1$ or 2) molecules on an Al(111) surface for a coverage of $\theta_3 = 2.36 \cdot 10^{-2} \text{ molecule} \cdot \text{Å}^{-2}$. Al atoms of the top layers are shown in blue and Al atoms of the other layers are shown in grey.



5.3.4 Conclusion

In vacuum, the energy and charge of the adsorption modes of the qX molecules on the Al(111) surface showed chemisorption for all derivatives and coverage, and the four qX species could form stable compact monolayer on Al(111) (corresponding to a coverage of $\theta_3 = 2.36 \cdot 10^{-2} \text{ molecule} \cdot \text{Å}^{-2}$). Globally, the stability of these compact monolayers are the result of both the iono-covalent bonding of the molecules on the Al(111) surface and the van der Waals interactions between the molecules and the Al(111) surface (14% to 17% van der Waals contribution to the interaction energy $E_{int}^{mol/Al(111)}$). Appart from the existence of higher interactions between the molecules in the organic layer for qSH (hydrogen bond discussed in Sections 5.2.3 and 5.2.4) than for q and qBr , no significant differences were found

between the qX molecules at θ_3 . However, it is worth noting that the compact monolayers presented in this work contain some bias as they were obtained at periodic constraint of one molecule per cell. The strongest difference found in the adsorption of the qX species lies in the relative stabilities of the different modes at low coverage ($\theta_1 = 4.72 \cdot 10^{-3}$ molecule $\cdot \text{\AA}^{-2}$), which can be associated to the case of a lone molecule adsorbed on a Al(111) surface. The q most stable adsorption mode (*tilt*) was found to be different than those of the qBr , qS and qSH molecules (*paral*), because of i) the strong van der Waals interactions of qBr with Al(111) in *paral* mode; ii) the iono-covalent bonding of the SO_3/SO_3H group of qS and qSH with Al(111) in *paral* mode. Considering that the formation process of an adsorbed monolayer begins by the adsorption of single molecules on the Al(111) surface, the adsorption geometry of the first adsorbed molecules could affect the geometry of the subsequently formed compact monolayer, as energy barriers will need to be overcome to increase the coverage up to one monolayer.

In aqueous environment, the calculations performed on qX^{n-} ($n = 1$ or 2) charged molecules showed geometries and most stable adsorption modes similar to those found in vacuum. The interaction of the X groups with the solvent influenced slightly the adsorption geometry, with the SO_3 and SO_3^- groups of the qS and qS^{2-} further away from the Al(111) surface both for *tilt* and *paral* modes. Adsorption energies were found weaker than in vacuum, but still indicated a strong adsorption, and stable layers at θ_3 coverage. At θ_1 coverage, the adsorption of deprotonated species validated the use of dehydrogenated species as model, in terms of adsorption geometry and net charge on the molecule after adsorption. The most notable differences were found for the case of the charged qX^{n-} ($n = 1$ or 2) molecules at θ_3 , where both adsorption energy and net charge on molecules were very different from the case of the qX molecules both in vacuum and water. However, additional calculations with non-interacting Na^+ and Mg^{2+} ions need to be performed in order to further discuss these results.

Overall, the modification of the X groups influences to a large extent the adsorption of the molecules on the Al(111) surface at low coverage (θ_1). For the compact monolayer model, the variation of the X groups does not change the adsorption geometry, but the formation process of a layer could be influenced by the single molecule (θ_1) adsorption geometries, possibly influencing the corrosion inhibition efficiency. The addition of a solvent model was shown to be useful to obtain more accurate results in the case of calculations involving species with groups interacting strongly with the solvent (in our case SO_3H/SO_3^- with

water).

In this chapter, two biases were included in our work. First, the periodic conditions (one molecule per simulation cell) constrained the degrees of freedom of the systems. Second, a perfect Al(111) surface was used, which neglected the effects of the steps, vacancies and adatoms that are present in experimental conditions. In the next chapter, we use a defective Al(111) surface, containing an Al adatom and noted Al-*Al*(111), and simulate up to three molecules adsorbed on the adatom.

Chapter 6

Alq₃ complexes on an aluminum surface

A mechanism of aluminum corrosion inhibition by the Hq molecule has been proposed in experimental studies, involving the presence on the aluminum surface of chelates (Alq₃) formed between deprotonated molecules and Al atoms or Cu and Mg atoms, which can be present as impurities. [38–40, 55, 138]. Although experimental works evidence some chemical bonding of the molecules with the Al surface, the exact structure of such complexes on the Al surface is not known.[55, 138] Previous theoretical work[116] have already studied the deposition of Alq₃ on the Al(111) surface showing both physisorbed and chemisorbed states of the complex on the surface, but without considering the possibility of having a geometry highly different from the complex in vacuum. In addition, the presence of dispersive interactions was not taken into account during geometry optimization. Therefore, we aim to obtain a broader picture of the possible structures of the Alq₃ complex on the Al(111) surface, and the results of these studies are presented in this chapter. We first perform calculations on *mer* and *fac* Alq₃ complexes, performed in vacuum, and adsorbed on an Al(111) surface in the framework of the dispersion corrected DFT. Different adsorption modes associated to the different isomers and orientations of the complex are investigated. Another possible process is the formation of complexes on the Al(111) surface, formed by the interaction of three q molecules with an Al adatom present on the surface. To explore these new geometries, we perform Molecular Dynamics simulations on the system, and extract a set of geometries that are subsequently optimized. From these two formation process, we get insights of the structures of Alq₃ complexes present on an Al surface.

6.1 Computational details

6.1.1 Adsorption of an Alq_3 complex on an Al(111) surface.

The Al(111) surface is modelled by a 8×8 asymmetric slab of 3 layers (64 atoms per layer), with the two top layers set free to relax. Periodic images of the complex across the surface are separated by at least 12 Å. After adsorption, about 21 Å separate the top of the complex from the bottom of the image slab in the direction normal to the surface. The local potential is checked for the geometry where the complex is the closest to the image slab (Figure C.1, Appendix C), and is found constant with respect to the direction perpendicular to the surface in the vacuum area, indicating that the adsorbed complex and the image slab do not interact. The reciprocal space is sampled by a Monkhorst-Pack[130] $2 \times 2 \times 1$ k-points grid. The energy values associated to these calculations are the adsorption, interaction and deformation energies:

The adsorption energy of the Alq_3 complex on the Al(111) slab is defined as:

$$E_{ads}^{cx/Al(111)} = E^{cx/Al(111)} - E^{cx} - E^{Al(111)} \quad (6.1)$$

Where $E^{cx/Al(111)}$ is the total energy of the optimized system containing the complex adsorbed on the Al(111) slab, E^{cx} is the total energy of the optimized free complex, and $E^{Al(111)}$ is the total energy of the optimized free Al(111) slab.

The interaction energy between the complex and the Al(111) slab is defined as:

$$E_{int}^{cx/Al(111)} = E^{cx/Al(111)} - E_{SP}^{cx} - E_{SP}^{Al(111)} \quad (6.2)$$

Where E_{SP}^{cx} is the total energy of the isolated complex at the geometry after adsorption, and $E_{SP}^{Al(111)}$ is the total energy of the isolated slab at the geometry after adsorption.

The deformation energy of the adsorbed Alq_3 complex and of the Al(111) slab are defined as:

$$E_{def}^{cx} = E_{SP}^{cx} - E^{cx} \quad (6.3)$$

$$E_{def}^{Al(111)} = E_{SP}^{Al(111)} - E^{Al(111)} \quad (6.4)$$

6.1.2 Adsorption of n q molecules (n = 1 or 3) on an Al-Al(111) surface

The Al-Al(111) slab, detailed in more details in Chapter 4, contains 3 layers of 64 atoms each (8×8 asymmetric slab), plus an Al adatom, with the two top layers plus the adatom set free to relax and the bottom layer fixed. The adatom was placed on a hcp site as it was found to be more stable than on a fcc site for a 6 layer slab (see Chapter 4). One or three q molecules are adsorbed on the adatom. In both cases (n = 1 and n = 3 molecules), the periodic images of the molecules or complexes on the surface are more than 10 Å away from each other. On the direction normal to the surface, more than 21 Å of vacuum separate the top of a molecule from the bottom of the image slab. A Molecular Dynamics exploration of the conformations space is performed on the systems with three q molecules (n = 3) adsorbed on the Al-Al(111) surface. The details and parameters of the MD simulations are listed in section 6.1.3. Geometries selected from the MD exploration are then optimized.

The adsorption energy of n (n = 1 or 3) molecules on the Al-Al(111) slab is defined as:

$$E_{ads}^{n mol / Al-Al(111)} = E^{n mol / Al-Al(111)} - nE^{mol} - E^{Al-Al(111)} \quad (6.5)$$

Where $E^{n mol / Al-Al(111)}$ is the total energy of the system containing n q molecules adsorbed on the Al-Al(111) surface, E^{mol} is the total energy of the optimized free q molecule, and $E^{Al-Al(111)}$ is the total energy of the free optimized Al-Al(111) slab.

The interaction energy between two subparts (part 1 and part 2) of the system to locally quantify the interactions is calculated as:

$$E_{int}^{part1/part2} = E^{part1+part2} - E_{SP}^{part1} - E_{SP}^{part2} \quad (6.6)$$

For instance, the interaction energy between the n molecules and the Al-Al(111) slab is defined as:

$$E_{int}^{n mol / Al-Al(111)} = E^{n mol / Al-Al(111)} - E_{SP}^{n mol} - E_{SP}^{Al-Al(111)} \quad (6.7)$$

Where $E_{SP}^{n\ mol}$ is the total energy of the n q molecules at the geometry after adsorption, isolated from the slab, and $E_{SP}^{Al-Al(111)}$ the total energy of the Al-Al(111) surface at the geometry after adsorption, isolated from the molecules. All energies introduced in this section are calculated in vacuum.

6.1.3 Geometry exploration by *ab initio* molecular dynamics

The conformation space of three q adsorbed on an Al-Al(111) surface is explored by *ab initio* molecular dynamics. The simulated temperature is maintained by a Langevin thermostat [139–141] ($T = 500\text{K}$), with 1.5 ps between steps of the trajectory. At each step, the electronic structure is calculated with the following parameters: a cutoff energy of 300 eV, a convergence criterion of 10^{-4} eV and gamma k-point sampling. The Al atom (including the adatom) positions are fixed, and the atoms of the molecules are set free to move. Runs of 10 ps each are performed from two different initial geometries. The starting geometries of these two runs vary. For the first run, noted MD1, the three q molecules are initially positioned close to parallel to the surface, with O1 atoms bonded to the Al adatom. For the second run, noted MD2, two of the molecules are positioned parallel to the surface and a third is positioned on top of the Al adatom.

From the trajectories of the MD runs, geometries are extracted every 320 steps and are optimized using a cutoff energy of 300 eV, an electronic convergence criterion of 10^{-4} eV, a convergence criterion on forces of $5 \cdot 10^{-3}$ eV \AA^{-1} and a gamma k-point sampling. The most stable geometries (geometries 10 for MD1 and geometry 17 for MD2), are then optimized more accurately with an electronic convergence criterion of 10^{-6} eV, a convergence criterion on forces of $5 \cdot 10^{-3}$ eV \AA^{-1} and $2 \times 2 \times 1$ k-points sampling of the reciprocal space.

6.2 Alq_3 complexes adsorbed on an Al(111) surface.

The two isomers of the complexes are adsorbed on the Al(111) surface such as to orient the O1 and N1 atoms towards the surface. The *mer* isomer has one face containing two O atoms and one N atom, and one face containing one O atom and two N atoms. The *fac* isomer has one face containing three O atoms and the other one containing three N atoms. In his work, Yanagisawa [116] proposed a classification of the configurations of adsorbed complexes on

Al(111) depending on the orientation of the permanent dipole of the adsorbed complex. When the dipole moment is directed towards the vacuum, the configuration is denoted "up". When it is directed towards the Al(111) surface, the configuration is denoted "down". In terms of geometry, a *up* configuration is obtained when the face containing a majority of O atoms is directed towards the surface, and a *down* configuration is obtained when the face containing a majority of N atoms is directed towards the surface. The dipole on the isolated *mer* and *fac* isomers were checked (See Figure A.1, Appendix A), leading to values and orientations similar to those indicated by Yanagisawa *et al.* [116]. The *mer/up*, *mer/down*, and the *fac/up* adsorption modes are shown in Figure 6.1. The *fac/down* mode has been shown to be the less stable [116] and is not studied. Calculated energies, as well as the position of the Al atom of the complex and the charge on the Al atom and on the complex, are presented in Table 6.1.

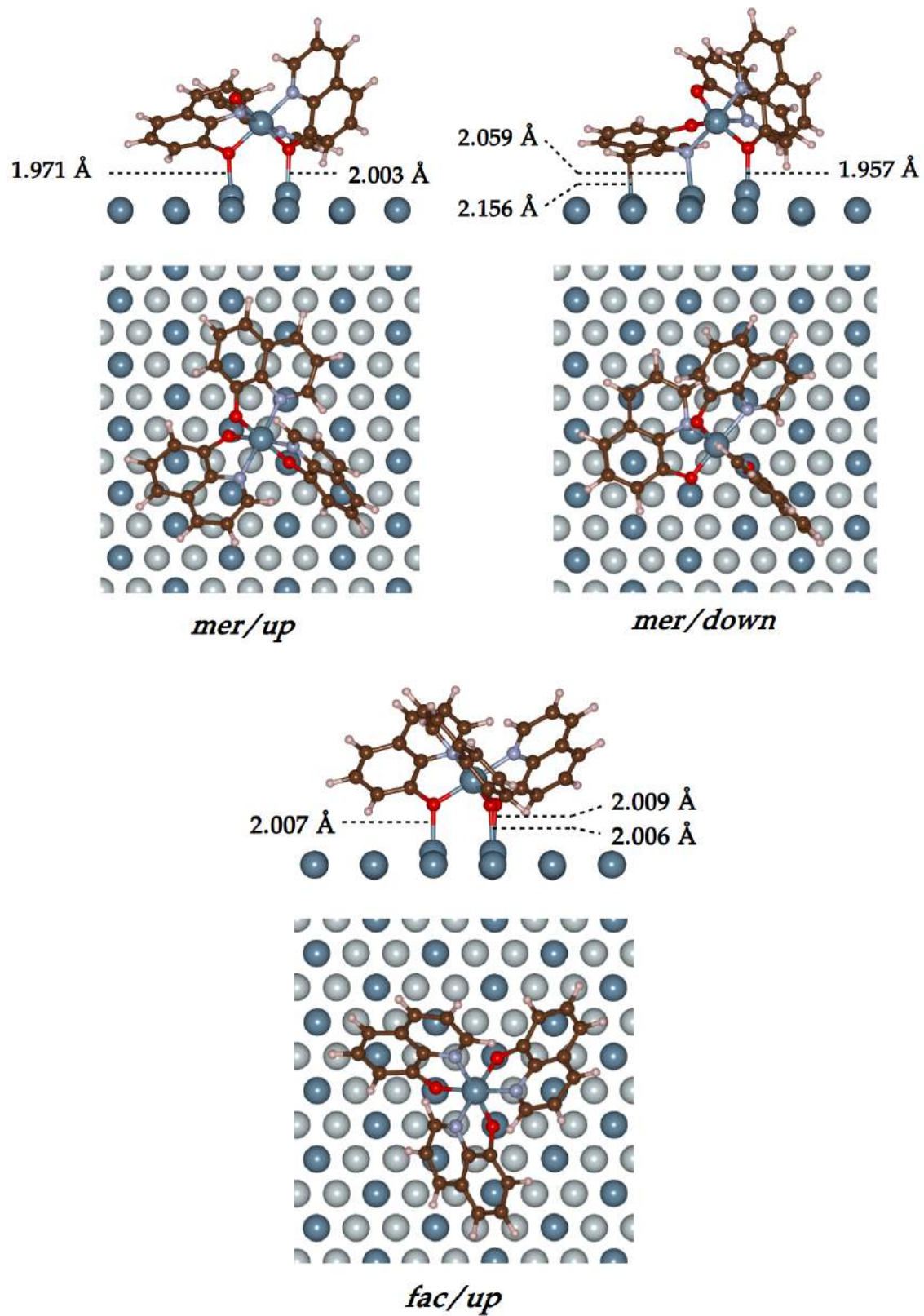
TABLE 6.1: Adsorption of the *mer* and *fac* Alq_3 complexes on Al(111). Relative total energies, adsorption energies, interaction energies, complex and Al(111) slab deformation energies (in eV), distance between the Al atom of the complex and the Al(111) surface (in Å), net charge on the Al atom of the complex and net charge on the complex (in e).

Geometry	<i>fac/up</i>	<i>mer/up</i>	<i>mer/down</i>
$\Delta E^{cx/Al(111)}$	+0	+0.54	+0.69
$E_{ads}^{cx/Al(111)}$	-2.21	-1.68	-1.52
$E_{int}^{cx/Al(111)}$	-3.45	-3.12	-4.25
E_{def}^{cx}	+0.73	+0.88	+2.09
$E_{def}^{Al(111)}$	+0.51	+0.56	+0.63
z_{Al}^{cx}	3.509	3.862	3.897
q_{Al}^{cx}	+2.45	+2.44	+2.36
Q_{cx}	-0.97	-0.73	-1.57

The *fac/up* geometry, where three O atoms are bonded to the surface ($d_{O-Al} = 2.007 \pm 0.002$ Å), is found to be the most stable geometry, with the *mer/up* and *mer/down* geometries being less stable by 0.54 eV and 0.69 eV respectively. Two O atoms form bonds with the Al(111) surface in the *mer/up* geometry ($d_{O-Al} = 1.971$ Å and 2.003 Å), while one O atom, one N atom and one C atom form bonds with the Al(111) surface in the *mer/down* geometry ($d_{O-Al} = 1.957$ Å, $d_{N-Al} = 2.059$ Å and $d_{C-Al} = 2.156$ Å).

The values of the adsorption energy (-1.52 eV to -2.21 eV) and of the interaction energy (-3.12 eV to -4.25 eV) show a strong interaction between the complexes and the Al(111) surface. The strongest interaction energy is obtained for the *mer/down* geometry (-4.25 eV), due to the bonding of O, N and C atoms with the Al(111) surface. However, it is the less stable

FIGURE 6.1: Adsorbed *mer* and *fac* Alq_3 on Al(111). The top Al layer of the Al(111) slab and the Al atom of the complex are in dark blue. The other Al atoms of the slab are in grey.



geometry, because of a very high deformation energy (2.09 eV), explained by the strong deformation on the molecule forming N-Al and C-Al bonds (see in Figure 6.1). For the two other geometries, deformations of the complexes are lower, with values of 0.88 eV and 0.73 eV respectfully for the *mer/up* and *fac/up* geometries. The slab is deformed upon adsorption of the complexes, with values of the deformation energy of 0.57 ± 0.06 eV in all cases.

The Al atom of the complex is closer to the surface in the *fac/up* geometry ($z_{Al}^{cx} = 3.509$ Å) than in the *mer/up* and *mer/down* geometries (3.862 Å and 3.897 Å respectively). The charge on this atom is close to +2.45 e in all cases, with a slightly lower charge (+2.36 e) for the case of the *mer/down*, which shows no or very small difference from the case of the free complex. Charge transfer takes place between the surface and the complexes upon adsorption, with the highest electron gain found for the *mer/down* geometry (gain of $1.57 e^-$), which is consistent with the high interaction between the surface and the complex discussed above. In the other two geometries, 0.73 to 0.97 electrons are transferred from the surface to the complex.

In order to investigate the strength of the adsorption of the complex, molecular dynamics runs of 3 ps were performed using the *fac/up* geometry as initial geometry. The temperature is first set to 300K, then to 500K, and no O-Al bond is broken during the runs. This indicates that once adsorbed, the complex is likely to stay adsorbed, even at high temperature.

In the work of Yanagisawa *et al.*, using the GGA functional on *mer* and *fac* complexes on 3 layer slabs of dimensions 8x8, the *fac/up* geometry was also found to be the most stable. A very different *mer/down* geometry than ours was found, which was found more stable than the *mer/up* geometry. This difference can be due to the different functional and calculation parameters used, as well as the fact that no dispersion corrections were employed in their calculations. Indeed, van der Waals interactions contribute to 50% to 59% of the interaction energy $E_{int}^{cx/Al(111)}$ in our calculations and are thus of capital importance to determine accurate adsorption geometries.

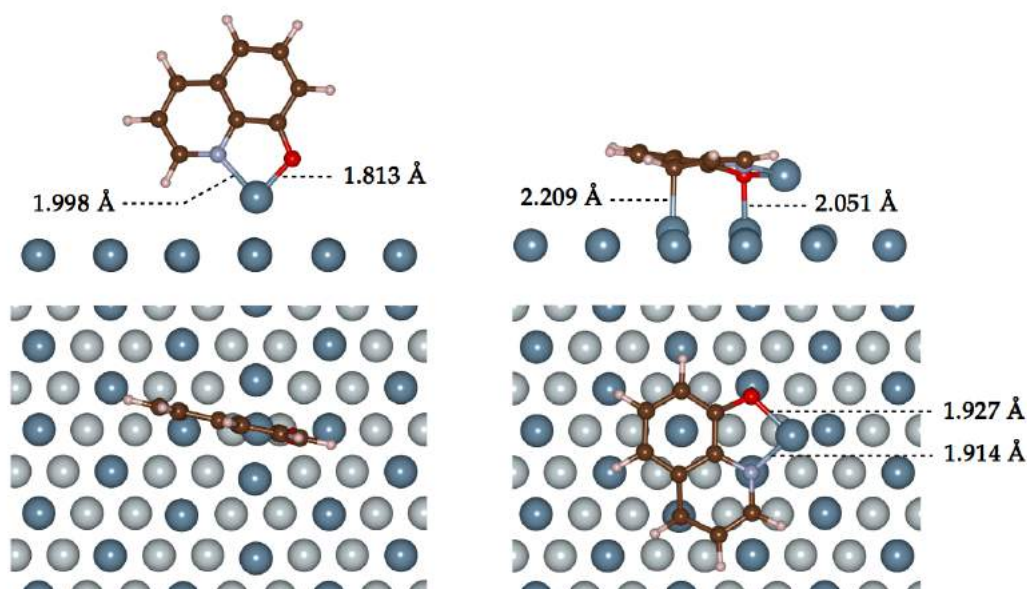
In this section, we showed that both *mer* and *fac* isomers of the Alq_3 complex can be strongly adsorbed on the Al(111) surface, with the *fac/up* geometry being the most stable one. We proceed to the exploration of geometries obtained by direct formation of the complex on an Al-Al(111) surface, which could lead to even more stable geometries. We purposely chose a system with the same amount and type of atoms than the one discussed above, in order to allow the direct comparison of total energies.

6.3 Formation of Alq_3 complexes on an Al-Al(111) surface

In this section, we first investigate the interaction of one q molecule with an Al-Al(111) surface, and then proceed to the MD exploration of the conformations space of the system containing three q molecule and a Al-Al(111) surface.

6.3.1 One q molecule adsorbed on an Al-Al(111) surface.

FIGURE 6.2: One q molecule adsorbed on an Al-Al(111) surface. Left: *tilt* mode. Right: *para* mode. The top Al layer and Al adatom of the Al-Al(111) slab are in dark blue. The other Al atoms of the slab are in grey.



The two adsorption modes of the q molecule on the Al-Al(111) surface are shown in Figure 6.2. In the *para* mode, the molecule is bonded to the adatom by the O1 and N1 atoms ($d_{O-Al} = 1.927 \text{ \AA}$, $d_{N-Al} = 1.914 \text{ \AA}$), and to the Al(111) surface by the O1 and C7 atom ($d_{O-Al} = 2.051 \text{ \AA}$, $d_{C-Al} = 2.209 \text{ \AA}$), while in the *tilt* mode, the molecule is positioned above the Al adatom and is only bonded to the adatom ($d_{O-Al} = 1.813 \text{ \AA}$, $d_{N-Al} = 1.998 \text{ \AA}$)

Energies, distances from the surface to the adatom and charges on the molecules are summarized in Table 6.2. Both modes show a strong adsorption of the molecules, with adsorption energies of at least -4 eV. These results show close adsorption energies between the two modes, with the *para* mode more stable by 0.13 eV. The interaction energy is stronger for the *para* mode than for the *tilt* mode, which is consistent with the higher number of bonds formed between the molecule and Al-Al(111) surface, as well as with the overall

TABLE 6.2: One q molecule adsorbed on an Al-Al(111) surface. Adsorption energy, interaction energy, deformation energies (in eV), distance between the Al adatom and the surface and its variation upon adsorption (in Å), net charge on the Al adatom and its variation upon adsorption (in e), net charge on the q molecule upon adsorption.

Geometry	<i>tilt</i>	<i>paral</i>
$E_{ads}^{mol/Al-Al(111)}$	-4.04	-4.17
$E_{int}^{mol/Al-Al(111)}$	-4.57	-6.14
E_{def}^{mol}	+0.40	+1.42
$E_{def}^{Al-Al(111)}$	+0.14	+0.55
$z_{Al\ adatom}(\Delta z_{Al\ adatom})$	1.981 (+0.054)	2.407 (+0.373)
$q_{Al\ adatom}(\Delta q_{Al\ adatom})$	+1.03 (+0.93)	+0.82 (+0.70)
Q_{mol}	-0.95	-2.11

smaller distances between the molecule and the surface (Figure 6.2). The molecule and surface are both more deformed in the *paral* mode ($E_{def}^{mol} = 1.42$ eV and $E_{def}^{Al-Al(111)} = 0.55$ eV) than in the *tilt* mode ($E_{def}^{mol} = 0.42$ eV and $E_{def}^{Al-Al(111)} = 0.14$ eV). As for the *paral* modes found for the flat Al(111) surface (Chapter 5), the formation of the C7-Al bond induces a high deformation of the pyridine ring of the molecule. The high deformation of the surface in the *paral* mode is explained by the Δz_{Al} value showing important displacement of the Al adatom upon adsorption (+0.373 Å).

The charge on the Al adatom is close to +1 e (Al^I oxidation state) for both modes, with the charge on the adatom (+1.03 e and +0.82 e) very close to the one obtained from the isolated Alq complex (+0.86 e). In the case of the *tilt* mode, the charge on the molecule (-0.95 e) and the deformation energy of the molecule (0.40 eV) are also very close to the values obtained for the Alq species (-0.86 e and 0.36 eV). This shows that the adsorption one q molecule on an ad-atom in *tilt* position leads to the formation of an Alq-like complex on Al(111), with the most noticeable difference being the length of the N1-Al bond (1.998 Å for the adsorbed q molecule, 2.187 in the free Alq complex). The charge transfer from the surface to the molecule is of about one electron higher in the *paral* mode (-2.11 e) than in the *tilt* mode (-0.95 e). In the *tilt* mode, the majority of the charge received by the molecule comes from the adatom (-0.91 e), while in the *paral* mode, the molecule can receive electrons from the Al(111) part of the surface (-1.41 e).

To form an Alq₃-like species on the aluminum surface, three q molecules have to be adsorbed on Al-Al(111). A broad exploration of the possible geometries for this system is

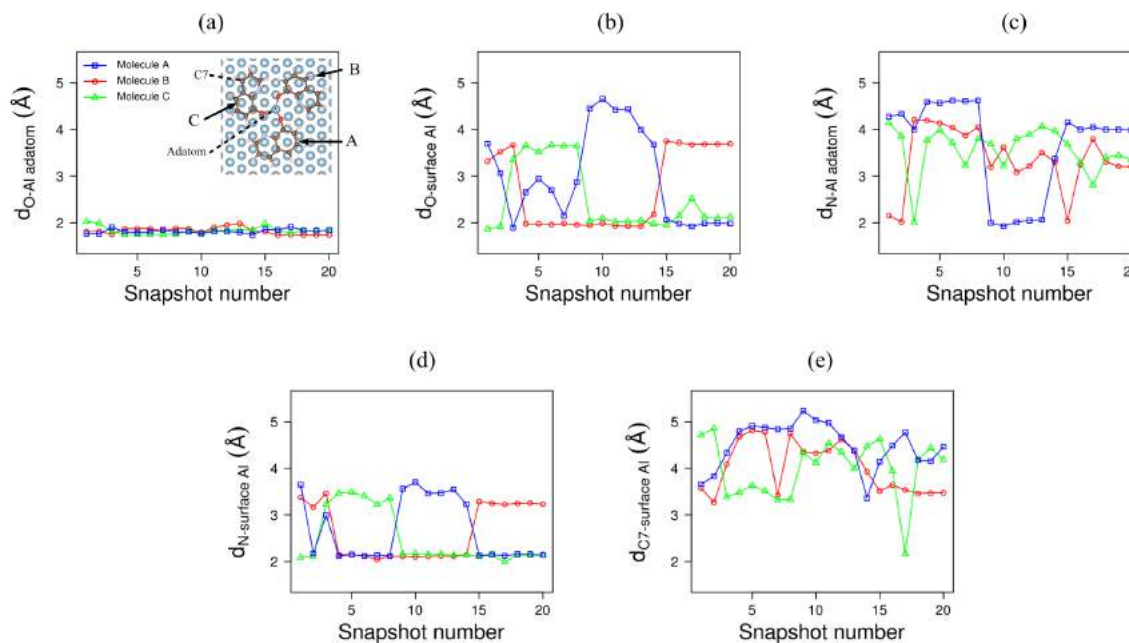
presented below.

6.3.2 Three q molecules adsorbed on an Al-Al(111) surface.

The conformation space of the system containing three q molecules adsorbed on an Al-Al(111) surface was explored by two molecular dynamics runs. From each MD trajectory, twenty geometries were extracted and a first level of optimization was performed on them (see section 6.1.3). Distances of interest in all these geometries are presented in Figure 6.3 for MD1 and in Figure 6.4 for MD2. Number of bonds between the molecules and the Al-Al(111) surface, as well as the energy of each geometry, are shown in Figure 6.5 for MD1 and in Figure 6.6 for MD2. In all geometries, three O1-Al adatom bonds are formed (see Figures 6.3(a) and 6.4(a)), therefore they are not shown in the histograms of Figures 6.5 and 6.6. For the MD1 trajectory, the variations of distances between atoms of the **A**, **B** and **C** molecules and the atoms of the Al-Al(111) surface are shown in 6.3. In addition to O1 bonding to the Al adatom, up to two O1-Al bonds are formed between the molecules and the Al(111) surface (Figure 6.3(b)). The bonding of the N1 (Figure 6.3(d)) and C7 (Figure 6.3(e)) atoms on the surface vary depending on the geometry. In some geometries, the N1 atom is also bonded to the Al adatom (Figure 6.5(c)).

The relative total energy of the different geometries, taking the most stable geometry (geometry 10) as the reference in energy, is shown in black in Figure 6.5 for MD1. Two groups of geometry, separated by at least 0.2 eV, appear clearly. Lower energies are obtained for the geometries 1-2, 9-13, 15 and 17, and higher energies are obtained for the geometries 3-8, 14, 16, and 18-20. For the lower energies, geometries 1 and 2 excluded, two O1-surface Al atoms are found, and at least one N1-Al adatom bond is found, except for geometry 17. This last geometry is the only one where a C7-Al bond exists, which stabilizes the system and seems to compensate the absence of N1-Al adatom bond. In MD2, the geometry and energy varies much less than for MD1. Both the distances of interest shown in Figure 6.4 and the number of bonds presented in Figure 6.6 show that only the bonding of the C7 and C9 atoms vary between the geometries, while the number of O1-surface Al bonds (2), N1-Al adatom bonds (1) and N1-surface Al bonds (2) are the same in all geometries extracted from the MD2 trajectory. In Figure 6.6, the energy values make three geometries (2, 17 and 18) stand out from all other geometries, which have similar energies (variations < 0.05 eV). In the case of geometry 2, the bonding of the C9 atom with the Al(111) surface leads to the

FIGURE 6.3: Three q molecules adsorbed on an Al-Al(111) surface. Geometries from 20 snapshots of the MD1 trajectory, optimized at a first level of accuracy; distances (in Å) (a) between the O atom and the Al adatom, (b) between the O atom and the surface Al atom (shortest distances), (c) between the N atom and the Al adatom, (d) between the N atom and a surface Al atom (shortest distances), (e) between the C7 atom and a surface Al atom (shortest distances). Values for molecules **A** in blue, **B** in red and **C** in green.



deformation of the **B** molecule ($E_{def}^{molB} = 1.82$ eV), which makes this geometry the less stable of MD2. In geometry 17 and 18, the bonding of the C7 atom on the Al(111) surface stabilizes the system and makes these geometries more stable than all others, with the geometry 17 being the most stable of all.

FIGURE 6.4: Three q molecules adsorbed on an Al-Al(111) surface. Geometries from 20 snapshots of the MD2 trajectory, optimized at a first level of accuracy; distances (in Å) (a) between the O atom and the Al adatom, (b) between the O atom and the surface Al atom (shortest distances), (c) between the N atom and the Al adatom, (d) between the N atom and a surface Al atom (shortest distances), (e) between the C7 atom and a surface Al atom (shortest distances), (f) between the C9 atom and a surface Al atom (shortest distances). Values for molecules **A** in blue, **B** in red and **C** in green.

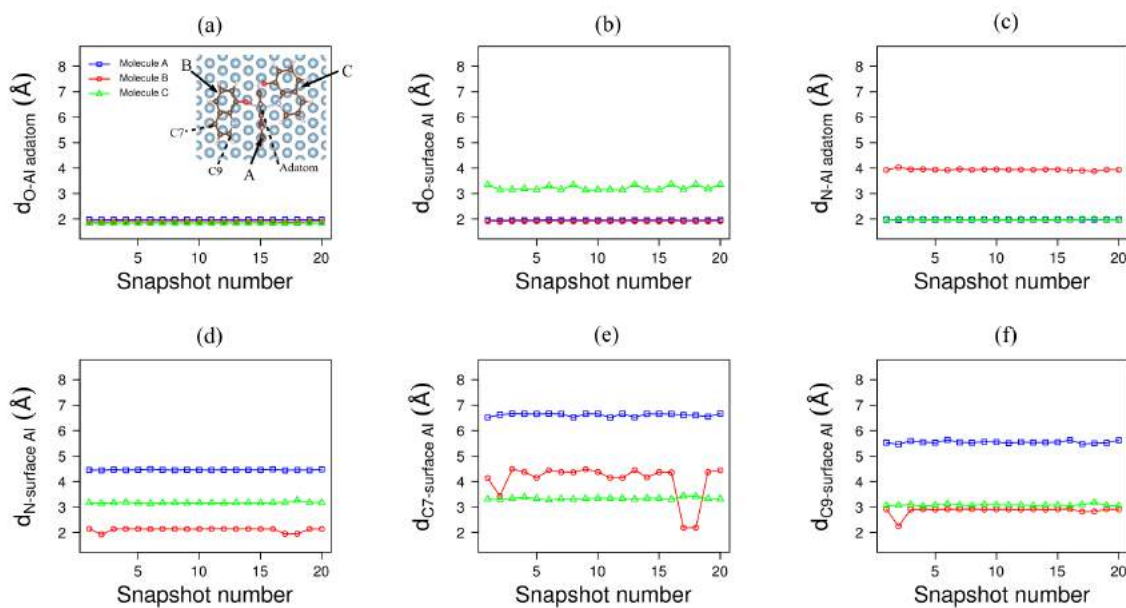


FIGURE 6.5: Three q molecules adsorbed on Al-Al(111). Geometries from 20 snapshots of the MD1 trajectory; relative total energies ΔE (in eV) in black (the reference is the energy of the geometry 10); number of bonds between O atoms and Al(111) surface atoms in dark orange; number of bonds between N atoms and the Al adatom in green-blue; number of bonds between N atoms and Al(111) surface atoms in light blue; number of bonds between C7 atoms and Al(111) surface atoms in brown. Atoms a and atom b are considered bonded if $d_{a-b} < 2.3 \text{ \AA}$.

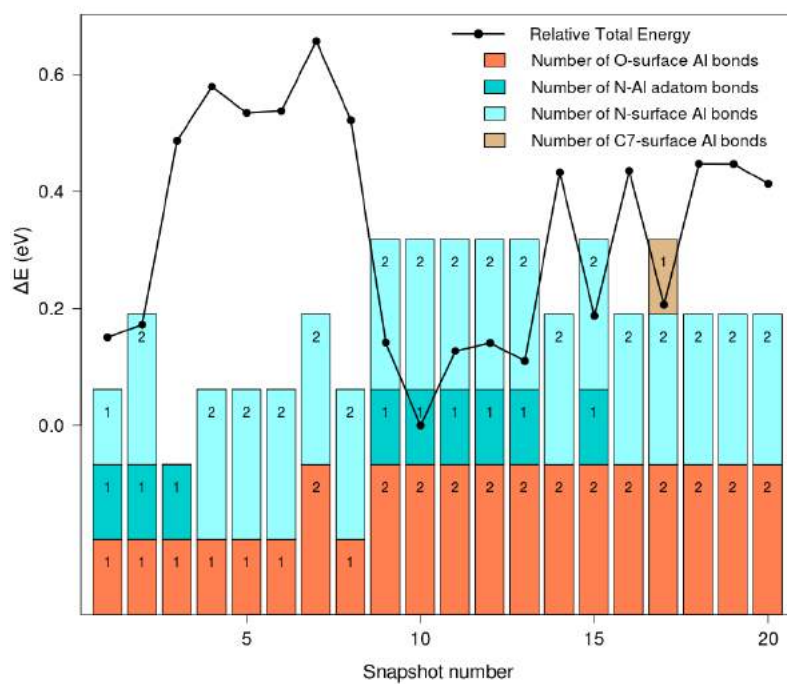
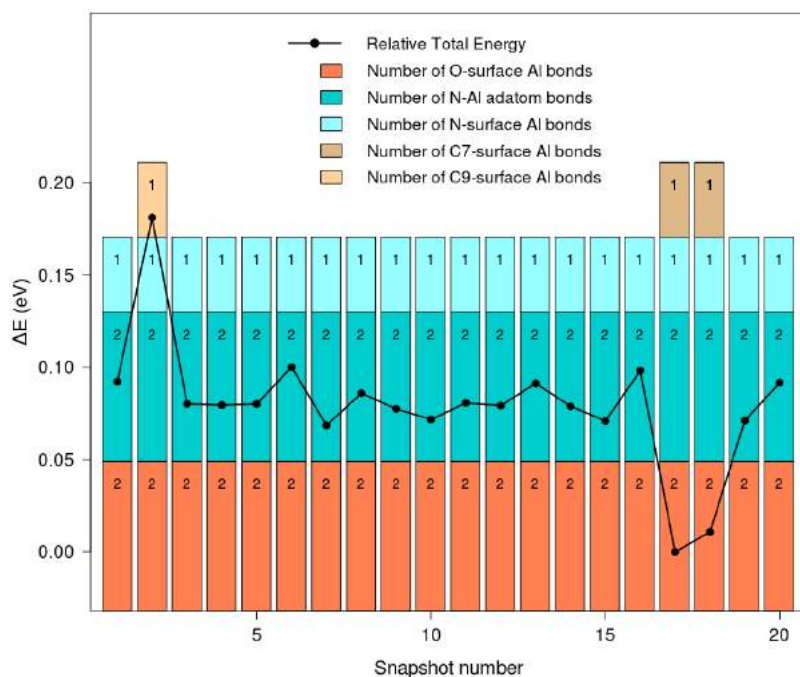


FIGURE 6.6: Three q molecules adsorbed on Al-Al(111). Geometries optimized from 20 snapshots of the MD2 trajectory; relative total energies ΔE (in eV) in black (the reference is the energy of the geometry 17); number of bonds between O atoms and Al(111) surface atoms in dark orange; number of bonds between N atoms and the Al adatom in green-blue; number of bonds between N atoms and Al(111) surface atoms in light blue; number of bonds between C7 atoms and Al(111) surface atoms in brown; number of bonds between C9 atoms and surface Al(111) surface atoms in beige. Atoms a and atom b are considered bonded if $d_{a-b} < 2.3 \text{ \AA}$.

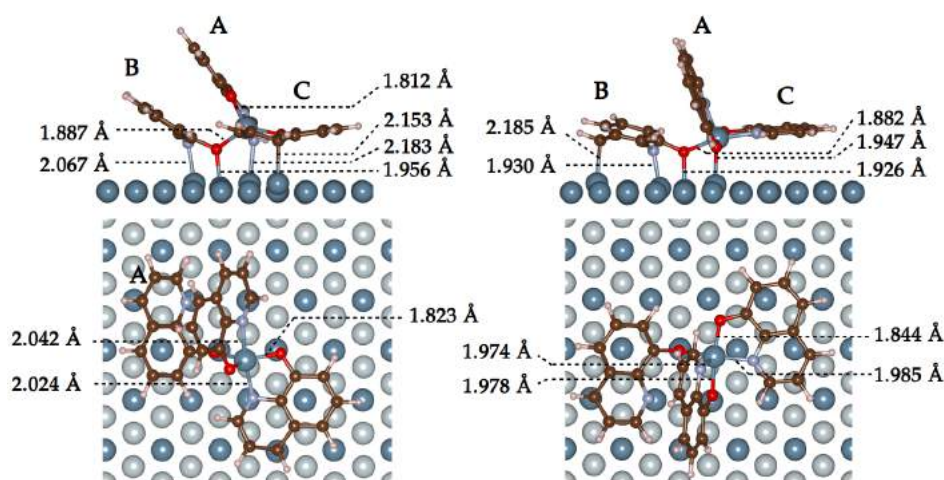


Most stable geometries for three q molecules adsorbed on an Al-Al(111) surface.

The most stable geometries from MD1 (geometry 10) and MD2 (geometry 17) were optimized using more accurate parameters than the ones used above. The optimization of the geometry 10 of MD1 leads to the formation of additional bonds. The corresponding geometries are presented in Figure 6.7. Geometry 17 of MD2 is found to be the most stable of the two by 0.38 eV. In both geometries, one molecule is positioned on top of the Al adatom, while the other two molecules are parallel or slightly tilted to the surface, on opposite sides of the Al adatom.

The **A** molecule is positioned on top of the Al adatom and is almost perpendicular to the surface. Both O1 and N1 atoms are bonded to the adatom, and the O1 atom is bonded to the surface in the case of the geometry 17. The **B** molecule is bonded to the adatom by the O1

FIGURE 6.7: Three q molecules adsorbed on an Al-Al(111) surface. Left: geometry 10 from MD1. Right: geometry 17 from MD2 (most stable form). The top Al layer and Al adatom of the Al-Al(111) slab and the Al atom of the complex are in dark blue. The other Al atoms of the slab are in grey.



atom, and to the surface by the O1 and N1 atoms in both geometries. In the geometry 17, the C7 atom is also bonded to the Al(111) surface, which is associated with a more parallel orientation of the molecule than for the geometry 10.

The **C** molecule is bonded to the Al adatom by the O1 and N1 atoms in both cases, and bonded to the surface by the C7 atom in geometry 10. Overall, the bonds formed by the molecules with the adatom are shorter than for the free complex, where bond distances are equal to 1.873 ± 0.018 Å for O-Al and 2.071 ± 0.032 Å for N-Al (See Table 4.3 in Chapter 4).

In Table 6.3 are presented the relative energies of the systems and the atomic charges across the systems for geometries 10 and 17. The atomic charge on the Al adatom is of +2.56 e and +2.48 e respectfully for geometries 10 and 17, which is similar to the case of the isolated and adsorbed Alq_3 complexes. A total of -4.28 e and -4.40 e are transferred from the Al-Al(111) surface to the molecules for geometries 10 and 17 respectfully, with the charge on each molecule depending on how the molecule is bonded to the surface.

TABLE 6.3: Properties of the geometry 10 and 17 obtained from the MD exploration and of the geometries obtained from the adsorbed complexes performed in vacuum. Relative total energies (in eV, the reference is the energy of geometry 17), charge on the Al atom in the complex, charge on the Al adatom, and charge on molecules **A**, **B** and **C** (in e); distance from the Al atom in the complex to Al(111) and distance from the Al adatom to Al(111) (in Å).

Geometry	Geometry 17	Geometry 10	<i>fac/up</i>	<i>mer/up</i>	<i>mer/down</i>
ΔE	0	+0.38	+0.25	+0.79	+0.94
$q_{Al\ adatom}$	+2.48	+2.56			
q_{Al}^{cx}			+2.45	+2.44	+2.36
Q_{molA}	-0.97	-0.85	-1.08	-0.94	-1.26
Q_{molB}	-2.18	-1.25	-1.19	-1.26	-1.49
Q_{molC}	-1.25	-2.18	-1.14	-0.98	-1.25
$z_{Al\ adatom}$	2.738	3.206			
z_{Al}^{cx}			3.509	3.862	3.897

For instance, the charge on the molecule **A** is lower for the geometry 10 (-0.85 e) than for the geometry 17 (-0.97 e), where an additional bond between the O1 atom and the Al(111) surface is present. The molecules bonded to the surface by the C7 atom receive a high charge (2.18 e). This is the case of the **C** molecule in geometry 10 and of the **B** molecule in geometry 17. The last molecule (**B** in geometry 10 and **C** in geometry 17) is less bonded to the surface and receives 1.25 e.

In geometry 17, the adsorption geometry of the three q molecules is equal to -13.08 eV. This corresponds to a stronger adsorption than three times the adsorption energy of a single q molecule on a Al-Al(111) surface ($-4.17 \times 3 = -12.51$ eV), indicating a synergistic behavior of the adsorption of the three molecule on the Al-Al(111) surface. To get a better understanding of the various interactions taking place in the system, interaction energies between subparts of the system are calculated and listed in Table 6.4. Deformation energies of the subparts are also calculated. The very strong bonding of the three molecules with the Al-Al(111) surface is quantified by the high interaction energy of the three q molecules with the Al-Al(111)

surface (-17.20 eV).

The interaction energy of the **A** molecule with the rest of the system (-6.40 eV) corresponds to a strong bonding, with a small but significant van der Waals contribution of up to 14% of the interaction energy. The molecule is only slightly deformed (0.49 eV) upon adsorption. The interaction of the **B** molecule with the rest of the system (-6.91 eV) contains a higher van der Waals contribution (22%), because of the molecule's proximity to the Al(111) surface, and the **B** molecule is highly deformed (2.03 eV) due to the formation of the C7-Al bond. The **C** molecule is also close to the surface, inducing high van der Waals interaction (22% of a total of -5.87 eV), but is not chemically bonded to the Al(111) surface, and thus only slightly deformed (0.43 eV).

TABLE 6.4: Most stable geometry for three q molecules adsorbed on Al-Al(111). Interaction energies between subparts of the system, van der Waals energy contribution and deformation energies (in eV)

Part 1	Part 2	$E_{int}^{part1/part2}$	$E_{int}^{part1/part2}(vdW)$	E_{def}^{part1}
molA + molB + molC	Al-Al(111)	-17.20	-2.82	2.95
molA	molB + molC + Al-Al(111)	-6.40	-0.91	0.49
molB	molA + molC + Al-Al(111)	-6.91	-1.55	2.03
molC	molA + molB + Al-Al(111)	-5.87	-1.30	0.43
molA	Al-Al(111)	-4.56	-0.49	0.49
molB	Al-Al(111)	-6.15	-1.23	2.03
molC	Al-Al(111)	-4.78	-1.11	0.43
molA + molB + molC	Al adatom	-13.48	-0.20	2.95
molA + molB + molC + Al adatom	Al(111)	-6.23	-2.83	

We can calculate the interaction energy between the three molecules and the Al adatom and compare it to the values obtained for the isolated Alq_3 complex, in order to see how close is this system to the Alq_3 complex. This value is of -13.48 eV, and is to be compared to the $E_{int}^{3mol/Al} = -15.13 \pm 0.07$ eV obtained for the isolated complexes, indicating that the bonding is almost as stabilizing in the two cases. If we consider that the (molA + molB + molC + Al adatom) subpart of the system is a Alq_3 -like complex, we can calculate an interaction energy of this subpart with the Al(111) surface, and compare it to that of the adsorbed complexes 6.2. This interaction energy is of -6.23 eV for the case of geometry 17, and of -3.61 ± 0.49 eV for the adsorbed complexes pre-formed in vacuum, which shows a much stronger bonding in the case of geometry 17 than in the case of the adsorbed complexes.

6.3.3 Overall Discussion

In Table 6.3 are presented the relative total energies of the systems obtained by direct adsorption of Alq_3 on the Al(111) surface and by adsorption of the 3 q molecules on the Al-Al(111) surface. The geometry 17 is found to be more stable than the geometry 10 as well as the *mer/up*, *mer/down* and *fac/up* geometries, respectively by 0.38 eV, 0.79 eV, 0.94 eV and 0.25 eV. The charge on the Al adatom or Al of the complex is similar in all geometries, indicating Al^{III} oxidation state in all cases. The position of the Al adatom or Al atom of the complex is very different between the geometry 10 and 17 on one hand and the *mer/up*, *mer/down* and *fac/up* on the other hand, with the latter being further away from the Al(111) surface by about 1 Å. This gives a clear picture of the significant difference in structure between the two groups of geometries. The relatively small energy difference (0.25 eV) between the most stable geometries of the two groups shows that the two could coexist, depending on factors such as the proportion of single molecules versus complexes in the solution, the defects on the surface, and the various energy barriers involved in the process.

6.4 Conclusion

In this chapter, the conformation of Alq_3 complexes on an Al(111) surface has been investigated using two approaches, the adsorption of Alq_3 complexes pre-formed in vacuum on an Al(111) surface and the direct formation of an Alq_3 complex by adsorption of three q molecules on an Al adatom on the Al(111) surface. The results showed a high number of stable geometries, associated to energies comprised in a range of about 1 eV ($\Delta E = 0$ to 0.93 eV). Regardless of the method used, the most stable structure of the complex on the surface is close to the geometry of an Alq_3 complex formed in vacuum, with at least five O1-Al adatom or N1-Al adatom bonds (versus six in the complex formed in vacuum), and the Al adatom in Al^{III} oxidation state.

Comparison between systems of this chapter and those of Chapter 5 is not straightforward as slabs of different number of layers (3 or 4) and different surface coverage were used. However, we can compare qualitatively the most stable configuration obtained in this chapter (geometry 17 of MD2) to the one obtained in Chapter 5, choosing the coverage θ_1 , which is the closest to the coverage of this chapter ($\theta = 6.64 \cdot 10^{-3}$ molecule $\cdot \text{Å}^{-2}$ in this chapter, $\theta_1 = 4.72 \cdot 10^{-3}$ molecule $\cdot \text{Å}^{-2}$ in Chapter 5). The adsorption energy per molecule is equal to

-4.36 eV for geometry 17 of MD2, and -3.59 eV for θ_1 of Chapter 5 (neutral q molecule, in vacuum). This could already suggest that the formation of complex-like species is favored on the aluminum surface at this low coverage. Further investigations are needed and prospects are presented in the next chapter.

General conclusion

In this work, we studied the 8-hydroxyquinoline (Hq) and two of its derivatives: the 5,7-dibromo-8-hydroxyquinoline (HqBr) and the 8-hydroxyquinoline-5-sulfonic acid (HqSH), in the framework of the dispersion corrected Density Functional Theory (DFT). We investigated the influence of the X groups (X = H, Br, SO₃H) at ortho and para positions of the phenol ring on the interactions of the HqX species with aluminum. This was carried out both for the interaction of the deprotonated species with an Al³⁺ ion to form Al(qX)₃ complexes, and for the interaction of deprotonated and dehydrogenated species with an Al(111) surface.

For the Al(qX)₃ complexes, the QTAIM and ELF topological analyses performed on the Al-O and Al-N bonds showed no significant differences in the bonding of the different deprotonated species with the aluminum ion, which was found in Al^{III} oxidation state. The properties of the charge density in Al-O and Al-N bonds, described by QTAIM descriptors, argued for ionic bonding with a weak covalent contribution. This showed that the differences in experimentally observed properties between the HqX molecules do not directly originate from differences in metal chelation properties of the derivatives.

The Hq molecule, known for its efficiency as an aluminum corrosion inhibitor, has been shown in previous work to form stable and compact layers on Al(111), when adsorbed in dehydrogenated form. By adsorbing the dehydrogenated molecules on Al(111), we aimed to see how the X groups influenced this adsorption. The q, qBr, qS and qSH species were adsorbed on Al(111) in vacuum at three surface coverage, corresponding to i) a single adsorbed molecule (θ_1), ii) molecules adsorbed and in interaction with neighbouring molecules (θ_2), iii) a compact monolayer (θ_3). At all coverage, chemisorption of the molecules on Al(111) is demonstrated. Van de Waals interactions were shown to highly contribute to the adsorption, with 14% to 26% van der waals contribution to the interaction energy between the molecules and the aluminum surface. At the higher coverage θ_3 , all species formed stable and compact monolayers, with the only difference being the stronger inter-molecular interactions in

the monolayer for qSH due to hydrogen bonds. It is important to note that these monolayer geometries were obtained without taking into account the energy barriers involved in the monolayer formation process, and by imposing a periodic constraint of one molecule per simulation cell. Overall, at θ_1 and θ_2 , the parallel (*para*) adsorption geometries were favored, except for the case of the q molecule at θ_1 coverage, where the tilted (*tilt*) geometry was favored. This difference in adsorption of single molecules on Al(111) could impact the monolayer formation process, leading to different monolayers for the different species.

The use of a solvent model to simulate the influence of water on the molecules and the Al(111) surface lead to similar adsorption geometries for q and qBr, while some differences were found for qS, resulting of the stabilization of the SO₃ group in water. This did not differ qualitatively from our results in vacuum, but showed the necessity of including a solvent model to obtain more accurate results for species with highly hydrophobic or hydrophilic groups.

In order to verify the reliability of the modeling of the adsorption of deprotonated species by using dehydrogenated species, which is assumed in our work, we investigated the adsorption of deprotonated molecules, in presence of counter ions and in water, on Al(111). For the θ_1 coverage, the geometry and net charges on the adsorbed deprotonated molecules were found similar to the case of the dehydrogenated molecules. As expected, different adsorption energies were found, but showing strong adsorption in both cases. At θ_3 , further calculations need to be performed before reaching a conclusion.

All these results relied on three assumptions: i) The aluminum surface under the organic layer is a perfectly flat Al(111) surface, ii) The organic layer respects a periodicity of one molecule per simulation cell, iii) single molecules, rather than pre-formed complexes, are adsorbed on the aluminum surface. In order to go further than these assumptions, we considered two new adsorption processes.

First, we adsorbed Alq₃ complexes pre-formed in vacuum, on a flat Al(111) surface. Both *mer* and *fac* isomers were considered, as well as *up* and *down* adsorption geometries, defined by the orientation of the dipole moment of the complexes relatively to the aluminum surface. The *fac/up* geometry, where the three O atoms of the complex were bonded to the surface, was found to be the most stable.

Then, we considered the adsorption of three q molecules on an Al adatom of a defective

Al(111) surface. The high number of degrees of freedom of this system made necessary a broad exploration of the conformation space. This was carried out using *ab initio* molecular dynamics. The most stable geometries corresponded to those with the highest number of bonds between the molecules and the Al adatoms, leading to an Al₃-like geometry with an Al^{III} oxidation state of the adatom, close to that of the Al atom in the free or adsorbed complex.

Although for these two processes, the most stable geometry was obtained by the adsorption of three q molecules on an Al adatom of Al(111), the different geometries explored could coexist depending on the layer formation dynamics. The adsorption energy per molecule showed stronger adsorption for the three q molecules on an Al adatom of Al(111) than for the q molecule adsorbed on a flat Al(111). This result needs to be confirmed with systems of same surface coverage and same number of layers for the Al(111) surface model.

Overall, this work showed that the modification of the H atoms of the Hq at para and ortho positions of the phenol ring by Br or SO₃H groups does only influence locally the electronic structure of the molecule. It therefore does not modify the chelation of the aluminum ion by the molecules. Further studies are needed to evaluate the influence of chemical modifications on the properties of the metal-organic cx, i.e. solubility and light emission properties. When adsorbed on an Al(111) surface, the direct interaction of the X groups with Al(111) or the inter-molecular interactions in the organic layers leads to different most stable adsorption modes for the different molecules at low coverage, but close adsorption modes at high coverage. In this regard, it is worth noting that the only molecule which is an effective corrosion inhibitor (Hq) is adsorbed favorably in a different geometry (*tilt*) than the two other molecules (HqBr and HqSH) at low coverage, which could influence the first steps of the formation of the layer. Following this work, several studies can be carried out. First, other imperfect surfaces, such as adatom dimers or atomic steps, could be tested in order to get closer to realistic surfaces. The presence of an oxide layer could allow us to better model the aluminum surface at cathodic sites of the corrosion process. Finally, cells containing more than one molecule, at maximum coverage, could allow the investigation of monolayer geometries less biased by imposed periodicity.

Appendix A

A.1 Free molecules and complexes

TABLE A.1: Bond lengths (in Å) in free dehydrogenated qBr and deprotonated qBr⁻ in vacuum and water.

Species	qBr		qBr ⁻	
	Vacuum	Water	Vacuum†	Water
d_{C1-C2}	1.395	1.395	1.389	1.385
d_{C2-C3}	1.390	1.387	1.391	1.400
d_{C3-C4}	1.469	1.461	1.444	1.430
d_{C4-C5}	1.499	1.491	1.498	1.484
d_{C5-C6}	1.432	1.428	1.452	1.447
d_{C6-C7}	1.413	1.411	1.418	1.419
d_{C7-C8}	1.384	1.383	1.380	1.379
d_{C8-C9}	1.407	1.405	1.409	1.411
d_{C1-C6}	1.434	1.434	1.411	1.417
d_{C4-O1}	1.239	1.249	1.246	1.272
d_{C5-N1}	1.343	1.346	1.349	1.359
d_{C9-N1}	1.332	1.335	1.326	1.329
d_{C1-Br1}	1.897	1.887	1.935	1.924
d_{C3-Br2}	1.878	1.881	1.921	1.920

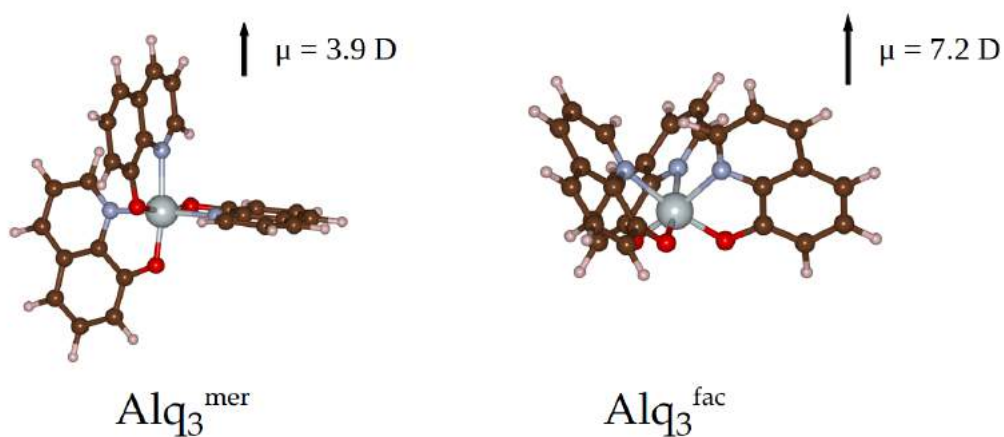
† Molecular calculation from Chapter 3.

TABLE A.2: Bond lengths (in Å) in free dehydrogenated qS and deprotonated qS²⁻ in vacuum and water.

Species	qSH	qSH ⁻	qS ²⁻	
	Vacuum	Vacuum†	Vacuum†	Water
d_{C1-C2}	1.403	1.409	1.393	1.393
d_{C2-C3}	1.308	1.379	1.397	1.397
d_{C3-C4}	1.455	1.443	1.433	1.426
d_{C4-C5}	1.499	1.501	1.493	1.484
d_{C5-C6}	1.433	1.444	1.454	1.445
d_{C6-C7}	1.417	1.421	1.423	1.422
d_{C7-C8}	1.384	1.382	1.380	1.380
d_{C8-C9}	1.406	1.404	1.410	1.410
d_{C1-C6}	1.438	1.434	1.424	1.428
d_{C4-O1}	1.246	1.248	1.267	1.280
d_{C5-N1}	1.342	1.327	1.358	1.360
d_{C9-N1}	1.334	1.349	1.326	1.329
d_{C1-S1}	1.785	1.731	1.810	1.782
d_{S1-O2}	1.434	1.460	1.486	1.480
d_{S1-O3}	1.440	1.451	1.483	1.476
d_{S1-O4}	1.627	1.667	1.486	1.480

† Molecular calculation from Chapter 3.

FIGURE A.1: Dipole moment (in Debye) for Alq₃^{mer} and Alq₃^{fac} complexes.



Appendix B

B.1 Molecule adsorbed on an Al(111) surface

TABLE B.1: Relative total energies (in eV) of q^- and q^{2-} molecules adsorbed on an Al(111) surface at θ_3 coverage for different distances (in Å) between the top layer of the slab and the bottom layer of the image slab. The Na^+ and Mg^{2+} ions are always at about equidistance between the molecule and the bottom layer of the image slab.

Property	q^-			qS^{2-}		
	<i>tilt_{bridge}</i>			<i>tilt_{bridge}</i>		
Distance	27	33	38	27	33	38
ΔE	0.00	+0.04	+0.08	0.00	+0.18	+0.31

TABLE B.2: Relative total energies (in eV) of the q^- molecule adsorbed on an Al(111) surface at θ_1 coverage for different distances (in Å) between the top layer of the slab and the bottom layer of the image slab. The Na^+ ion is always at about equidistance between the molecule and the bottom layer of the image slab.

Property	q^-	
	<i>tilt_{bridge}</i>	
Distance	27	33
ΔE	0.00	+0.01

FIGURE B.1: Local potential in the direction normal to the surface for the *tilt* mode of the q molecule adsorbed on Al(111) in vacuum (top) and in water (bottom). θ_3 coverage.

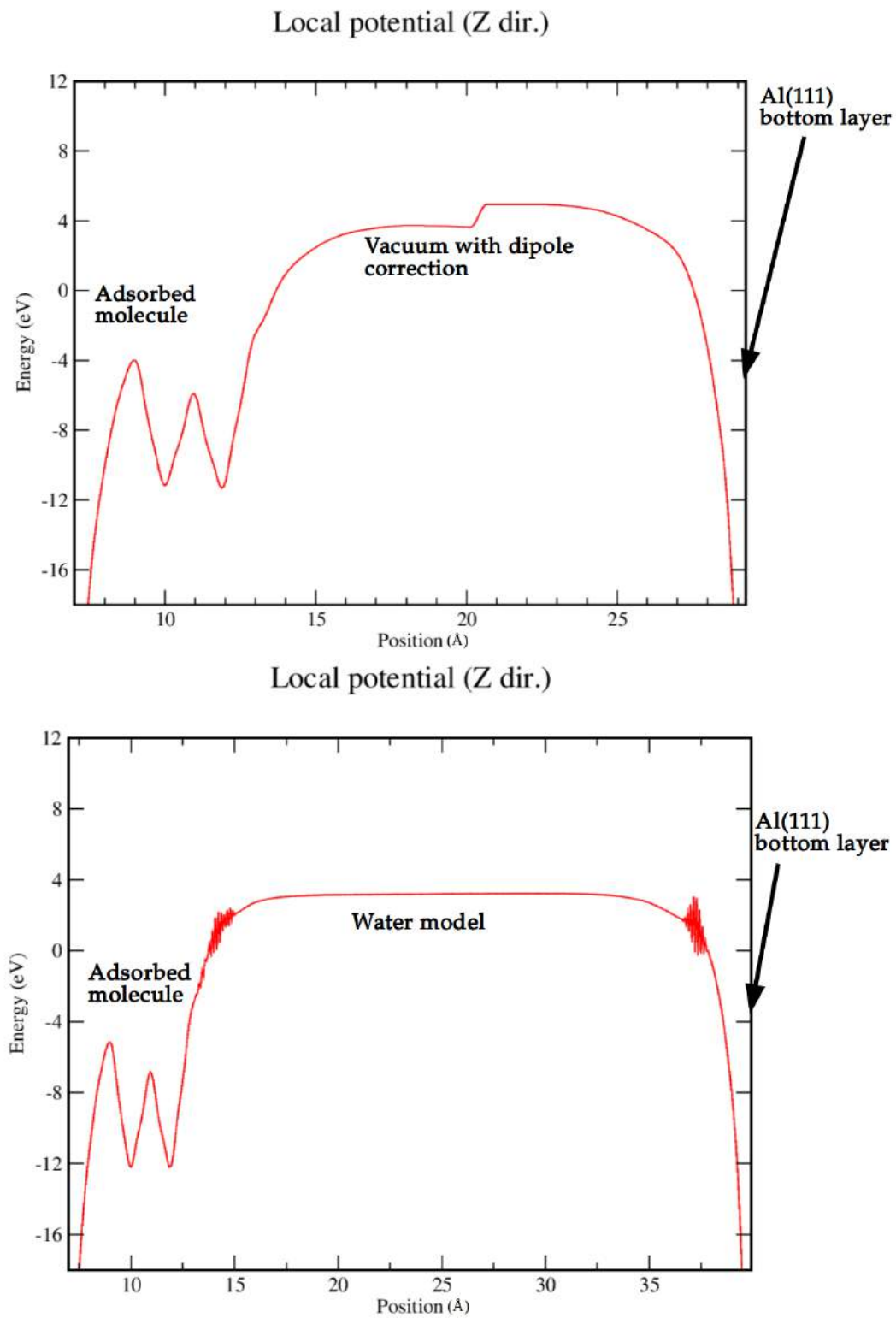


FIGURE B.2: Local potential in the direction normal to the surface for the *tilt* mode of the qS molecule adsorbed on Al(111) in vacuum at θ_3 coverage.

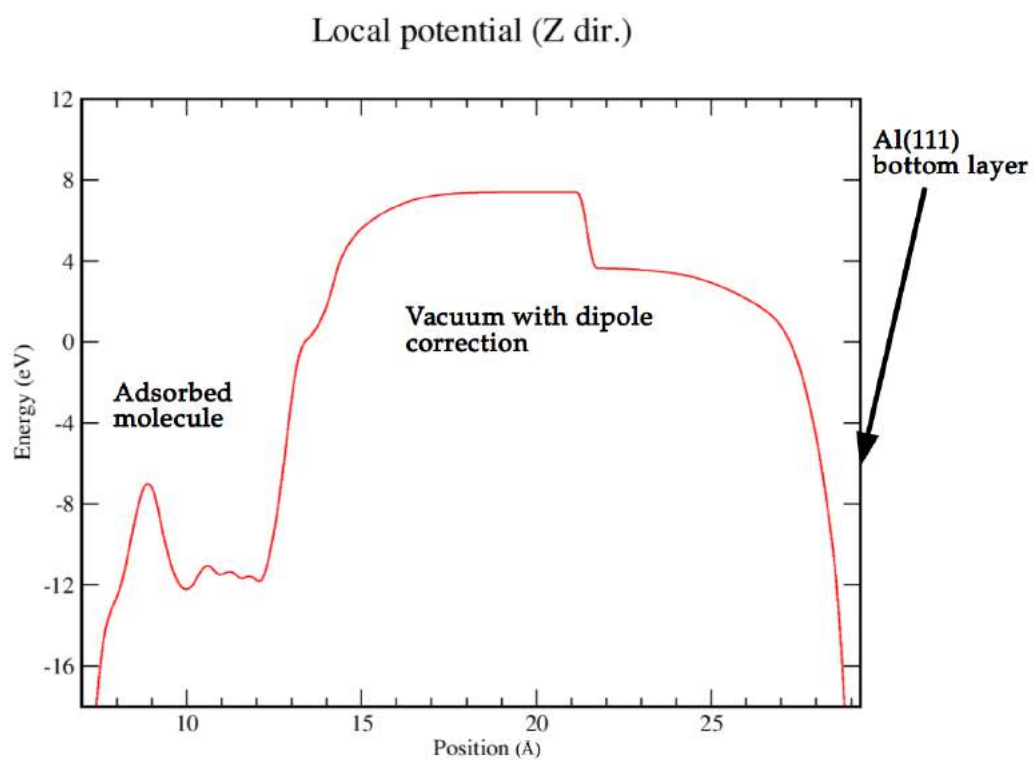
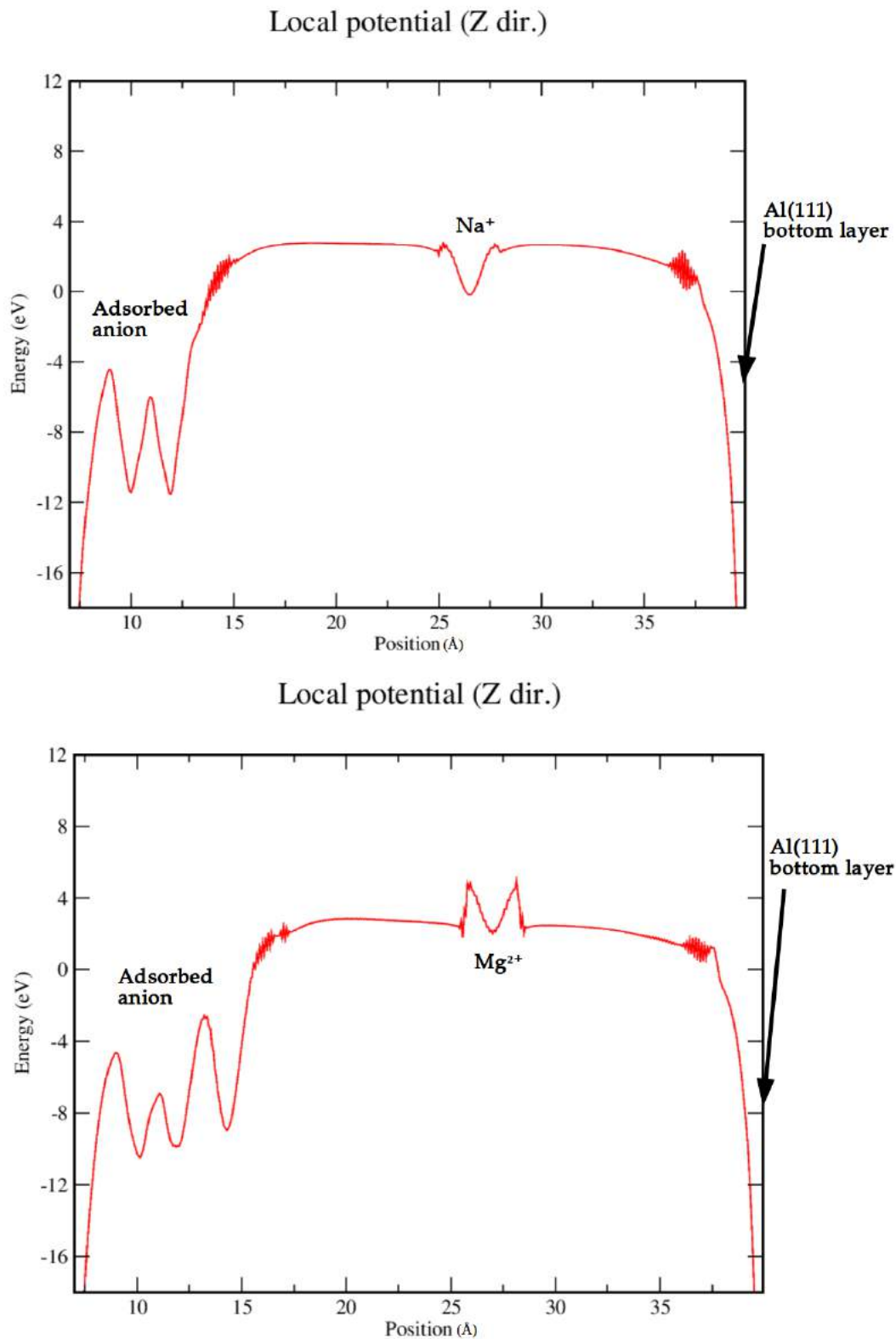


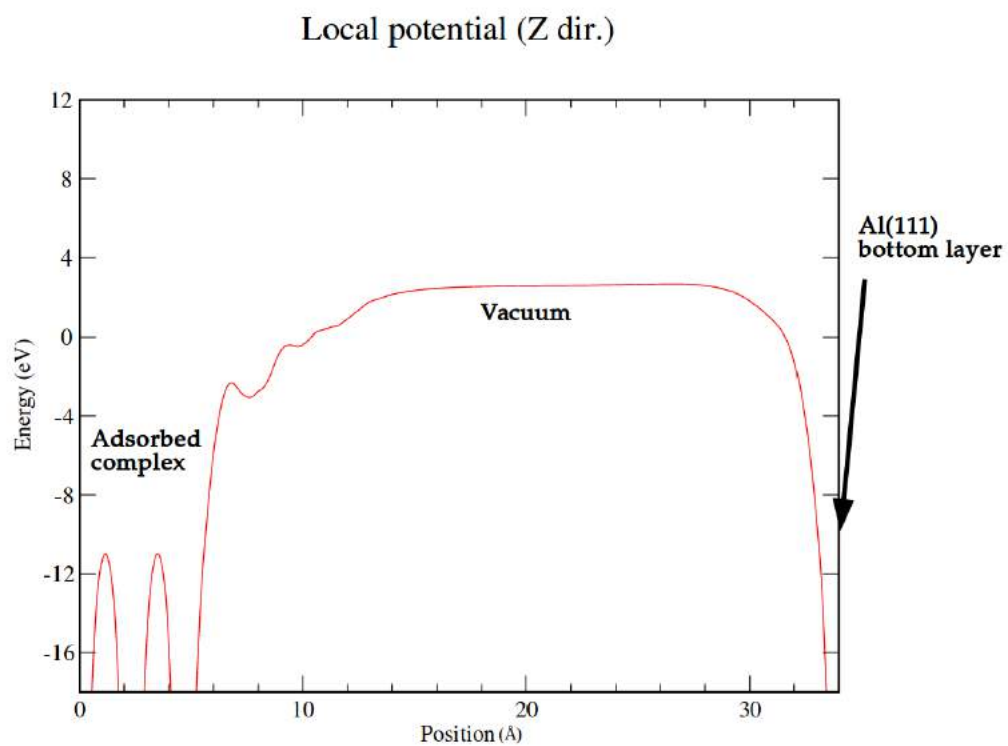
FIGURE B.3: Local potential in the direction normal to the surface for the *tilt* modes of the q^- molecule adsorbed on Al(111) (top) and for the qS^{2-} molecule adsorbed on Al(111) (bottom) in water at θ_3 coverage.



Appendix C

C.1 Complex adsorbed on an Al(111) surface

FIGURE C.1: Local potential in the direction normal to the surface for the *mer/down* geometry.



Bibliography

- (1) Yalkowsky, S. H.; Dannenfelser, R. M. *College of Pharmacy, University of Arizona, Tucson, AZ* **1992**, 189.
- (2) Albert, A.; Phillips, J. N. *J. Chem. Soc.* **1956**, 1294–1304.
- (3) Hollingshead, R. G. W., *Oxine and its Derivatives*; Butterworths Scientific Publications: 1956; Vol. 4.
- (4) Fresco, J.; Freiser, H. *Inorganic Chemistry* **1963**, 2, 82–85.
- (5) United States Environmental Protection Agency.
- (6) Wu, Z.; Shen, C.; Li, W.; Wu, J.; Zhao, H. *Journal of Chemical & Engineering Data* **2020**, 65, 2088–2097.
- (7) Roychowdhury, P.; Das, B. N.; Basak, B. S. *Acta Crystallographica Section B* **1978**, 34, 1047–1048.
- (8) Summers, K. L.; Pushie, M. J.; Sopasis, G. J.; James, A. K.; Dolgova, N. V.; Sokaras, D.; Kroll, T.; Harris, H. H.; Pickering, I. J.; George, G. N. *Inorganic Chemistry* **2020**, 59, PMID: 32936627, 13858–13874.
- (9) Verma, C.; Quraishi, M.; Ebenso, E. E. *Surfaces and Interfaces* **2020**, 21, 100634.
- (10) Baker, B. C.; Sawyer, D. T. *Analytical Chemistry* **1968**, 40, 1945–1951.
- (11) Soroka, K.; Vithanage, R. S.; Phillips, D. A.; Walker, B.; Dasgupta, P. K. *Analytical Chemistry* **1987**, 59, 629–636.
- (12) Brinkmann, M.; Gadret, G.; Muccini, M.; Taliani, C.; Masciocchi, N.; Sironi, A. *Journal of the American Chemical Society* **2000**, 122, 5147–5157.
- (13) Painuly, D.; Mogha, N. K.; Masram, D. T.; Singhal, R.; Gedam, R.; Nagpure, I. *Journal of Physics and Chemistry of Solids* **2018**, 121, 396–408.
- (14) Nghia, N. N.; Lee, Y.-I., et al. *Microchimica Acta* **2019**, 186, 36.

- (15) Wang, J.; Li, Y.; Li, K.; Meng, X.; Hou, H. *Chemistry – A European Journal* **2017**, *23*, 5081–5089.
- (16) Guo, W.; Meng, X.; Liu, Y.; Ni, L.; Hu, Z.; Chen, R.; Meng, M.; Wang, Y.; Han, J.; Luo, M. *Journal of Industrial and Engineering Chemistry* **2015**, *21*, 340–349.
- (17) Soliman, M. A.; Rashad, G. M.; Mahmoud, M. R. *Chemical Engineering Research and Design* **2019**, *144*, 459–471.
- (18) Jashni, E.; Hosseini, S. *Separation and Purification Technology* **2020**, *234*, 116118.
- (19) Kumbasar, R.; Şahin, *Journal of Membrane Science* **2008**, *325*, 712–718.
- (20) Ramos, M. L.; Justino, L. L. G.; Fonseca, S. M.; Burrows, H. D. *New J. Chem.* **2015**, *39*, 1488–1497.
- (21) Duvenhage, M.; Visser, H.; Ntwaeaborwa, O.; Swart, H. *Physica B: Condensed Matter* **2014**, *439*, 5th South African Conference on Photonic Materials (SACPM 2013), 46–49.
- (22) Fukushima, T.; Kaji, H. *Organic Electronics* **2012**, *13*, 2985–2990.
- (23) Cölle, M.; Dinnebier, R. E.; Brütting, W. *Chem. Commun.* **2002**, 2908–2909.
- (24) Singh, D.; Nishal, V.; Bhagwan, S.; Saini, R. K.; Singh, I. *Materials Design* **2018**, *156*, 215–228.
- (25) Prachayasittikul, V.; Prachayasittikul, S.; Ruchirawat, S.; Prachayasittikul, V. *Drug design, development and therapy* **2013**, *7*, 1157.
- (26) Oliveri, V.; Vecchio, G. *European Journal of Medicinal Chemistry* **2016**, *120*, 252–274.
- (27) Revie, R. W., *Uhlig's corrosion handbook*; John Wiley & Sons: 2011; Vol. 51.
- (28) Pourbaix, M.; Burbank, J. *Journal of The Electrochemical Society* **1964**, *111*, 14C.
- (29) Pyun, S.-I.; Moon, S.-M. *Journal of Solid State Electrochemistry* **2000**, *4*, 267–272.
- (30) Vargel, C., *Corrosion of aluminium*; Dunod: 1999.
- (31) Smialowska, Z. S. *Corros. Sci* **1999**, *41*, 1743–1767.
- (32) Williams, E. S.; Panko, J.; Paustenbach, D. J. *Critical reviews in toxicology* **2009**, *39*, 553–575.
- (33) Khanari, K.; Finšgar, M. *Arabian Journal of Chemistry* **2019**, *12*, 4646–4663.
- (34) Obot, I.; Macdonald, D.; Gasem, Z. *Corrosion Science* **2015**, *99*, 1–30.
- (35) Khanari, K.; Finšgar, M. *RSC Adv.* **2016**, *6*, 62833–62857.

- (36) Jadhav, S. *Open Chemistry* **2011**, *9*, 369–378.
- (37) Sherif, E.-S. M. *Journal of Industrial and Engineering Chemistry* **2013**, *19*, 1884–1889.
- (38) Marcelin, S.; Pébère, N. *Corros. Sci.* **2015**, *101*, 66–74.
- (39) Balaskas, A. C.; Curioni, M.; Thompson, G. E. *Surf. Interface Anal.* **2015**, *47*, 1029–1039.
- (40) Garrigues, L.; Pebere, N.; Dabosi, F. *Electrochimica Acta* **1996**, *41*, 1209–1215.
- (41) Zheludkevich, M.; Yasakau, K.; Poznyak, S.; Ferreira, M. *Corrosion Science* **2005**, *47*, 3368–3383.
- (42) Winkler, D. A.; Breedon, M.; Hughes, A. E.; Burden, F. R.; Barnard, A. S.; Harvey, T. G.; Cole, I. *Green Chem.* **2014**, *16*, 3349–3357.
- (43) Kokalj, A.; Peljhan, S.; Finšgar, M.; Milošev, I. *Journal of the American Chemical Society* **2010**, *132*, PMID: 21033661, 16657–16668.
- (44) Winkler, D.; Breedon, M.; White, P.; Hughes, A.; Sapper, E.; Cole, I. *Corrosion Science* **2016**, *106*, 229–235.
- (45) Costa, D.; Ribeiro, T.; Cornette, P.; Marcus, P. *The Journal of Physical Chemistry C* **2016**, *120*.
- (46) Poberžnik, M.; Chiter, F.; Milošev, I.; Marcus, P.; Costa, D.; Kokalj, A. *Applied Surface Science* **2020**, *525*, 146156.
- (47) Kovačević, N.; Kokalj, A. *Corrosion Science* **2013**, *73*, 7–17.
- (48) Kokalj, A.; Peljhan, S.; Koller, J. *The Journal of Physical Chemistry C* **2014**, *118*, 944–954.
- (49) Gustinčič, D.; Kokalj, A. *Metals* **2018**, *8*, 310.
- (50) Chiter, F.; Lacaze-Dufaure, C.; Tang, H.; Pébère, N. *Phys. Chem. Chem. Phys.* **2015**, *17*.
- (51) Chiter, F.; Bonnet, M.-L.; Lacaze-Dufaure, C.; Tang, H.; Pébère, N. *Phys. Chem. Chem. Phys.* **2018**, *20*, 21474–21486.
- (52) Shen, S.; Zuo, Y.; Zhao, X. *Corrosion Science* **2013**, *76*, 275–283.
- (53) Zong, Q.; Wang, L.; Sun, W.; Liu, G. *Corrosion Science* **2014**, *89*, 127–136.
- (54) Mei LI, S.; rui ZHANG, H.; hua LIU, J. *Transactions of Nonferrous Metals Society of China* **2007**, *17*, 318–325.
- (55) Lamaka, S.; Zheludkevich, M.; Yasakau, K.; Montemor, M.; Ferreira, M. *Electrochimica Acta* **2007**, *52*, 7231–7247.

- (56) Chiter, F. Étude théorique d'inhibiteurs verts de corrosion : adsorption de la 8-hydroxyquinoléine sur surfaces d'aluminium, Ph.D. Thesis, 2015.
- (57) Born, M.; Oppenheimer, R. *Annalen der Physik* **1927**, 389, 457–484.
- (58) Thomas, L. H. **1927**, 23, 542–548.
- (59) Fermi, E. *Rend. Accad. Naz. Lincei* **1927**, 6, 5.
- (60) Hohenberg, P.; Kohn, W. *Phys. Rev.* **1964**, 136, B864–B871.
- (61) Kohn, W.; Sham, L. J. *Phys. Rev.* **1965**, 140, A1133–A1138.
- (62) Perdew, J. P.; Zunger, A. *Phys. Rev. B* **1981**, 23, 5048–5079.
- (63) Adamo, C.; Barone, V. *The Journal of Chemical Physics* **1998**, 108, 664–675.
- (64) Kim, K.; Jordan, K. D. *The Journal of Physical Chemistry* **1994**, 98, 10089–10094.
- (65) Perdew, J. P.; Burke, K.; Ernzerhof, M. *Phys. Rev. Lett.* **1996**, 77, 3865–3868.
- (66) Perdew, J. P.; Burke, K.; Ernzerhof, M. *Phys. Rev. Lett.* **1997**, 78, 1396–1396.
- (67) Gaussian 09 Revision D.01, F. M. J. et al., *Gaussian 09*; Gaussian, Inc.: Wallingford, CT, 2016.
- (68) Kresse, G.; Hafner, J. *Phys. Rev. B* **1993**, 47, 558–561.
- (69) Kresse, G.; Furthmüller, J. *Phys. Rev. B* **1996**, 54, 11169–11186.
- (70) Kresse, G.; Furthmüller, J. *Computational Materials Science* **1996**, 6, 15–50.
- (71) Hehre, W. J.; Stewart, R. F.; Pople, J. A. *The Journal of Chemical Physics* **1969**, 51, 2657–2664.
- (72) Collins, J. B.; von R. Schleyer, P.; Binkley, J. S.; Pople, J. A. *The Journal of Chemical Physics* **1976**, 64, 5142–5151.
- (73) Ditchfield, R.; Hehre, W. J.; Pople, J. A. *The Journal of Chemical Physics* **1971**, 54, 724–728.
- (74) Weigend, F.; Ahlrichs, R. *Physical Chemistry Chemical Physics (Incorporating Faraday Transactions)* **2005**, 7, 3297.
- (75) Weigend, F. *Phys. Chem. Chem. Phys.* **2006**, 8, 1057–1065.
- (76) Kittel, C., *Introduction to Solid State Physics*; Wiley: 1996.
- (77) Grimme, S. *Journal of Computational Chemistry* **2006**, 27, 1787–1799.
- (78) Grimme, S.; Antony, J.; Ehrlich, S.; Krieg, H. *The Journal of Chemical Physics* **2010**, 132, 154104.

- (79) Mathew, K.; Kolluru, V. S. C.; Hennig, R. G. VASPsol: Implicit solvation and electrolyte model for density-functional theory, <https://github.com/henniggroup/VASPsol>, 2018.
- (80) Mathew, K.; Sundararaman, R.; Letchworth-Weaver, K.; Arias, T. A.; Hennig, R. G. *J. Chem. Phys.* **2014**, *140*, 084106.
- (81) Steinmann, S. N.; Sautet, P.; Michel, C. *Phys. Chem. Chem. Phys.* **2016**, *18*, 31850–31861.
- (82) Becke, A. D.; Edgecombe, K. E. *J. Chem. Phys.* **1990**, *92*, 5397–5403.
- (83) Savin, A.; Jepsen, O.; Flad, J.; Andersen, O. K.; Preuss, H.; von Schnering, H. G. *Angewandte Chemie International Edition in English* **1992**, *31*, 187–188.
- (84) Silvi, B.; Savin, A. *Nature* **1994**, *371*, 683–686.
- (85) Weizsäcker, C. F. V. *Zeitschrift für Physik* **1935**, *96*, 431–458.
- (86) Fuster F.; Sevin, A. S. B. *J. Phys. Chem. A* **2000**, *104*, 852–858.
- (87) Bader, R. F. W.; Clarendon Press.
- (88) Murgich, J.; Franco, H. J. *Journal of Physical Chemistry A* **2009**, *113*, 5205–5211.
- (89) Contreras, R.; Domingo, L. R.; Silvi, B. In *Encyclopedia of Physical Organic Chemistry*; American Cancer Society: 2017, pp 1–114.
- (90) Abramov, Y. A. *Acta Crystallographica Section A* **1997**, *53*, 264–272.
- (91) Noury, S.; Krokidis, X.; Fuster, F.; Silvi, B. *Computers Chemistry* **1999**, *23*, 597–604.
- (92) Marenich, A. V.; Cramer, C. J.; Truhlar, D. G. *The Journal of Physical Chemistry B* **2009**, *113*, PMID: 19366259, 6378–6396.
- (93) Schiavo, E.; Munoz-Garcia, A.; Barone, V.; Vittadini, A.; Casarin, M.; Forrer, D.; Pavone, M. *Chemical Physics Letters* **2018**, *693*.
- (94) Blöchl, P. E. *Phys. Rev. B* **1994**, *50*, 17953–17979.
- (95) Kresse, G.; Joubert, D. *Phys. Rev. B* **1999**, *59*, 1758–1775.
- (96) Methfessel, M.; Paxton, A. T. *Phys. Rev. B* **1989**, *40*, 3616–3621.
- (97) Press, W. H.; Flannery, B. P.; Teukolsky, S. A.; Vetterling, W. T., et al. *Numerical recipes*, 1989.
- (98) Pulay, P. *Chemical Physics Letters* **1980**, *73*, 393–398.
- (99) Keith, T. A. AIMALL, version 19.10.12, TK Gristmill Software, Overland Park KS, USA, 2019, 1997.

- (100) Vega, D.; Almeida, D. *Journal of Computational Methods in Science and Engineering* **2014**, *14*, 131–136.
- (101) Tang, W; Sanville, E; Henkelman, G *Journal of Physics: Condensed Matter* **2009**, *21*, 084204.
- (102) CSCS Molekel, version 4.3.
- (103) Momma, K.; Izumi, F. *Journal of Applied Crystallography* **2011**, *44*, 1272–1276.
- (104) Bahers], T. L.; Adamo, C.; Ciofini, I. *Chemical Physics Letters* **2009**, *472*, 30–34.
- (105) Le Bahers, T.; Adamo, C.; Ciofini, I. *The Journal of Physical Chemistry A* **2010**, *114*, PMID: 20402487, 5932–5939.
- (106) Banerjee, T.; Saha, N. N. *Acta Crystallographica Section C* **1986**, *42*, 1408–1411.
- (107) Fuster, F; Grabowski, S. J. *J. Phys. Chem. A* **2011**, *115*, 10078–10086.
- (108) Poater, J.; Duran, M.; Sola, M.; Silvi, B. *Theoretical . Chem. Rev.* **2005**, *105*, 3911–3947.
- (109) Curioni, A.; Boero, M.; Andreoni, W. *Chemical Physics Letters* **1998**, *294*, 263–271.
- (110) Li, H.; Zhang, F.; Wang, Y.; Zheng, D. *Mater. Sci. Eng.: B* **2003**, *100*, 40–46.
- (111) Saxena, A. K. *Synth. React. Inorg. Met. Org. Chem.* **1999**, *29*, 1747–1767.
- (112) Muccini, M.; Kenevey, M. A. L. K.; Zamboni, R.; Masciocchi, N.; Sironi, A. *Adv. mater.* **2004**, *16*, Relation: <https://www.rug.nl/zernike/> date_submitted : 2007Rights : UniversityofGroningen. 861–864.
- (113) Katakura, R.; Koide, Y. *Inorganic Chemistry* **2006**, *45*, PMID: 16841973, 5730–5732.
- (114) Halls, M. D.; Schlegel, H. B. *Chemistry of Materials* **2001**, *13*, 2632–2640.
- (115) Wang, Y.-P.; Han, X.-F.; Wu, Y.-N.; Cheng, H.-P. *Phys. Rev. B* **2012**, *85*, 144430.
- (116) Yanagisawa, S.; Lee, K.; Morikawa, Y. *The Journal of chemical physics* **2008**, *128*, 244704.
- (117) Chiter, F.; Nguyen, V. B.; Tarrat, N.; Benoit, M.; Tang, H.; Lacaze-Dufaure, C. *Materials Research Express* **2016**, *3*, 046501.
- (118) Da Silva, J.; Stampfl, C.; Scheffler, M. *Surface Science* **2006**, *600*, 703–715.
- (119) Tyson, W.; Miller, W. *Surface Science* **1977**, *62*, 267–276.
- (120) Noonan, J. R.; Davis, H. L. *Journal of Vacuum Science & Technology A* **1990**, *8*, 2671–2676.
- (121) STAMPFL, C.; SCHEFFLER, M. *Surface Review and Letters* **1995**, *02*, 317–343.

- (122) Bogicevic, A.; Hyldgaard, P.; Wahnström, G.; Lundqvist, B. I. *Phys. Rev. Lett.* **1998**, *81*, 172–175.
- (123) Barth, J. V.; Brune, H.; Fischer, B.; Weckesser, J.; Kern, K. *Phys. Rev. Lett.* **2000**, *84*, 1732–1735.
- (124) Chang, C. M.; Wei, C. M.; Chen, S. P. *Phys. Rev. Lett.* **2000**, *85*, 1044–1047.
- (125) Peljhan, S.; Koller, J.; Kokalj, A. *The Journal of Physical Chemistry C* **2014**, *118*, 933–943.
- (126) Poberžnik, M.; Costa, D.; Hemeryck, A.; Kokalj, A. *The Journal of Physical Chemistry C* **2018**, *122*, 9417–9431.
- (127) Li, X.; Deng, S.; Xie, X. *Corrosion Science* **2014**, *81*, 162–175.
- (128) Chiter, F.; Costa, D.; Maurice, V.; Marcus, P. *Applied Surface Science* **2021**, *537*, 147802.
- (129) Vernack, E.; Costa, D.; Tingaut, P.; Marcus, P. *Corrosion Science* **2020**, *174*, 108840.
- (130) Monkhorst, H. J.; Pack, J. D. *Phys. Rev. B* **1976**, *13*, 5188–5192.
- (131) Neugebauer, J.; Scheffler, M. *Phys. Rev. B* **1992**, *46*, 16067–16080.
- (132) Makov, G.; Payne, M. C. *Phys. Rev. B* **1995**, *51*, 4014–4022.
- (133) Wang, D.; Yang, D.; Zhang, D.; Li, K.; Gao, L.; Lin, T. *Applied Surface Science* **2015**, *357*, 2176–2183.
- (134) Bianchi, R.; Gervasio, G.; Marabello, D. *Inorg. Chem.* **2000**, *39*, 2360–2366.
- (135) Raissi, H.; Yoosefian, M.; Mollania, F.; Farzad, F.; Nowroozi, A. R.; Iloghmaninejad, D. *Computational and Theoretical Chemistry* **2011**, *966*, 299–305.
- (136) Halder, A.; Data, D.; Seelam Prabhakar, P.; Bhattacharyya, D.; Mitra, A. *ACS Omega* **2019**, *4*, 7354–7368.
- (137) Ahmadi, M. A. In *Fundamentals of Enhanced Oil and Gas Recovery from Conventional and Unconventional Reservoirs*, Bahadori, A., Ed.; Gulf Professional Publishing: 2018, pp 187–205.
- (138) Soliman, H. *Corrosion Science* **2011**, *53*, 2994–3006.
- (139) Allen, M. P.; Tildesley, D. J., *Computer Simulation of Liquids*; Oxford University Press: 1991.
- (140) Hoover, W. G.; Ladd, A. J. C.; Moran, B. *Phys. Rev. Lett.* **1982**, *48*, 1818–1820.
- (141) Evans, D. J. *J. Chem. Phys.* **1983**, *78*, 3297–3302.

RÉSUMÉ

La 8-hydroxyquinoléine (Hq) et ses dérivés (Hq chimiquement modifiée) sont connus pour leur capacité à complexer des ions métalliques. Ils sont mis en œuvre dans la dépollution des effluents aqueux, la conception de composants électroluminescents, et l'inhibition de la corrosion de surfaces métalliques. Les propriétés de ces molécules et des complexes formés avec des ions métalliques dépendent des modifications chimiques réalisées sur la Hq. Nous effectuons des études théoriques sur la Hq et deux de ses dérivés, la 5,7-dibromo-8-hydroxyquinoléine (HqBr) et l'acide 8-hydroxyquinoléine-5-sulfonique (HqSH), dans le cadre de la Théorie de la Fonctionnelle de la Densité et en prenant en compte les forces de dispersion (DFT-D).

Dans un premier temps, nous avons déterminé les formes stables des complexes issus de l'interaction entre un cation Al^{3+} et les molécules Hq, HqBr et HqSH déprotonées, puis nous avons effectué des analyses topologiques (ELF et QTAIM) de la structure électronique de ces complexes. Des liaisons iono-covalentes sont formées entre les molécules et l'ion Al^{3+} .

Puis, nous avons étudié l'adsorption des molécules Hq, HqBr et HqSH déshydrogénées sur une surface Al(111), dans le vide et en présence d'eau (modèle de solvant implicite). Les trois types de molécules peuvent former des couches stables compactes sur la surface Al(111).

A contrario, les topologies d'adsorption d'une molécule isolée sont différentes pour la Hq, dont l'efficacité en tant qu'inhibiteur de la corrosion de l'aluminium a été démontré expérimentalement, et pour les HqBr et HqSH, qui ne démontrent aucune efficacité en tant qu'inhibiteurs de corrosion. Ces conformations différentes des molécules sur la surface Al(111) en début du processus de formation des couches organiques, pourraient jouer sur leur propriété de protection de l'aluminium contre la corrosion.

Enfin, la formation de complexes directement sur la surface Al(111) a été étudiée par dynamique moléculaire *ab initio* afin d'explorer l'espace des conformations. De nombreuses géométries stables ont été déterminées et la formation d'un complexe sur la surface par adsorption de trois molécules déshydrogénées sur une surface Al(111) présentant un ad-atome est favorisée par rapport à la précipitation d'un complexe Alq_3 préalablement formé dans le vide.

Ainsi, nous présentons dans ce travail une description : i) de la nature précise des liaisons dans les complexes Alq_3 , ii) des géométries des dérivés de la Hq adsorbés sur une surface Al(111), iii) de la formation sur Al(111) de complexes de type Alq_3 par adsorption de molécules Hq déshydrogénées sur une surface Al(111).

ABSTRACT

The 8-hydroxyquinoline (Hq) and its derivatives (chemically modified Hq) are known for their ability to chelate metallic cations. They are used in applications such as depollution, light emitting devices, medicine and inhibition of the corrosion of metallic surfaces. The properties of these molecules and of their metal-organic complexes depend on the chemical modifications made on Hq. In the present work, in addition to Hq, two derivatives are studied: the 5,7-dibromo-8-hydroxyquinoline (HqBr) and the 8-hydroxyquinoline-5-sulfonic acid (HqSH). Our investigation is carried out in the framework of the dispersion corrected Density Functional Theory (DFT-D), and focuses on the study of the interactions of Hq, HqBr and HqSH species with aluminum.

First, we investigate the geometries of the complexes formed by deprotonated Hq, HqBr and HqSH with an aluminum cation, and characterize the bonds formed between the molecules and the cation from ELF and QTAIM topological analyses of the electronic structure of the complexes. The three molecules form similar iono-covalent bonds with the Al^{3+} ion.

We then focus on the interaction of the dehydrogenated Hq, HqBr and HqSH species with an Al(111) surface, in vacuum and in water, to get insight on the adsorption properties of the three molecules. While all three molecule can form stable and compact layers on Al(111), the adsorption a single molecule is different for Hq, which has been shown experimentally to be an efficient corrosion inhibitor of aluminum, than for HqBr and HqSH, which have shown no inhibition efficiency against aluminum corrosion. These different geometries could influence the dynamics of the layer formation, and thus the protection of the aluminum surface against corrosion.

Finally, the formation of Hq complexes, noted Alq_3 , on Al(111) is investigated, using *ab initio* molecular dynamics to explore the conformation space of the system. The work shows a large amount of possible stable geometries that could coexist. The formation of a complex on the surface by the adsorption of three dehydrogenated molecules on an Al adatom of the Al(111) surface is favored over the deposition of an Alq_3 complex preformed in vacuum.

This work gives: i) an accurate description of the nature of the bonding in aluminum complexes, in vacuum and solution, ii) an insight of the interactions of dehydrogenated Hq derivatives with the Al(111) surface, iii) new possible configurations of dehydrogenated Hq adsorbed on a defective Al(111) surface, forming Alq_3 -like complexes on the surface.